January 2015

Native chromatin extraction and its structure analysis

Zhongwu Zhou
Purdue University

Graduate School Form 30
Updated 1/15/2015

PURDUE UNIVERSITY
GRADUATE SCHOOL
Thesis/Dissertation Acceptance

This is to certify that the thesis/dissertation prepared

By Zhongwu Zhou

Entitled
NATIV CHROMATIN EXTRACTION AND ITS STRUCTURE ANALYSIS

For the degree of Doctor of Philosophy

Is approved by the final examining committee:

Joseph M K Irudayaraj
Chair

Christopher J Gilpin

Wen Jiang

Abigail S Engelberth

To the best of my knowledge and as understood by the student in the Thesis/Dissertation Agreement, Publication Delay, and Certification Disclaimer (Graduate School Form 32), this thesis/dissertation adheres to the provisions of Purdue University's "Policy of Integrity in Research" and the use of copyright material.

Approved by Major Professor(s): Joseph M K Irudayaraj

Approved by: Joseph M K Irudayaraj 12/1/2015

Head of the Departmental Graduate Program Date

NATIVE CHROMATIN EXTRACTION AND ITS STRUCTURE ANALYSIS

A Dissertation

Submitted to the Faculty

of

Purdue University

by

Zhongwu Zhou

In Partial Fulfillment of the

Requirements for the Degree

of

Doctor of Philosophy

December 2015

Purdue University

West Lafayette, Indiana

致中国留学基金委，我的爱人和孩子

ACKNOWLEDGEMENTS

I would like to give special thanks to my advisor Joseph M. K. Irudayaraj, who gave me freedom to choose research topics and professional guides to conduct a research. I would also like to thank my advisory committee members, Chris Gilpin, Wen Jiang and Abigail S Engelberth for spending their valuable time to review this work.

I especially thank Yixiu Liu for her encouragement and support, which have been the main sources of my motivation and happiness. I thank Sophie Lelievre, Ann L. Kirchmaier, Arnold Stein, John Anderson, Zhi Shan, Don Ready, Yunfeng Bai, Pengfei Wang, Xiaolei Wang, Ren Wen, Yan Rui, Kunpeng Li and Yi Yang for their inspiring discussion. Finally, I would like to thank Chris Woodcock, Guohong Li, Ping Zhu, Jeffrey Hansen and Jacques Dobuchet for their critical comments on my research.

Funding from both Purdue University and China Scholarship Council are appreciated.

TABLE OF CONTENTS

Page

Page

LIST OF TABLES

LIST OF FIGURES

Figure Page

Figure Page

Figure Page

Figure Page

ABSTRACT

Zhou, Zhongwu. Ph.D., Purdue University, December 2015. Native Chromatin Extraction and Its Structure Analysis. Major Professor: Joseph M. K. Irudayaraj.

Structure determines function. Properly ordered chromatin organization is fundamental for accurate regulation of gene expression inside eukaryotes. A native chromatin extraction method is developed based on solid phase reversible immobilization (SPRI) using magnetic nanoparticles as carriers. This method provides a quick, simple, inexpensive and an environmental-friendly means of chromatin extraction, and preserves the native structure of chromatin. The purified chromatin consists of DNA, histones, chromatin associated RNAs (CARs) and other non-histone proteins. Using the purified chromatin as a source, we developed a biotin-streptavidin mediated enzyme-based immunosorbent assay for simultaneous detection of epigenetic modifications on DNA and histone proteins. In order to analyze the CARs, we also developed a magnetophoretic chromatography method to remove the free RNAs, and the CARs were further extracted from the collected chromatin. The extracted CARs were reverse transcribed as cDNA and further characterized by real-time qPCR. The total assay time taken for cell separation, chromatin purification and chromatin associated RNAs extraction can be accomplished in less than 2h. Finally, we further applied cryogenic electron microscopy to analyze higher order chromatin structure in near-native state. We found that the chromatin fibers hold a branching structure and this structure generally exist in eukaryotic cells.

CHAPTER 1. GENERAL INTRODUCTION

1.1 Introduction

1.1.1 Chromatin

Over 3 billion base pairs of nucleotides arranged in a linear sequence along deoxyribonucleic acid (DNA) are within the genome and encode every protein and genetic trait in each type of cell of the human body. DNA in each cell can reach 2-meter in length when fully extended (Kulić and Schiessel, 2003). A series of processes must therefore take place that enable the cell to package DNA within the confines of the nucleus (with a general diameter of 10 μm) while retaining its ability to transcribe and duplicate the entire DNA sequence and maintain its integrity. This is achieved through an elaborate process of DNA condensation that sees DNA packaged into 46 chromosomes (or 23 chromosome pairs) in humans.

In the interphase nucleus, chromosomes are difficult to distinguish from each other. However, they are not randomly distributed inside a nucleus but do occupy a discrete space inside the nucleus – so called chromosome territory (Heard and Bickmore, 2007). Lighter stained euchromatin (transcriptionally active) and the patches of darker heterochromatin (transcriptionally silent) are, on the other hand, easy to visualize. During

the cell division, chromosome territories transform into highly condensed chromosomes, which then can be clearly distinguished from one another.Chromosomes reach their highest level of condensation during cell division, or mitosis, where they will acquire a discrete 4-armed or 2-armed morphology that represents approximately 10,000-fold compaction (Cremer and Cremer, 2001). Although this heavily condensed mitotic form has become the most common way of depicting chromosomes, their structure is significantly different during the interphase. Compared to mitotic chromosomes, interphase chromosomes are less condensed and occupy the entire nuclear space, making them somewhat difficult to distinguish.

Like the formation of metaphase chromosomes, the compaction required to fit a full set of interphase chromosomes into the nucleus is achieved through a series of DNA folding, wrapping and bending events that are facilitated by histones, which are highly conserved basic nuclear proteins that enable DNA compaction by neutralizing DNA's negative charge. Histones generally arrange as an octamer in complex with DNA to form the nucleosome. The combination of DNA and histone proteins that make up the nuclear content is often referred to as chromatin (Gardner et al., 2011).

Recently chromatin is recognized as a complex of macromolecules consisting of DNA, RNA, histones and other associated protein. The primary functions of chromatin are 1) to package DNA into a smaller volume to fit in the cell, 2) to reinforce the DNA macromolecule to allow mitosis, 3) to prevent DNA damage, and 4) to control gene expression and DNA replication (Hansen, 2002).

1.1.2 Chromatin Structure

Chromatin structure may be defined as any assemblage of nucleosomes that assumes a reproducible conformation in 3D space. Classically, the chromatin structure is reviewed at different levels. The DNA, an extended 2 nm flexible polymer following a hierarchical packing pathway, first packs into an 11 nm “bead-on-a-string’ structure wherein DNA wraps around the histone octamer with 1.7 turns. The basic repeating unit of this structure is called a nucleosome. With the linker DNA and linker histones, the 11 nm fibers are further compacted into 30 nm fiber. Recent advance in chromatin structure biology reveals that there are four nucleosomes in each turn to form the 30 nm fiber (Song et al., 2014). The 30 nm structure could further associate with chromosome scaffold to form a “300 nm’ structure. The ‘300 nm’ structure can further fold into a metaphase chromosome with a size around 1400 nm.

The classical review of chromatin structure may help the beginners to associate the chromatin structure to its delicate function. However, it is far from enough for a complete understanding of chromatin function inside the nucleus. Using electron microscopies, we confirm the DNA structure, the nucleosome structure and the 11 nm ‘bead-on-a-string’ structures. Though the structure of *in vitro* reconstituted 30 nm fiber is resolved by cryo electron microscopy using single particle method, there is a hot debate whether the 30 nm fiber exists inside the nucleus. The knowledge of higher order chromatin structure beyond 30 nm fiber is unknown, which humbles our understanding of chromatin organization inside the nucleus, such as how each chromosome forms chromosome territory inside the nucleus; how the nucleolus is formed etc. Thus, there is a resolution

gap between the ‘bead-on-a-string’ structure and the chromosome territory structure, as shown in Fig 1.1.

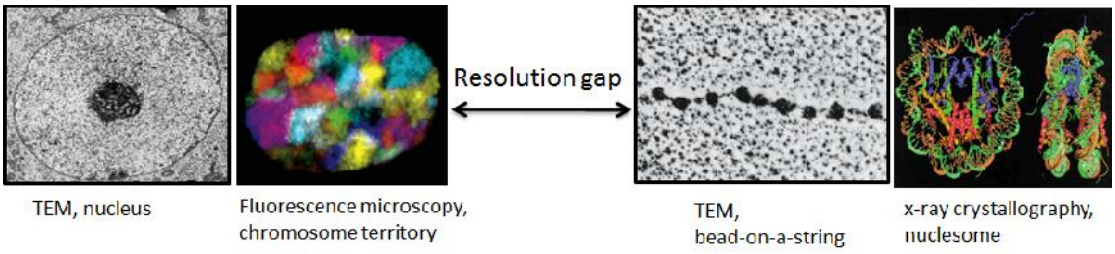

Figure 1.1 The resolution gap between the ‘bead-on-a-string’ structure and the chromosome territory structure.

1.1.3 Chromatin Structure Beyond 30 nm

On one hand, cryogenic electron microscopy (cryo-EM) studies initiate the observation of the 30 nm chromatin fiber in the near-native state from sperm, chicken erythrocytes and Hela S3 cells chromatin. Using electron tomography (ET) to study chromatin structure of chicken erythrocyte nuclei (both in the native form and in the isolated form), Horowitz et al. revealed that the 30-nm fiber could be modeled by a two-start zigzag helical conformation (Fussner et al., 2011b; Tremethick, 2007). However, in the study the samples were chemically fixed, dehydrated, embedded in resin, and stained by heavy metal. The corresponding observation could be attributed to the probable structure rearrangement and staining artifacts. Li et al prepared ultra-thin sections of Hela cells using different techniques such as chemical fixation, high pressure freezing with freeze substitution and cryo-ultromicrotomy with SEM-FIB (focused ion beam), to make a better preservation of the native status of the nuclei. Their results suggested that the chromatin fibers in Hela cells are likely organized in architecture with a diameter of about 30 nm (Li et al., 2015). This work was consistent with their previous study that the

in vitro reconstituted 30 nm chromatin fiber present a left-handed double helix structure revealed by Cryo EM single particle method.

On the other hand, Cryo EM studies of sectioned nuclei argued that the 30-nm chromatin fibers are not existed (Eltsov et al. 2008) (Eltsov et al., 2008). Another study using small angle x-ray scattering to exam the chromatin fiber in nuclei also suggest that RNase treated nuclei does not contain the 30-nm fiber. The observed 30-nm fiber might be rRNA complexes. Thus, it is concluded that the organization of the genome based on 10 nm chromatin fibers is sufficient to describe the complexities of nuclear organization and gene regulation (Maeshima et al., 2014).

While there is a hot debate on the existence of the 30 nm chromatin fibers, the higher order chromatin structure beyond 30 nm chromatin fiber is generally unknown. And it is too easy to conclude that the native chromatin fiber is not uniform. Several experimental attempts using electron microscopy including atomic force microscopy and cryo electron tomography have been used to visualize these structures. Atomic force microscopy allows the direct three-dimensional visualization of chromatin fiber in solution. Results reveal that the fiber retained a zigzag organization. However, the *in vitro* reconstituted short chromatin fibers can’t represent native chromatin fibers in nuclei. Due to the low contrast of chromatin compared to its surrounding nuclear content, which has similar molecule mass as chromatin, it is difficult differentiate chromatin from others in the cryo sectioned nuclei.

1.1.4 Native Chromatin Extraction

Due to the low contrast of chromatin inside the nucleus in Cryo EM, it is better to extract chromatin in its native state and determine its structure in near-native state by Cryo

electron tomography. However, native chromatin extraction is hard to achieve using the conventional method. Conventionally, the extracted chromatin is of fragment and suitable for chromatin immuno-precipitation related assay, but can't be used for chromatin structure determination since the higher order structure of chromatin is disrupted.

We applied the concept of solid-phase reversible immobilization (SPRI), the non-specific binding between magnetic nanoparticles (MNPs) and polymer-like macromolecules, for native chromatin extraction. We first applied the SPRI method to extract DNA using salicylic acid coated magnetic nanoparticles, and further explored for native chromatin extraction. Chromatin from bulk cell populations was magnetically isolated from cell lysates without any further filtration or high-speed centrifugation, which would introduce shear forces on chromatin, causing damage. Unlike chemically cross-linked chromatin, the extracted native chromatin is suitable of single-nucleosome-level resolution and avoids nonspecific modification signals from different nucleosomes carried over through protein-protein interaction. The process for DNA/chromatin extraction is shown as following:

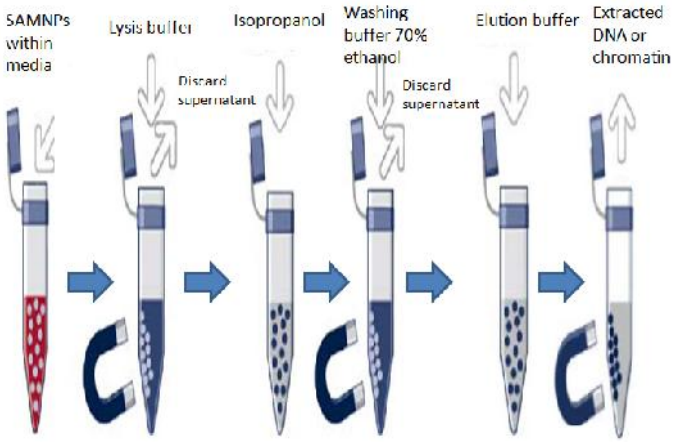

Figure 1.2 Solid phase reversible immobilization for DNA/native chromatin extraction based on magnetic nanoparticles.

1.1.5 Chromatin Associated RNAs (CARs)

High-throughput transcriptomic analyses have revealed more the 90% of human genome is transcripted. A small portion of these transcripts code for proteins, the others are non-coding RNAs (ncRNAs). ncRNAs are classified as snoRNAs, microRNAs, siRNAs, snRNAs, exRNAs, and piRNAs and the long ncRNAs, for example Xist and HOTAIR. Only a limit number of ncRNAs have been assigned biological functions. These ncRNAs inside nucleus have been found to affect local chromatin conformation and gene expression in diverse biological processes. Recent findings suggest that they are an integral component of the chromatin and that they involve in heterochromatin formation by organization the heterochromatic components, such as HP1 and repressive histone marks.

1.1.6 Extraction of CARs

Purification of CARs is extremely important for down-stream applications such as transcriptomic analyses. Conventionally, CARs are typically isolated from soluble chromatin, which is collected from different fractions in a sucrose gradient for overnight centrifugation after soluble chromatin has been released from the isolated nuclei by MNase digestion. The total assay time, including nuclei preparation, chromatin purification and RNA isolation, is about 16 h. Unfortunately, the RNAs isolated from soluble chromatin-containing fractions often do not fully represent the true CARs population, since RNAs also associate with insoluble heterochromatin fragments. For example, repetitive RNAs can form more complex and less soluble structures with heterochromatin. Moreover, when compared to mRNA, the half life of CARs varies over a wide range with some less than 2 h. Although the sequences of CARs extracted by

conventional methods can be systematically identified at the global level using high-throughput genomic platforms, these approached often exhibit some bias due to the fact that some RNAs are resistant to extraction and some RNAs are degraded during the long handling process. Thus, developing an ultrafast and unbiased method for the extraction of CARs is essential to ensure the accuracy of transcriptomic analyses.

1.1.7 Epigenetic Code and Its Determination

Epigenetic regulation is essential for normal development and maintenance of tissue-specific gene expression patterns in mammals. There are two levels of epigenetic regulation in cells: one constitutes the DNA modifications containing methylation and hydroxymethylation on the 5th carbon of cytosine (5mC and 5hmC, respectively) among others, another is the posttranslational histone modifications including methylation, acetylation, phosphorylation, ADP-ribosylation and ubiquitination. Global epigenetic modifications in some cases have been considered as the hallmark of leukemogenesis and in general can be used to assess the state of health of cells in blood. A simple test to detect and quantify epigenetic biomarkers on DNA and histones from cells in whole blood can be valuable for screening and prognosis purposes.

Leucocytes present in hemocytes with a ratio less than 1% and are the one of the only cell types containing chromatin in blood. In patients with leukemia, these cells are immature and do not function properly. Enrichment of leucocytes from whole blood is a required first step of diagnosis. The conventional density gradient centrifugation method for enriching leucocytes is labor and time consuming (30 min) and the commercialized kits using anti-human leukocyte coated particles are not robust (due to fragility of bioactivity of the antibodies) and expensive for routine analysis ($18 per reaction). Conventional

chromatin-preparation methods involving precipitation and centrifugation cannot adapt to the micro total analysis systems ("μTAS" or called "lab-on-a-chip"). We reported a chromatin extraction method from cultured mammalian cells using salicylic acid coated magnetic nanoparticles. However, this approach still required enrichment of cells with centrifugation, not ideal for lab-on-a-chip analysis. Here, we developed a rapid and reliable protocol to prepare chromatin from whole blood using carboxyl-functionalized magnetic nanoparticles, which can be used to enrich leucocytes and further to nonspecifically adsorb chromatin from the enriched cells. The magnetic separation protocol demonstrated in this effort based on the one-pot method could be easily used for constructing a lab-on-a-chip system for clinical screening.

Based on the novel chromatin extraction method from cells in blood, we further developed a biotin-streptavidin mediated enzyme-based immunosorbent assay (two-step EIA) to simultaneously detect epigenetic marks on DNA and histone proteins in a 96-well plate format using our enhanced immunoassay platform. Compared to conventional methods, which requires separate sample preparation steps to detect DNA modifications or histone modifications, our approach is fast, cheap and robust. By coupling cell separation, chromatin purification and epigenetic mark quantification, we demonstrate a facile approach where the whole operation can be accomplished within 8 hours, which otherwise would take 2-3 days.

1.2 Significance of This Work

A serial of studies have been performed on chromatin related research. Based on SPRI, we developed a native chromatin extraction method. The epigenetic code contained inside the chromatin has been analyzed by enhance EIA method; The CARs, one of the important composites of chromatin, have been purified and characterized by qPCR, which are ready for tanscriptomic analysis; The branching chromatin structure has been discovered by cryogenic electron microscopy.

CHAPTER 2. GENOMIC DNA EXTRACTION BY SOLID PHASE REVERSIABLE ADSORPTION

2.1 Introduction

In recent years, using magnetic micro/nano-materials for the separation of biomolecules has attracted significant interest because of the wide range of practical applications in biomedicine and biology. Magnetic nanoparticles (MNPs) have been used as solid supports to enrich cells, cell organelles and biomolecules, including nucleic acids, proteins and xenobiotics, directly from chemical or biological suspensions (Šafařík and Šafaříková, 1999; Sarkar and Irudayaraj, 2008). The use of MNPs provide a number of advantages over other conventional techniques specifically in biological separations and extraction (Šafařík and Šafaříková, 1999). Traditional separation techniques used in molecular biology, biochemistry, and chemistry rely on centrifugation and/or filtration. Although these define the standards in various applications and processes, neither of them is amenable to automation or rapid and often times require intense mechanical forces for separation. Magnetic separation techniques have the potential to be fast and selective and does not require elaborate protocols, expensive equipment or filtration devices (Šafařík and Šafaříková, 1999).

Magnetic separation and purification of cells and nucleic acids offer various benefits over conventional methods, especially in its ease of use and the possibility of an environmentally friendly extraction process (does not require a high volume of toxic chemicals) at ambient temperature conditions. Molecular biology approaches, such as PCR amplification and restriction digestion, require high-molecular-weight DNA. Compared with centrifugation and filtration based techniques that exert shearing forces on the DNA, magnetic separation exerts only a magnetic drag, which is nondestructive and nonintrusive on the biomolecules. In this procedure, the MNPs are added to a solution or suspension containing the target. The target is by means of specifically or non-specifically adsorbed onto the MNPs surface, and then, the formed MNPs-target complexes are recovered from the suspension using an appropriate external magnetic separator. Due to the superparamagnetism of MNPs, using MNPs instead of magnetic microparticles has advantage that we can prepare suspensions that are stable against sedimentation in the absence of an applied magnetic field (Akbarzadeh et al., 2012). In addition, the larger volume-to-surface ratio enable MNPs enrich more targets compared to magnetic macroparticles.

Today, DNA based assays are the most common research methods in molecular biology and are fundamental to life science research. Separation assays based on MNPs can provide DNA with improved quality for use in enzymatic digestion, polymerase chain reaction, detection of epigenetic marks, and sequencing (Křížová et al., 2005; Prodělalová et al., 2004; Saiyed et al., 2007; Shan et al., 2010a; Shan et al., 2012a), because the method is simple and is almost free of toxic chemicals(Shan et al., 2012a) or force-based separation protocols as in centrifugation. However, the steps involved in the

preparation of functionalized and monodispersed MNPs and the cost of using commercialized magnetic separation kits hinder routine application of this facile technology for biochemical or clinical screening.

Salicylic acid (SA) is a chemical ligand with a carboxylic and a phenolic functional site, commonly used as the modifier in chelating resins and has shown to possess excellent sorption properties (Shishehbore et al., 2011; Zhou et al., 2013a). It has also been used to coat MNPs and for solid phase extraction and concentrating of some heavy metal ions from various impure samples (Shishehbore et al., 2011; Unal et al., 2010). However, the application of salicylic acid coated magnetic nanoparticles (SAMNPs) as a solid phase, for genomic DNA (gDNA) separation has not been reported. Herein we report on a modified, easy and reliable technique to synthesize SAMNPs, and demonstrate its utility as a robust one-stop gDNA extraction process from crude cell culture media. The quality and quantity of SAMNPs purified gDNA were confirmed by agarose gel electrophoresis and PCR amplification.

2.2 Synthesis and Characterization of SAMNPs

Water dispersible SAMNPs were prepared via a one-step wet chemical strategy, modified from a previous method by Unal et al. (Unal et al., 2010). Briefly, a solution of a mixture of NaOH and SA was added to a sterilized three necked-bottle until the pH was raised to ~11 under vigorous stirring with Ar gas, followed by the addition of an aqueous solution comprising of a mixture of Fe (III) and Fe (II) salts with a molar ratio of 2Fe (III): 1Fe (II): 4SA until the formation of a black suspension. After refluxing at 90 °C for 4 h, a

dark brown suspension was noted. Using sodium hydroxide instead of ammonium hydroxide is effective in controlling liquid flooding. Moreover, the prepared SAMNPs by this method were much smaller than previous reported ones. The smaller size makes the SAMNPs have higher surface-to-volume ratio. The final product (Fig.2.1A) was separated from the aqueous solution by magnetic separation and further washed with pure water until a neutral pH was reached. The SAMNPs were then dispersed in pure water at a concentration of 10 mg/ml. Fig.2.1A shows a representative TEM image of ~10 nm SAMNPs dispersed in water.

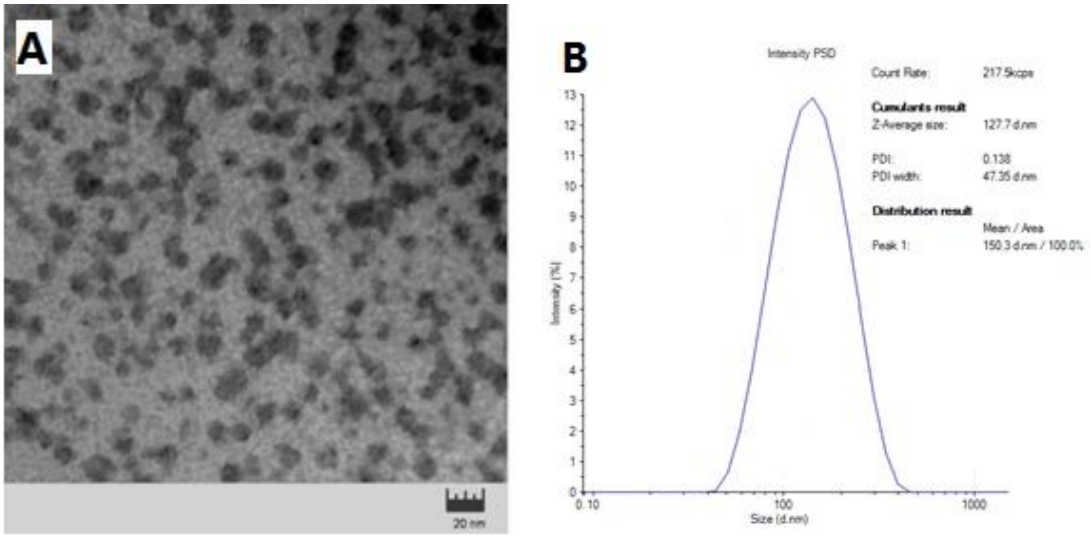

Figure.2.1 (A) Transmission electron microscopy (TEM) image of SAMNPs. The scale bar represents 20 nm; (B) Dynamic light scattering curves of the dispersion of SAMNPs in pure water.

Dynamic light scattering analysis of the same samples revealed that the synthesized SAMNPs were highly monodispersed and had a hydrodynamic diameter of ~122.7 nm (Wan et al., 2007). Zeta potential analysis confirmed that the zeta potential –was 38.1 mV in water, data not shown. Samples with zeta potentials between -30mV and +30mV

typically tend to aggregate, because higher level of zeta potential results in greater electro-static repulsion between the particles, minimizing aggregation(Liu and Liu, 2010). According to Unal et al, the chemisorptions of SA onto Fe_3O_4 nanoparticles via the carboxylic acid oxygens, which are symmetrically bonded to the Fe_3O_4 nanoparticle surface, allows these particles easily dispersible in water due to exposed OH group. The ability to have nanocomposite materials which are easily dispersible in water is a highly desirable feature and implies that water soluble nanoparticle suspensions at physiological pH could be useful in a wide range of biomedical applications and treatments, whereas other forms of MNPs currently are not. The high surface-to-volume ratio of the even distributed SAMNPs and monodispersed property render them higher possibility to interact with their potential targets like suspended cells and DNA, compared to their counterparts.

2.3 Genomic DNA extraction by SAMNPs

Genomic DNA (gDNA) purification from crude HeLa cell culture media was performed as follows. HeLa cells were grown in DMEM supplemented with 10% FBS, 2 mM glutamine, 100 U/ml penicillin and 10 μg/ml streptomycin, in a 5% CO_2 incubator at 37 °C. When the cells were ~80% confluent, 1 ml trypsin was added to suspend the adhered cells at 37 °C for 3 min, and the trypsin digestion ceased with additional culture media. Cell concentration was determined with a hemocytometer as ~$5x10^5$ cells/ml. Without specific metion, the subsequent experiment was using the same concentration of cells. The cells were then transferred to a 1.5 ml tube containing 10 μl of SAMNPs. The

mixture was incubated at room temperature for 5 min to form cell-nanoparticle complexes, which were then immobilized to a magnetic separation stand following by aspiration of the supernatant and then discarded. Immobilized cells were lysed by adding 50 µl of lysis buffer (3M NaI; 5 M urea; 40 g/l Triton X-100; 10 nM EDTA, 25 nM Tris-HCl, pH 6.5) prior to incubation at room temperature for 5 min. 50 µl of isopropanol, which facilitates binding of the released DNA to the SAMNPs, was added to the suspension (and incubated for 3 min at room temperature). After magnetic separation of the DNA-nanoparticle complexes, the supernatant was discarded, and the immobilized DNA was rinsed once with 100 µl of cold 70% ethanol solution. After removal and evaporation of ethanol, the DNA was eluted in 20 µl TE buffer (10 mM EDTA, 25 Mm Tris-HCl, pH 8.0) at room temperature for 10 min. RNase digestion was performed if necessary. The SAMNPs were then immobilized with the supernatant transferred to a DNase/RNase free EP tube for further analysis. We also compared our results with traditional phenol-chloroform extraction (Liu and Harada, 2001; Shan et al., 2012a). Each experiment was repeated in triplicate.

TEM was used to characterize the cells captured by SAMNPs, with images obtained with a CM-100 instrument operating at 80 kV, as shown in Fig.2.2. The cell-SAMNPs complexes were fixed by 2% Glutaraldehyde in 0.1M cacodylate buffer and further fixed with 2% OsO4 in 0.1M cacodylate buffer. Then the complexes were washed and embedded in 1.5% agarose. After spinning down cell/agarose pellet, the gel was cooled and removed from tube with 10% ethanol, samples were diced and dehydrated. The complexes were further dehydrated in ethanol series and embedded in Epon. Thin sections of 80 nm thicknesses were cut and placeed on 200 mesh copper grids and then grids were stained 5

min with 2% UA in 70% MEOH, and 3 min in Lead Citrate. Compared to our previous study which used carboxyl coated MNPs to extract urine DNA(Shan et al., 2012a), the yield of cell collection by SAMNPs was higher since many more cells were present in the cell culture media compared to that in urine. The ratio of immobilized cells comparing to that in the media was determined by a hemocytometer as 68%. Fig.2.2 clearly shows that SAMNPs were attached to the surface of HeLa cells; some were even trapped in the cell membrane, allowing the magnetically labeled nucleated cells in the media to be easily recovered with an external magnet (SuperMag Multitube Separator™). It should be noted that the SAMNPs were randomly deposited on the surface of mammalian cells, in a manner similar to that observed with the carboxyl coated nanoparticles, indicating the non-specific nature of their interaction. The high yield of cells harvested by SAMNPs is expected to ensure a high yield of gDNA extracted from the samples.

During the initial lysis process, the SAMNPs attached to the cell surface need not be removed because the SAMNP-cell complexes can be directly lysed. For DNA extraction, the same MNPs were used. An equal volume of isopropanol was added to form DNA/nanoparticle complexes. As both the enrichment of mammalian cells and the adsorption of gDNA can be realized with the same nanoparticles, many residual impurities and enzyme inhibitors present in the cell culture media or cell lysate can be easily removed. Because of the non-specific interaction of DNA and SAMNPs, there is a possibility of proteins being bound to SAMNPs contributing to a possible loss of purity of the DNA. However, agarose gel electrophoresis confirmed that negligible proteins were observed in the final eluted DNA samples in TE buffer, as show in Fig.2.3A. The OD_{260}/OD_{280} ratio was 1.83, which also is indicative of the high purity of the extracted

gDNA. gDNA extracted by the traditional phenol extraction process displayed similar electrophoretic pattern of DNA fragments, but with lower yields, which is in agreement with previous study(Basu et al., 2013).

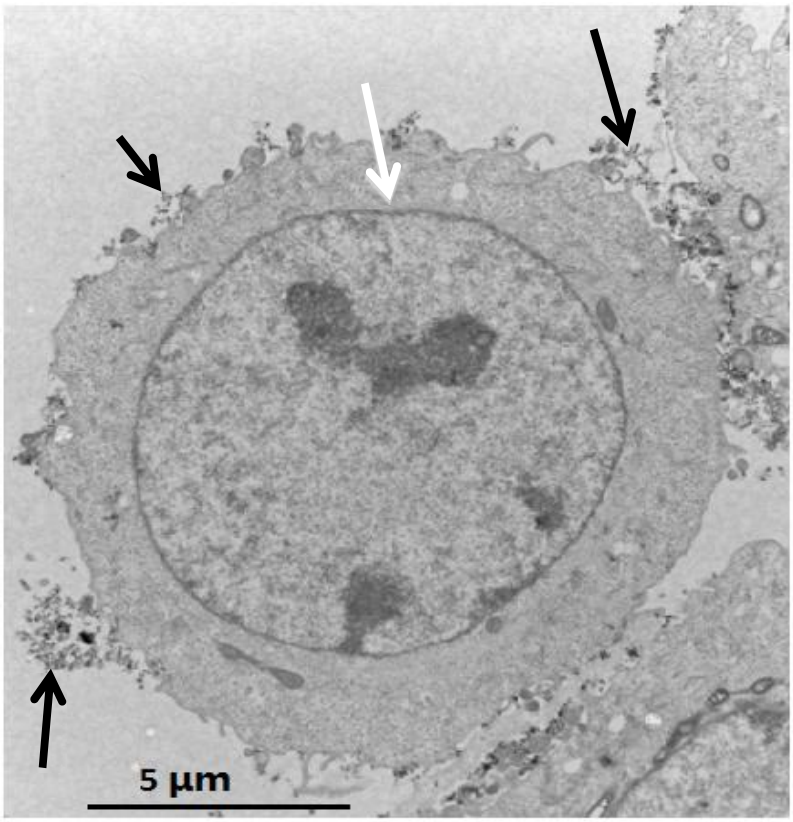

Figure. 2.2 Transmission electron microscopy (TEM) image of mammalian cells captured with SAMNPs. The scale bar represents 5 µm. Note that a few aggregates of SAMNP (indicated by black arrows) are visible at the surface of cells. The mammalian nucleus was indicated by white arrow.

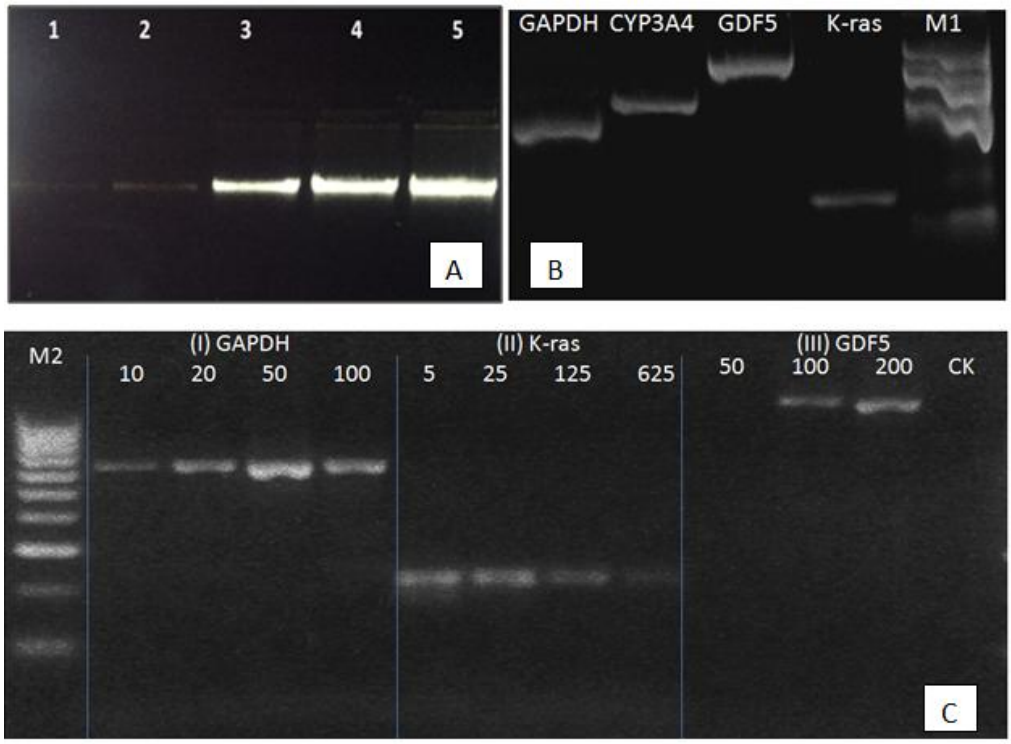

Figure.2.3 (A) Agarose gel electrophoresis of mammalian genomic DNA (gDNA). Lane 1, 2, 3 and 4: gDNA extracted by SAMNPs from 10, 20, 50 and 100 µl of culture media of mammalian cells (~$5x10^5$ cells/ml), respectively. Lane 5: gDNA extracted by traditional phenol-chloroform method from 1 ml of culture media from mammalian cells. (B) Agarose gel electrophoresis of PCR products obtained after amplification of gDNA extracted from 50 µl of cell suspension. (C) Agarose gel electrophoresis of PCR products. (I) GAPDH gene with a size of ~556 bps as amplified by PCR with 1 µl of DNA templates extracted from 10, 20, 50 100 µl of culture media with mammalian cells. (II) K-ras gene with a size of ~214 bps was amplified by PCR with 1 µl of 5, 25, 125, and 625 times diluted DNA from 100 µl of culture media with mammalian cells. (III) GDF5 gene with size 1106 bp was amplified by directly using purified cells by magnetic separation. The cells were from 50, 100 and 200 µl of culture media, respectively. All the negative controls show a lack of binding to the gel image.

2.4 PCR Reaction

The quality of extracted gDNA was determined by PCR amplification of four fragments (Table 2.1) with different sizes derived from genes possibly located at different chromatins using a Bio-Rad MyCycler Thermal Cycle (Bio-Rad Laboratories, Hercules,

CA). Amplification reactions were carried out in a final volume of 25 µl containing 12.5 µl 2 x PCR master mix, 1 µl of extracted DNA template, 1 µl of each of the PCR primers and pure water. Amplification profile for all of the four genes was the same: 95 °C for 5 min, followed by 34 cycles 60s at 94 °C, 30s at 53°C, 60s at 72 °C, and a final extension performed at 72 °C for 5 min. The final amplicons (5 µl) were loaded onto a 2.5% agarose gel in TBE buffer for electrophoresis, with bands visualized under ultraviolet light by RGB staining.

PCR was performed on K-ras, GAPDH, CYP3A4 and GDF5 genes with amplicon sizes ranging from 214-1106 bps, as shown in the agarose gel image (Fig.2.3B). The PCR reactions show excellent agreement, verifying the high quality of DNA extracted by the present method. All the negative controls show no binding on the gel image. All of the PCR templates contained 1 µl of gDNA extracted from 50 µl of HeLa cell suspensions and eluted in 20 µl of TE buffer. To further investigate the sensitivity of the gDNA preparation method, a 556-bp DNA sequence of GAPDH gene was amplified using different sample volumes (10, 20, 50 and 100 µl) tested by PCR, as shown in Fig.2.3C (I). As expected, the intensities of PCR bands became stronger with increased sample volume (from 10 to 50 µl). The high extraction performance can be attributed to the high binding affinity of SAMNPs to mammalian cells. Our results strongly suggest that the method developed is suitable for small-scale and PCR-ready mammalian gDNA extraction. Another set of PCR reaction was also performed using 1 µl of 5, 25, 125, and 625 times diluted gDNA extracted from 100 µl suspension. As expected, the intensities of PCR bands became weaker and weaker as the dilutions increased (from 5 to 625).

Table 2.1 Gene location, PCR primers and predicted sizes of amplified products.

Gene name	Primers (5' →3')	Location	Product size
K-ras	Forward: GTACACATGAAGCCATCGTATA	chr12(p12.1)	214 bp
	Reverse: CCACTTGTACTAGTATGCCTTAAG		
GAPDH	Forward: ACCACAGTCCATGCCATCAC	Chr12(p13.31)	556 bp
	Reverse: TCCACCACCCTGTTGCTGTA		
CYP3A4	Forward: AACAGGGGTGGAAACACAAT	chr7(q21.1)	592 bp
	Reverse: CTTTCCTGCCCTGCACAG		
GDF5	Forward: GGTGAGGTTGCAGGGAAT	Chr20(q11.2)	1106 bp
	Reverse: CAGGGGAATTGTGGATAA		

A noteworthy feature of our work is that the MNP approach developed can further simplify the process of direct DNA template preparation for PCR because of enrichment of the cell population by MNP targeting and separation. DNA template from 100 and 200 µl of media was obtained and the PCR amplification was successful for GDF5 gene with an amplicon size of ~1106 bp (Fig.2.3C). The negative control did not have any DNA template. An important point to note is that the nanoparticles attached on the cell membrane did not induce any adverse effect on the PCR amplification [14]. Further, the entire process can be completed within 7 min, a highly desirable feature for quick and simple PCR-based screening.

In conclusion, SAMNPs proved to be a superior solid phase carrier for gDNA purification. Compared to other functional MNPs used as solid phase carriers for DNA extraction, the preparation of SAMNPs was easy and did not require complex surface coating steps. Our method embraces a green chemistry approach because we attempt to

reduce or eliminate the use or generation of hazardous/toxic chemicals. The synthesized SAMNPs nonspecifically bind to the mammalian cells and further binds to the released gDNA. The entire procedure required less than 30 min without any lag in the process, and the extraction could be accomplished in one tube. Thus the developed method can be termed as “one-tube, one-stop genomic DNA extraction” that does not require elaborate sample handling or use hazardous reagents such as phenol or chloroform.

CHAPTER 3. NATIVE CHROMATIN EXTRACTION AND CHARACTERIZATION

3.1 Introduction

In order for the genomic DNA to fit inside the nucleus of a eukaryotic cell, the double DNA strands must fold into a compacted form by winding around proteins called histones, thereby forming an intricate complex material known as chromatin. Chromatin not only serves as a vector to package DNA within the nucleus, but also acts as a regulator to control a diverse range of biological processes including transcription and replication, by altering the accessibility of the DNA to regulatory factors (Saha et al., 2006). Chromatin status directly affects cell development and disease processes. Indeed chromatin is fundamental to nuclear function and is of significant interest both in elucidating fundamental biological processes and in advancing applied research for the development of disease biomarkers and the identification of new therapeutic targets. Eukaryotes use different levels of chromatin structure to influence nuclear processes. Interphase chromosomes occupy distinct chromosome territories (CTs), and the location of CTs is nonrandom and cell phenotype dependent (Cremer and Cremer, 2010; Takizawa et al., 2008). Generally, gene-rich chromosomes are positioned near the nucleus center, where active genes are generally located, and gene-poor chromosomes sit near the

nuclear periphery, a region associated with heterochromatin and gene silencing (Ragoczy et al., 2006). For example, the inactive X chromosome in female mammalian cell translocates to the periphery after interacting with *Xist* (Rego et al., 2008). Large-scale chromatin interactions recovered by chromatin conformation capture (3C) technology, including interactions between chromosomes, play important roles in gene regulation, recombination and other nuclear processes. In addition, chromatin is organized in functional compartments, such as transcription factories and repair centers. Chromatin structure is also altered by the chemical modification of histone proteins and DNA, by histone variants and histone champions, by remodeling of nucleosomes, and by non-coding RNAs and non-histone DNA binding proteins(Bartke et al., 2010; Cedar and Bergman, 2009; Glozak et al., 2005).

The classical view of chromatin organization is that the lowest organizational unit is the repeated nucleosome, consisting of two copies of the core histones H2A, H2B, H3, and H4, linked by histone H1, to form an obvious 10-nm, “bead-on-a-string” structure when viewed with an electron microscope (EM) (Woodcock et al., 1976a). The secondary structure is the so called “30-nm fiber”, which is formed by helically twisted strings of linked nucleosomes. This fiber is commonly thought to be folded into higher order chromatin loops, although the topological organization of this higher order structure in the nucleus remains unclear. However, new experimental approaches including chromatin conformation capture (3C) and cryo-electron microscopy, call into question the *in situ* evidence for the 30 nm chromatin fiber(Adomas and Wade, 2013; Fussner et al., 2011a; Horowitz-Scherer and Woodcock, 2006; Luger et al., 2012; van Steensel, 2011; Woodcock and Dimitrov, 2001).

Chromatin, containing both DNA and chromatin associated proteins (including histones and non-histone proteins), is a fundamental substrate for biological research. While DNA extraction and the purification of chromatin associated proteins were extensively studied(Bhorjee and Pederson, 1976; Zhang et al., 2013; Zhang et al., 2012), the chromatin extraction methods have not advanced significantly since the 1970s(Bhorjee and Pederson, 1973; Harlow and Wells, 1975; Kornberg et al., 1989; Monahan and Hall, 1975; Pederson, 1977). Based on our previous extensive studies on DNA extraction, we applied the concept of solid-phase reversible immobilization, the non-specific binding between magnetic nanoparticles (MNPs) and polymer-like macromolecules, to chromatin extraction. In this study, chromatin from bulk cell populations was magnetically isolated from cell lysates without any further filtration or high-speed centrifugation, which would introduce shear forces on chromatin, causing damage. Unlike chemically cross-linked chromatin, the extracted native chromatin is suitable of single-nucleosome-level resolution and avoids nonspecific modification signals from different nucleosomes carried over through protein-protein interaction (Cuddapah et al., 2009). The extracted chromatin is suitable for further analysis such as identification of chromatin associated proteins (ChAPs) by mass spectroscopy to uncover disease biomarkers, nucleosome position analysis using human chromatin, patterns of histone modifications and DNA modification as well as higher order chromatin structures.

3.2 Material and Methods

3.2.1 Cell Sample Preparation

Non-neoplastic S1 HMT-3522 human mammary epithelial cells (HMEC), between passages 56 and 60, were plated at 2.3 X 10^4 cells/cm^2 for propagation as monolayers on plastic in chemically defined H14 medium (Abad et al., 2007). When the cells were approximately 80% confluent after maintaining for 7-10 days, they were harvested by treatment with trypsin and diluted in 10 ml DMEM/F12 medium (Invitrogen, 11965-118). 180 µl of soybean trypsin inhibitor (SBTI) was added to stop the trypsin (0.05%) digestion. The cell concentration was adjusted to approximately 1.0×10^6 cells/ml.

3.2.2 Preparation of SAMNPs

Water-dispersible salicylic acid coated magnetic nanoparticles (SAMNPs) were synthesized by our previously reported method, as modified from Unal and coworkers(Unal et al., 2010; Zhou et al., 2013b) Briefly, a 2:1:4 molar ratio of Fe (III): Fe (II): SA (salicylic acid) was added to a sterilized three-neck bottle containing NaOH solution (pH 11.0) with vigorous stirring with Ar gas. After refluxing at 90 ^oC for 4 h, a dark brown suspension was formed. The magnetic nanoparticles in the suspension were collected by magnetic separation and further washed to neutral pH with distilled water. The SAMNPs were dispersed in distilled water at a concentration of 10 mg/ml.

3.2.3 Native Chromatin Extraction by SAMNPs

Chromatin was purified from mammalian cells as follows. Typically, ~ 10^6 cells were collected in an Eppendorf tube by centrifugation (1000g, 5 min), then lysed by the addition of 100-µl lysis buffer (250 mM SDS, 1 mM EDTA, 0.5 mM EGTA, 1 mM

PMSF and 2% Protease Inhibitor Cocktail (New England Biolabs)). The cell pellet was pipetted up and down slowly 20 times with a 200-µl pipette tip. After incubation for 10 min, 8-10 µl SAMNPs were added to form a chromatin-SAMNP complex. 100 µl of isopropanol was added to the suspension for 10 min at room temperature (RT) to facilitate the formation of chromatin-SAMNPs complexes. After magnetic separation of the chromatin-SAMNP complex, the supernatant was discarded and the immobilized chromatin was rinsed once with 200 µl of ice cold 70% ethanol. After removal and evaporation of ethanol, the chromatin was eluted in 50-100 µl of 1X phosphate buffered saline buffer (PBS) at RT for at least 1h. A further magnetic separation step was performed to obtain the released chromatin in the supernatant. The purified chromatin was then used for Western blotting (WB) and imaging analysis.

3.2.4 Western Blotting Analysis

Table 4.1 Antibody information for fluorescence immunostaining and Western blotting analysis.

Antibody	Company	Catalog NO.	Dilution times/application
H4	abcam	ab10158	500/WB
H3K9me3	abcam	ab8898	500/WB
Lamin B	abcam	ab16048	1000/WB
H3	abcam	ab1791	1000/IF
Goat-anti rabbit-Alexa 647	Life technologies	A-21245	1000/IF

The extracted chromatin was mixed with a 6X loading buffer (0.375M Tris pH 6.8, 12% SDS, 60% glycerol, 0.6M DTT, 0.06% bromophenol blue) and incubated at 37 ^{o}C for 20 min, then separated by electrophoresis through SDS-PAGE gels (crosslinking indicated in figure legends) and transferred to polyvinylidene fluoride membranes. The membranes were blocked with 5% milk to minimize non-specific antibody binding and then probed with specific primary antibodies histone 4, histone H3 trimethyl Lys27 (H3K27me3), nuclear matrix protein Lamin B and nuclear mitotic apparatus protein (NuMA). Table 4.1 contains detailed antibody information. All antibodies were diluted in the blocking buffer and incubated overnight at 4^{o}C in a wet chamber. The corresponding HRP-conjugated secondary antibodies were incubated with membranes at RT for 45 min. The membrane was developed in ECL buffer. Protein bands were visualized immediately after development using Western Lightning Plus-Enhanced Chemiluminescence Substrate (Perkin Elmer Life & Analytical Science).

3.2.5 Confocal Microscopy Analysis

50 µl of extracted chromatin was incubated with rabbit anti-human Histone 3 antibody at RT for 30 min, and washed 2 times with 1X PBS, then Alexa 647 conjugated goat-anti-rabbit IgG and Hoechst 34580 were added and incubated further for 45 min. The pellet was collected by centrifugation and washed 3 times with 1X PBS. The final product was dissolved in PBS and mounted on a glass cover slip. Directed staining by Hoechst 34580 was also performed in a similar manner. Fluorescence of Hoechst 34580 (excitation 405 nm, emission 461 nm) and Alexa 647 (excitation 650 nm, emission 668 nm) were detected using an inverted Zeiss LSM 710 (Carl Zeiss Microscopy Ltd, Cambridge, U.K.)

system and confocal images were collected using Zeiss LSM software (Carl Zeiss Microscopy Ltd, Cambridge, U.K.).

3.2.6 Atomic Force Microscopy (AFM) Imaging

A drop of 5 µl chromatin solution was spotted onto a freshly cleaved mica surface (Ted Pella, Inc.) and incubated for 10s to allow chromatin to absorb onto the substrate. The sample drop was then washed off with 30 µl 2 mM magnesium acetate solution, and dried with compressed air. Chromatin samples were imaged in air in the tapping mode on a Multimode AFM with Nanoscope IIIa controller (Veeco) using oxide-sharpened silicon probes with a resonance frequency in the range of 280-340 kHz (MikroMasch-NSC15). The tip-surface interaction was minimized by optimizing the scan set-point to the highest possible value. AFM imaging was performed at 25 °C. The images in TIFF format were prepared by NanoScope Analysis software.

3.2.7 Transmission Electron Microscopy (TEM) Imaging

A 10 µl drop of purified chromatin was placed on a copper grid coated with carbon. After 30 s the grid was air dried and then negatively stained with 1% uranyl acetate for 2 min. The grid was then air dried and viewed in a Tecnai T20 microscope which is a 200KV transmission electron microscope with LaB6 filament.

3.3 Results

3.3.1 Western Blotting Analysis of ChAPs

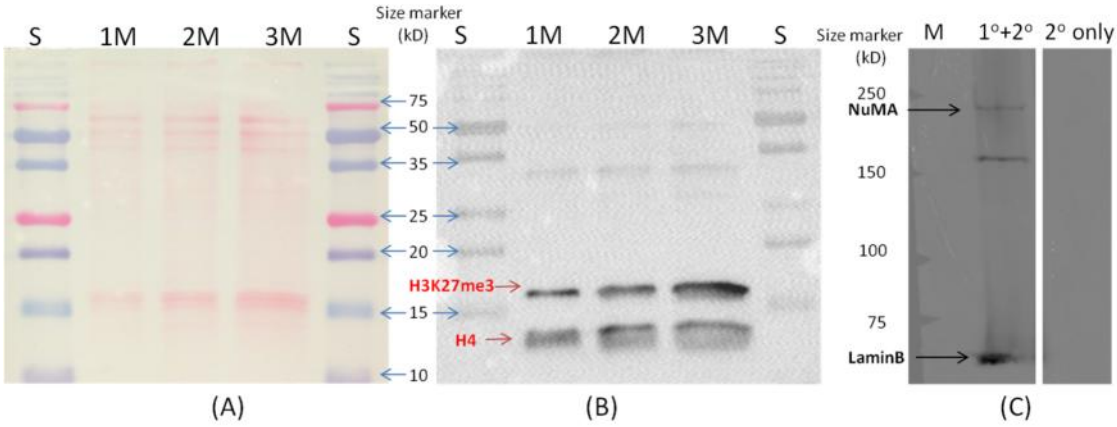

Figure 3.1 Western blotting of ChAPs. Chromatin extracted from different amounts of cells (~ 1, 2 and 3 M， M= million, respectively), and loaded on a 15% SDS-PAGE, transferred to membrane and further stained by Ponceau S solution (A), blocked, and then incubated with H3K27me3 and H4 antibodies. The membrane was developed two times to obtain the two bands (B). Chromatin from ~ 1 M cells were extracted, and loaded on a 5% SDS-PAGE, and incubated with NuMA and Lamin B antibodies. The band could only be detected with both the primary (1^o) and the corresponding secondary (2^o) antibodies. The negative control (2^o only) did not show the presence of any bands (C).

Western blotting was used to examine ChAPs, both the histone proteins and non-histone proteins. The protein bands corresponding to Histone 3 modification (H3K27me3, 15.3 kD) and histone 4 (H4, 11.3 kD) can be clearly noted in Fig.3.1(B). Two other non-histone proteins, nuclear mitotic apparatus protein (NuMA, 240kD) and nuclear matrix protein Lamin B (66kD), were also detected as shown in Fig.3.1(C). We were not able to detect splicing regulator SC35 by WB (data not shown), consistent with recent reports that this protein is absent in ChAP preparation(Zhang et al., 2012). To investigate the sensitivity of the chromatin preparation method, chromatin was extracted from different

numbers of cells (1, 2 and 3 million), and as expected, the intensity of H3K27me3 and H4 became stronger and stronger (Fig.3.1(B)). We also examined the ChAPs by SDS-PAGE, stained by coomassie blue, and presented in the Fig.3.2.

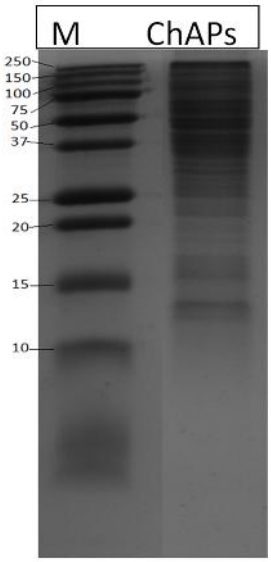

Figure 3.2 15% SDS-PAGE of ChAPs, stained by coomassie blue.

3.3.2 Immunofluorescence Staining of Extracted Chromatin

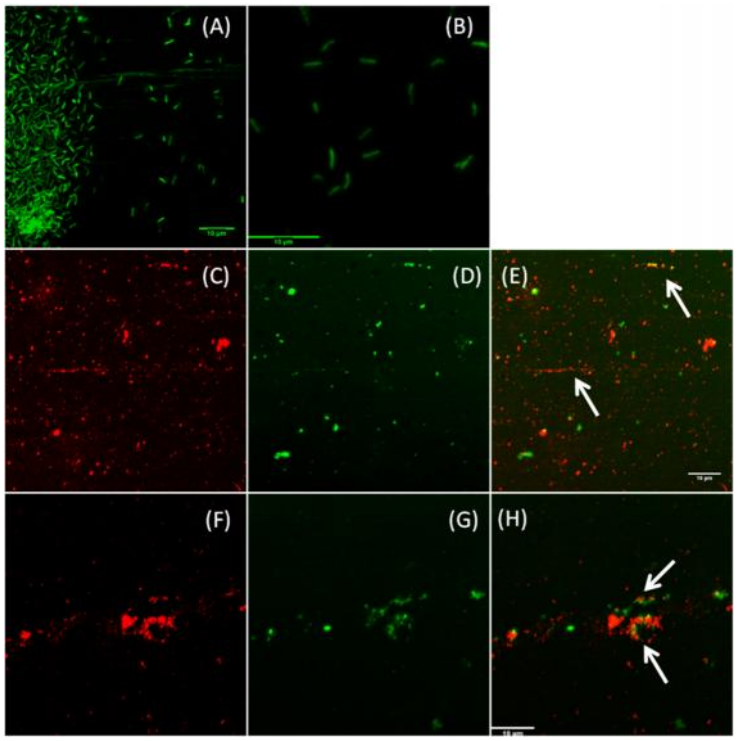

Figure 3.3 Hoechst 34580 stained chromatin visualized by confocal microscopy (A, B). Double staining of extracted chromatin (C~H). H3 was stained with Alexa 647 (red, C and F), and DNA was stained by Hoechst 34580 (green, D and G) for immunofluorescence experiments. ImageJ was used to obtain the merged images (E and H). The white arrows indicated the stained chromatin. Scale, 10 μm.

The extracted chromatin was stained with Hoechst 34580, a blue fluorescent dye specific for nucleic acids, and analyzed by confocal microscopy, as shown in Fig.3.3.The yield of chromatin was observed to be very high as noted in Fig.3.3A. Because of the relatively low resolution of light microscopy, most of the extracted chromatin appears rod-like, and its detailed structure could not be observed. Double staining studies were also performed on the extracted chromatin. Samples were stained first with Alexa 647-labeled anti-rabbit secondary antibody, and then with Hoechst 34580, and examined by confocal microscopy, as showed in Fig.3.3 (C~H).

3.3.3 Chromatin Fine Structures by AFM

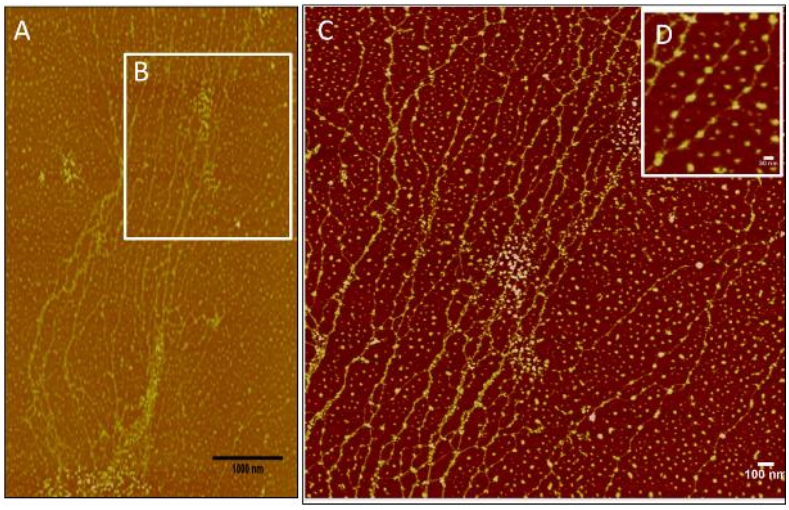

Figure 3. 4. AFM images of extracted chromatin. Images were obtained in air at ambient humidity. Large scale scanning was performed (A), chromatin fiber at different levels (from 10 ~ 300 nm) was observed. A detailed part of (B) (the white square) was rescanned in (C), the typical 10 nm, “bead-on-a-string” structure was clearly observed, and these fibers crosslink to one another to form larger fibers (about 20 nm). An enlarged part of C was given in D, and a replication fork-like structure was observed. Single nucleosome could be clearly observed. Scale bar are provided in the lower right of each figure by ImageJ.

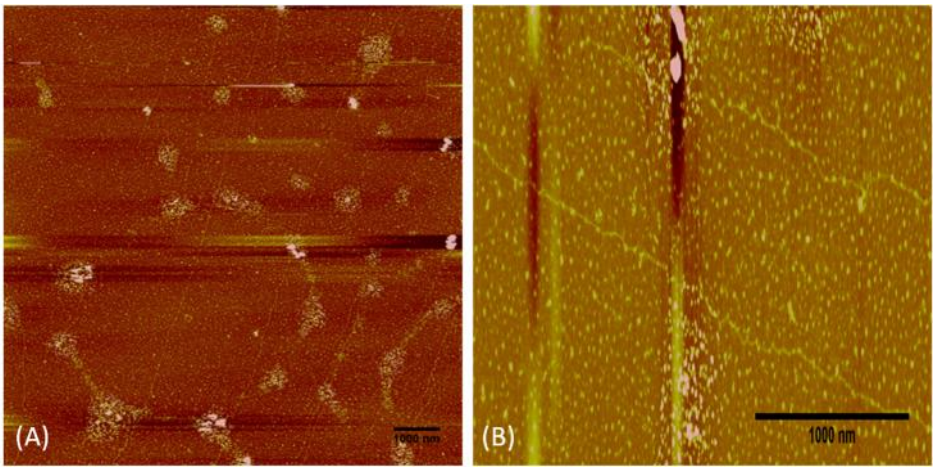

Figure 3.5 Long and single chromatin fibers (about 10 μm) is shown in (A), and a detailed structure in (B). Scale bar are provided in the lower right of each figure by ImageJ.

Since the first demonstration by Robert Feulgen which shows that the interphase chromatin and mitotic chromosomes contain DNA in 1914, many scientists have studied the chromatin structure, which is essential for the accurate transmission of genetic and epigenetic information to the daughter cells. Though metaphase chromosomes are easily observed by light microscopy, it is hard to obtain the fine structure of chromatin during interphase or metaphase. To observe higher-order structures of chromatin, past work has focused on TEM and AFM studies. Scanning probe microscopy, especially AFM, has significant advantages in obtaining nucleosome-level resolution in an aqueous environment. Thus in AFM experiments chromatin can remain unstained and hydrated; images are obtained in air at ambient humidity. Chromatin fibers at different levels (from 10 nm to 300 nm) were observed in Fig.3.4A, Single nucleosome resolution of chromatin is shown in Fig.3.4C. Interestingly, a clear bead-on-a-string structure was visible (Fig.3.4D). Long 10-nm fibers were also observed, Fig.3.5.

3.3.4 Higher Order Chromatin Structure by TEM

Fig. 3.6 shows TEM micrographs of the extracted chromatin at different resolutions. The chromatin was stained with uranyl acetate, and as expected, heterochromatin was observed at the compact regions of chromatin denoted by red arrows. Most of the extracted chromatin was highly condensed, which is consistent with our confocal microscopy data. The complex structure of chromatin makes it hard to measure the length of whole chromatin (scale bar is provided). Interestingly, in some micrographs (Fig.3.6 A~D), the terminal end of chromatin was heavily protected by the formation of a T shaped structure. This may help to explain how cells keep chromatin from fusing. Some fine chromatin structure was also observed (Fig.3.6 G~I).

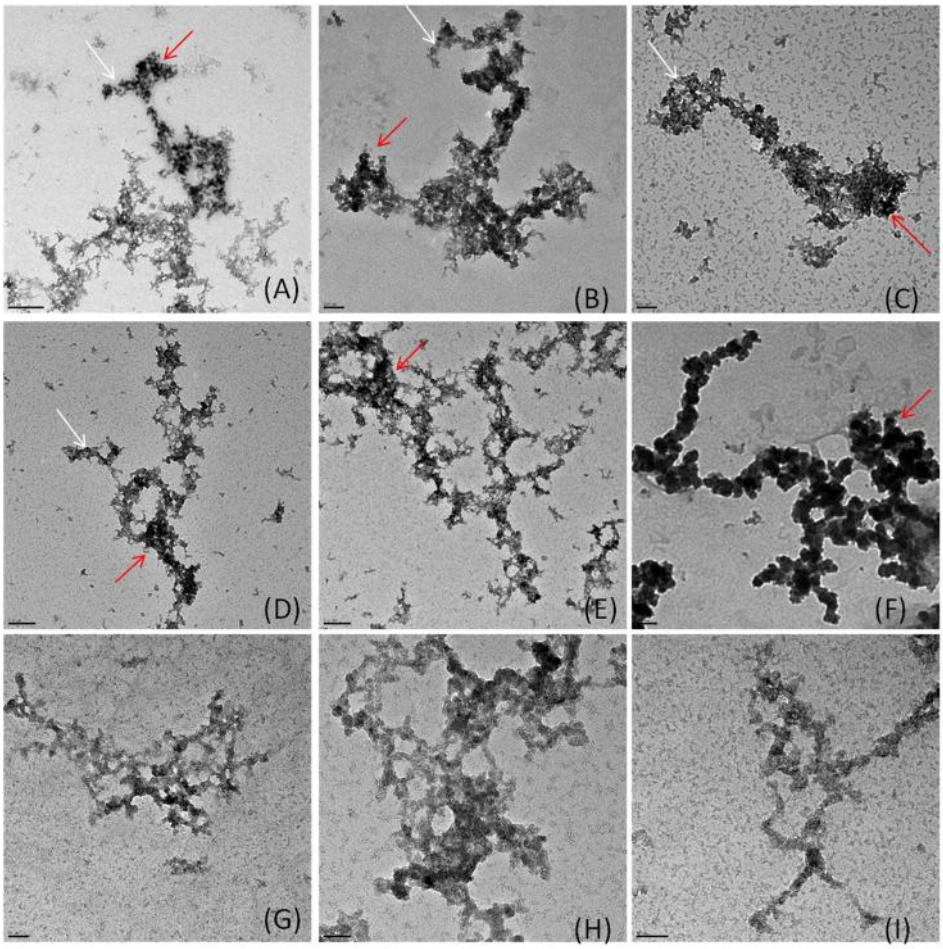

Figure 3.6 TEM image of extracted chromatin. The white arrows indicated a T shape structure, which may help to explain how cells keep chromatin from fusing. The red arrows indicated heterochroamtin at compact regions of chromatin. The scale bars from A to I were 500 nm, 100 nm, 100 nm, 200 nm, 200 nm, 100 nm, 50 nm, 50 nm and 50 nm, respectively.

3.4 Discussion

3.4.1 Advances of SPRI Approach for Native Chromatin Extraction

Magnetic nanoparticles are being used in both fundamental and applied biological research to facilitate mechanical separation and as contrast agents. These applications are made possible by the fact that most biological systems do not have a naturally occurring magnetic

component. This feature is useful when magnetic nanoparticles (MNPs) are applied as solid phase carriers to form MNPs-molecule complexes. These complexes can be selectively controlled and detected with high specificity and low background noise (Beveridge et al., 2011). We have previously applied the negatively charged MNPs for DNA extraction and purification (Zhou et al., 2013b). Long polymer-like macromolecules such as DNA tend to non-specifically wrap around nanoparticles and co-aggregate with the assistance of chaotropic agents like PEG/NaCl or isopropanol. These nanoparticles reversibly release long polymer-like macromolecules in the presence of low salt solution. For example, DNA-MNPs complexes disassociate from each other in TE buffer (pH 8.0). This is the basis for the solid-phase reversible immobilization (SPRI) introduced by Hawkins and coworkers (DeAngelis et al., 1995; Hawkins et al., 1994). In a similar manner, we extract chromatin from cell lysates using salicylic acid coated magnetic nanoparticles (SAMNPs). A similar approach has successfully been used for mammalian DNA extraction (Zhou et al., 2013b). We selected isopropanol instead of PEG/NaCl due to the high viscosity of the chromatin lysates. The high concentration of PEG would increase the viscosity of the solution and prolong the magnetic separation process.

There is no doubt that chromatin conformation is greatly influenced by the ionic milieu, yet the nuclei levels of cations and polyamines are not known with certainty (Bednar et al., 1995; Bednar et al., 1998; Carruthers et al., 1998; Woodcock and Dimitrov, 2001). In order to mimic the physiological condition and to reduce the structural variation of chromatin extracted from different cell samples, we eluted chromatin from SAMNPs using the 1X PBS buffer (137 mM NaCl, 2.7 mM KCl, 10 mM Na_2HPO_4 and 2 mM KH_2PO_4, pH 7.4). Because of the high ionic strength of PBS, the elution process was prolonged. Normally, it

takes ~15 min (at RT) to elute pure DNA from SAMNPs in TE, however it takes at least 1 h to obtain a similar concentration of chromatin in 1X PBS. Overnight elution at 4^{o}C is strongly recommended to obtain a highly concentrated chromatin solution. Even with elution for several days, it is still hard to obtain a 100% disassociation of chromatin from SAMNPs. When large amount of chromatin are needed, it is more efficient to elute two or three times. Another possible way to reduce the compaction of chromatin is to use a 50% isopropanol solution with 300 mM NaCl, 10 mM $MgCl_2$ and 25 mM EDTA (Murphy et al., 1999). However, in order to avoid introduction of artifacts on the extracted chromatin, this was not seen as a viable option.

When using SAMNPs for chromatin extraction, the released chromatin in the lysate should be soluble; otherwise it will precipitate before attaching on to the magnetic nanoparticle surface giving rise to an impure product. Thus, the concentration of SDS in the lysis buffer (at 250 mM, 7.2% m/v, or higher concentration) should be carefully chosen (Zhang et al., 2013; Zhang et al., 2012). Excessive SDS could lead to dissociation of ChAPs and DNA. Previous studies have shown that more than 1500 groups of nucleic acid associated proteins are extracted and identified from a million cells by mass spectroscopy (Zhang et al., 2012). Chromatin was also extracted with 500 µl of 0.72% SDS lysing buffer, and no significant differences were detected with regard to the thickness of the chromatin fiber compared to the one extracted with 50 µL of 7.2% SDS (noted in the Fig.3.7).

Another advantage of the present method is that cells were free of covalent crosslinking by formaldehyde or glutaraldehyde fixation. Though these aldehyde-based fixatives enable strong crosslinking and fixation of proteins, they may give rise to possible artifacts such as the destruction of epitopes for antibody staining and changed protein

conformation (Jiang et al., 2007; Zhang et al., 2012). Compared to cross-linked chromatin, the extracted chromatin was native, which provides single-nucleosome-level resolution and avoids non-specific modification signals from different nucleosomes carried over through protein-protein interaction (Cuddapah et al., 2009). Since the extracted native chromatin contains both ChAPs and DNA, the extracted chromatin with the associated proteins can be used for the global analysis of ChAPs to assess the pattern of histone and DNA modifications by mass spectroscopy.

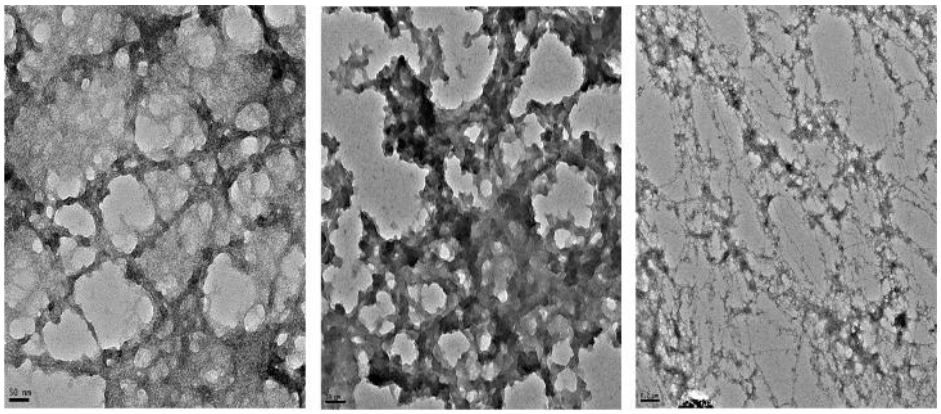

Figure 3.7 (A) chromatin extracted by 50 µl of 7.2% SDS; (B) chromatin extracted by 500 µl of 0.72% SDS; (C) DNA extracted by 50 µl of lysing buffer according to Zhou et al.

3.4.2 Chromatin Identification by WB and Confocal Fluorescence Microscopy

The successful identification of histones with the right size by WB confirmed that histone proteins exist in the extracted chromatin. The identification of H3K27me3 in the extracted chromatin implied that this specific epitope of modified histone was not masked by the high concentration of SDS. Failure to identify SC35, an internal negative control, implied that the extracted chromatin is free of other nuclear impurities or cellular impurities, such as nuclear membrane.

Due to the diffraction limit, with the resolution of confocal fluorescence microscopy being approximately 200~400 nm, it is impossible to observe the finer structure of chromatin, i.e., the 10 nm fiber, “bead-on-a-string” structure using this method. Only the larger fibers (hundreds nanometers) or highly condensed metaphase chromosomes could be observed. Thus, with high probability, the chromatin observed in this study is the heterochromatin form, a tightly packed form of DNA in the whole chromatin. We also observed the extracted chromatin by dark-field microscopy (Fig.3.8) because of its innate scattering signals. Though we could not obtain the finer structure of chromatin, we confirmed that both histones and DNA are present in the extracted chromatin by imaging. The absorption spectra of extracted chromatin and DNA are also provided (Fig.3.9).

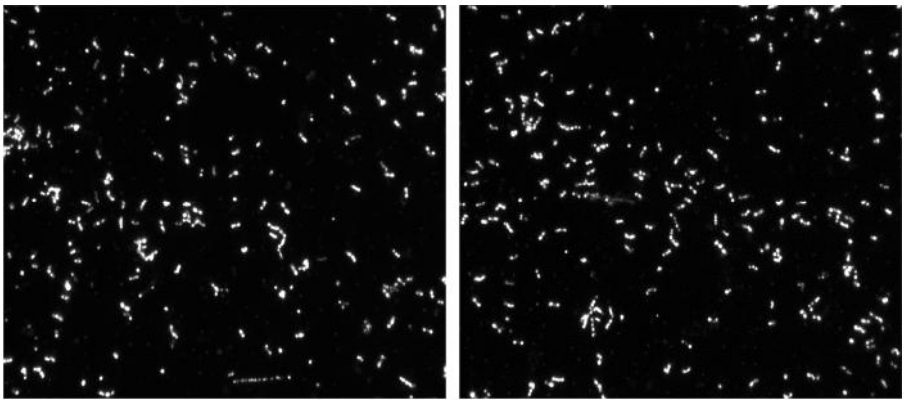

Figure 3.8 Chromatin observed by dark-field microscopy.

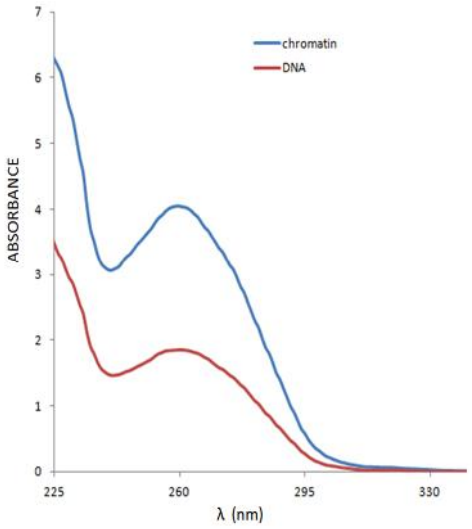

Figure 3.9 The absorption spectra of extracted chromatin and corresponding DNA. The DNA was prepared from chromatin by phenol/Chloroform extraction.

3.4.3 Nucleosomes at Replication Fork

DNA replication is a semiconservative process of producing two identical copies from one original DNA molecule, which occurs in all living organisms. In eukaryotic cells, in order to maintain identity within cell lineages, the epigenome as well as the genome needs to be faithfully replicated in each cell cycle, including DNA modifications, histone modifications and nucleosome positioning. After nascent DNA strands form behind the replication fork, they are rapidly reorganized into nucleosomes. The ‘old’ parental histones in coordination with the assembly of the newly synthesized histones are transferred to form histone octamers on the nascent DNA strands (Lucchini et al., 2001), which also are known as parental histone segregation and replication-dependent *de novo* nucleosome assembly, respectively (Groth et al., 2007). It is not yet known how these two processes are coordinated to preserve genetic stability in terms of nucleosome position. We addressed this issue through images of the replication fork. Each replication

fork is delimited by two bifurcations on the chromatin stand, producing a “bubble-like” configuration (McKnight and Miller Jr, 1977), as shown in Fig.3.10. Each strand of the replication fork was around 10 nm, which is the lowest level of chromatin fiber. From these images, it is easy to note that the nucleosomes are not evenly distributed on the two nascent strands on the replication fork. It indicates that parent H3-H4 tetramers are not equally split into H3-H4 dimers to the two nascent strands. Further studies are necessary to address this question.

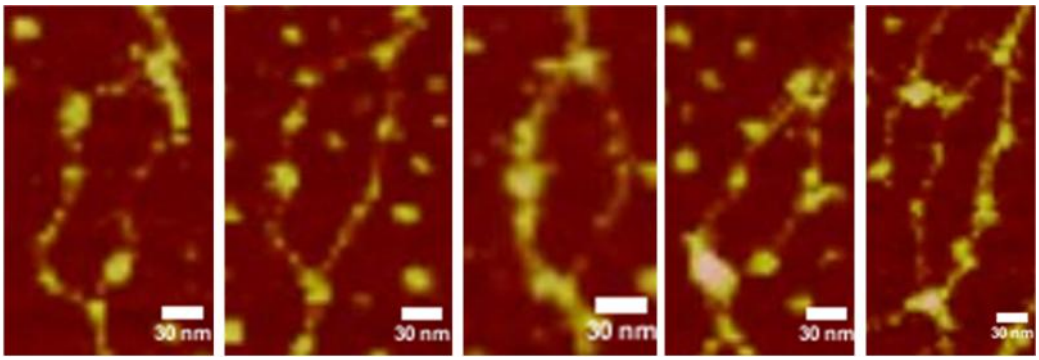

Figure 3.10 Non-evenly distributed nucleosomes on the two nascent DNA strands.

3.4.4 Reducing the Resolution Gap by AFM

Numerous studies have been reported on chromatin structure, either from the nuclear cross sections which provide general but blurred chromatin images or from the extracted chromatins examined by electron microscopy which provides a clear bead-on-a-string structure. However, a challenge is on how to integrate the two types of information (Cardoso et al., 2012; Horowitz-Scherer and Woodcock, 2006). Cryo sections of vitrified nuclei could provide intermediately resolved images that reduce the gap between the molecular and cellular scales. However, the high level of non-chromatin components (salts and small organic molecules) in the nucleus with the almost same electron

scattering power of chromatin can lead to very low resolution contrast images in which neither individual nucleosomes nor arrays of nucleosome can be recognized (Horowitz-Scherer and Woodcock, 2006). Thus, it is much more practical to focus on imaging and biophysical characterization of purified chromatin.

Combining our novel chromatin extraction method with AFM characterization provides a new means to view the interphase chromatin, as shown in Fig.3.4A~D. The images present different levels of chromatin fiber from 11 nm (Fig.3.4D) to 500 nm (Fig.3.4A). Fig. 4.4A clearly shows how the 11-nm fiber is organized into higher order chromatin from 20~62 nm. These 62-nm fibers would further assemble into 300-nm fiber and even 500-nm fiber. It is only reasonable to discuss whether the 30-nm fiber exists in the interphase chromatin in this context. We measured the diameter of these chromatin fibers, and found that the 11-nm fiber may occasionally assemble into ~ 30-nm fiber; however, the 30-nm fiber may not be a necessary condition to form higher order chromatin structures such as the 300-nm fiber. Only short fiber segments of chromatin with a mean diameter of about 30 nm could be found in the images. This is also consistent with the data obtained from TEM images. Thus, we first used the large-scale interphase chromatin imaging method to confirm that the 30-nm chromatin fiber may not always be necessary to form higher order chromatin structures.

3.4.5 Additional Structures and Characteristics

Chromatin conformation capture (3C) assays and related technologies have been used to identify long distance chromatin interaction, e.g. enhancer and promoter interaction. However, it is difficult to apply these data to paint the whole genome. As shown in Fig.3.4A and 4,4B, even in one single chromatin, several chromatin fibers exist and

interact with one another. Two novel structures were shown in Fig.3.11. In each image, two nucleosomes indicated by the black arrows, may be merging the two separate DNA strands together. This type of structure is not likely derived from the replication fork, and their function is still unknown.

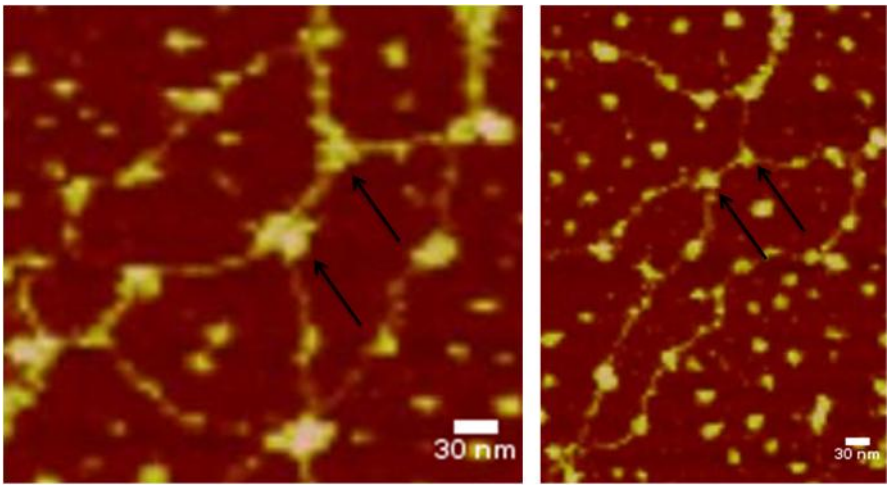

Figure 3.11 Complex chromatin structures. The black arrow indicates the nucleosome and/or ChAPs which merge the two separate DNA strands together.

Another noteworthy aspect of these studies is that the complicated chromatin network could shed light on the DNA repair process. It has been estimated that every cell could experience up to 10^5 spontaneous DNA lesions per day (Ciccia and Elledge, 2010). These lesions would block the progression of replication. Double-strand breaks in chromatin can be lethal if not repaired. And, if not repaired correctly, they can cause deletions, translocation, and fusions in the DNA. In order to avoid these problems and accelerate the replication process, single chromatin fibers crosslinking together to form a complex network would facilitate the repairing machinery to find the two ends of the broken chromatin.

The conventional protocols for embedding biological samples for electron microscopy involve extensive processing such as crosslinking, oxidation and solvent extraction. These processes can limit the extent of useful information obtained because of the poor quality of the specimen. Purified chromatin was directly imaged by TEM after simple negative staining. The rotary shadowing method is commonly used for observing the bead-on-a-string structure; however, since we have obtained this fine structure via AFM, we would like to observe the higher order chromatin structure. Images showed that the chromatin structure was preserved at the largest extent and we could observe the chromatin fiber at different levels from 10~800 nm. These TEM images (Fig.3.6) provides a better understanding of chromatin organized inside the compacted nucleus, which could not be seen by section (Woodcock and Ghosh, 2010).

CHAPTER 4. CROSS-PLATFORM DETECTION OF EPIGENETIC MODIFICATIONS FROM EXTRACTED CHROMATIN IN LEUCOCYTES FROM BLOOD

4.1 Introduction

Epigenetic regulation is essential for normal development and maintenance of tissue-specific gene expression patterns in mammals (Sharma et al., 2010). There are two levels of epigenetic regulation in cells: one constitutes the DNA modifications containing methylation and hydroxymethylation on the 5^{th} carbon of cytosine (5mC and 5hmC, respectively) among others, another is the posttranslational histone modifications including methylation, acetylation, phosphorylation, ADP-ribosylation and ubiquitination (Conway O' Brien et al., 2014). Global epigenetic modifications in some cases have been considered as the hallmark of leukemogenesis (Conway O' Brien et al., 2014; Greenblatt and Nimer, 2014; Gutierrez and Romero-Oliva, 2013; Voso et al., 2010) and in general can be used to assess the state of health of cells in blood. A simple test to detect and quantify epigenetic biomarkers on DNA and histones from cells in whole blood can be valuable for screening and prognosis purposes.

Leucocytes present in hemocytes with a ratio less than 1% and are the only cell type containing chromatin in blood (Xie et al., 2007). In patients with leukemia, these cells are immature and do not function properly. Enrichment of leucocytes from whole blood is a

required first step of diagnosis. The conventional density gradient centrifugation method for enriching leucocytes is labor and time consuming (30 min) (Chambers et al., 1983) and the commercialized kits using anti-human leukocyte coated particles are not robust (due to fragility of bioactivity of the antibodies) and expensive for routine analysis ($18 per reaction). Conventional chromatin-preparation methods involving precipitation and centrifugation cannot adapt to the micro total analysis systems ("μTAS" or called "lab-on-a-chip") (Bhorjee and Pederson, 1973; Harlow and Wells, 1975; Kornberg et al., 1989; Monahan and Hall, 1975; Pederson, 1977; Woodcock et al., 1976b; Xie et al., 2007). We reported a chromatin extraction method from cultured mammalian cells using salicylic acid coated magnetic nanoparticles (Zhou and Irudayaraj, 2015a). However, this approach still required enrichment of cells with centrifugation, not ideal for lab-on-a-chip analysis. Here, we developed a rapid and reliable protocol to prepare chromatin from whole blood using carboxyl-functionalized magnetic nanoparticles, which can be used to enrich leucocytes and further to nonspecifically adsorb chromatin from the enriched cells. The magnetic separation protocol demonstrated in this effort based on the one-pot method could be easily used for constructing a lab-on-a-chip system for clinical screening (Xie et al., 2007).

Based on the novel chromatin extraction method from cells in blood, we further developed a biotin-streptavidin mediated enzyme-based immunosorbent assay (two-step EIA) to simultaneously detect epigenetic marks on DNA and histone proteins in a 96-well plate format using our enhanced immunoassay platform. Compared to conventional methods, which requires separate sample preparation steps to detect DNA modifications or histone modifications, our approach is fast, cheap and robust. By coupling cell

separation, chromatin purification and epigenetic mark quantification, we demonstrate a facile approach where the whole operation can be accomplished within 8 hours, which otherwise would take 2-3 days.

4.2 Material and Methods

4.2.1 Materials and Chemicals

Carboxyl-functionalized magnetic nanoparticles (10 mg/ml) were synthesized according to previous reports (Shan et al., 2010b). Clinical blood samples were collected from 9 healthy donors (4 males and 5 females) and stored in -80 ^{o}C until further use. All studies were approved by Institutional Review Boards (IRB) protocols at their respective institutions. Informed consent forms were obtained from all subjects. Non-neoplastic S1 HMT-3522 human mammary epithelial cells (S1 cells) were cultured according to standard protocols. The S1 cells were treated with conjugated linoleic acid (CLA) and ethanol (as a control) to influence the histone modification profile.

DNA coating solution, succinimidyl-6-[biotinamido]-6-hexanamidohexanoate (NHS-LC-LC biotin), succinimidyl 4-(N-maleimidomethyl)cyclohexane-1-carboxy-(6-amidocaproate) (LC-SMCC), succinimidyl 6-[3(2-pyridyldithio) propionamido] hexanoate (LC-SPDP), dithiothreitol (DTT), horseradish peroxidase (HRP), Sephadex G-15, Mouse anti-rabbit IgG antibody were purchased from Pierce (Rockford, IL). Casein, Tween 20, tetramethylbenzidine (TMB), sodium dodecyl sulfate (SDS), phenylmethylsulfonyl fluoride (PMSF), ethylenediaminetetraacetic acid disodium salt (EDTA) and glutaraldehyde were obtained from Sigma (St. Louis, MO). Rabbit anti-

5hmC antibody was supplied by Active Motif (Carlsbad, CA). Streptavidin was purchased from Prozyme (Hayward, CA). 2% Protease Inhibitor cocktail was purchased from New England Biolabs.

4.2.2 Chromatin Extraction from Frozen Blood Samples

Chromatin was purified from frozen blood as follows. Typically, 0.3 - 1 ml of thawed blood sample was placed in 1.5 ml sterilized eppendorf tubes containing 10 µl carboxyl-functionalized magnetic nanoparticles (10 mg/ml). After gentle mixing, the blood samples and magnetic nanoparticles were incubated in room temperature for 10 min to allow the formation of leucocyte-magnetic nanoparticle complexes. These complexes are collected by magnetic separation (SuperMag Multitube Separator^{TM}, Ocean NanoTech, San Diego), and the red supernatant was discarded and the immobilized leucocytes were rinsed with PBS 1X 3 times.

In order to exam the complexes by TEM, one aliquot of the cell-MNPs complexes were fixed by 2% Glutaraldehyde in 0.1M cacodylate buffer and further fixed with 2% OsO4 in 0.1M cacodylate buffer. Then the complexes were washed and embedded in 1.5% agarose. After spinning down cell/agarose pellet, the gel was cooled and removed from tube with 10% ethanol, samples were diced and dehydrated. The complexes were further dehydrated in ethanol series and embedded in Epon. Thin sections of 80 nm thicknesses were cut and placeed on 200 mesh copper grids and then grids were stained 5 min with 2% UA in 70% MEOH, and 3 min in Lead Citrate.

The other aliquot of complexes were then lysed by the addition of 50 - 80 µl of lysis buffer (250 mM SDS, 1 mM EDTA, 0.5 mM EGTA, 1 mM PMSF and 2% Protease Inhibitor cocktail), by pipetting up and down slowly 20 times to denature and rupture the

cell/nuclear membrane and incubated for another 10 min. Cooled isopropanol (the same amount as the lysis buffer) was added to the lysates and incubated for 5 min. The chromatin-magnetic nanoparticle complexes were collected again via magnetic separation; the supernatant was discarded and the complex was rinsed once with 200 µl of cooled 70% ethanol. After the removal and evaporation of ethanol, chromatin was eluted in 50 µl of PBS 1X at room temperature for at least 1h. A further magnetic separation step was performed to collect the released chromatin in the supernatant. The concentration of purified chromatin was determined at OD_{260} and stored at -20ºC until further use.

4.2.3 Two-step Enzyme-linked Immunosorbent Assay

200 ng of purified chromatin was added to a polystyrene microwell plate followed by mixing with 50 µl DNA coating solution and 50 µl glutaraldehyde (1%) at room temperature for 2 h with gentle agitation. After washing with distilled water (DIW) three times, the residual surface was blocked with 0.5% (w/v) casein in PBS at 37 ºC for 1 hour. Subsequent incubation with the primary antibody (0.5 µg/ml, 100 µl), diluted in PBS 1X containing 0.5% casein and 0.1% Tween 20 was performed for 1 hour at 37 ºC to target relevant epigenetic modifications (5mC, 5hmC, H4 and H3K9me2). After washing, biotinylated secondary antibodies specific to each primary antibody (0.5 µg/ml, 100 µl) was added and incubated for 1 hour at 37 ºC. Finally, streptavidin conjugated to HRP (0.25 µg/ml, 100 µl) was added and incubated for 1 hour at 37 ºC. For signal generation, 200 µl of the colorimetric substrate mixture (1000: 10: 1 volume ratio of the following: 50 mM sodium acetate buffer, pH 5.1; 1% (w/v) tetramethylbenzidine; 3% (v/v) H_2O_2) was added to the microwell plate and kept at room temperature for 15

minutes followed by the addition of 50 µl of 2 M sulfuric acid to halt the reaction. The optical intensity was finally measured at 450 nm with the VersamaxTM absorbance microplate reader (Molecular Device; Sunnyvale, CA). Conventional EIA was performed under the same conditions by using secondary antibodies labeled with HRP instead of using biotinylated secondary antibody and streptavidin-HRP conjugate. A two-step EIA using DNA as substrate instead of chromatin was also performed for validation to assess whether chromatin extracted by our method could be used as a substrate to detect epigenetic modifications on DNA (Chowdhury et al., 2014).

4.2.4 Western Blotting Analysis

The extracted chromatin was mixed with a 6X loading buffer (0.375 M Tris pH 6.8, 12% SDS, 60% glycerol, 0.6 M DTT, 0.06% bromophenol blue) and incubated at 37 °C for 20 min, then separated by electrophoresis through SDS-PAGE gels (crosslinking indicated in figure legends) and transferred on to polyvinylidene fluoride membranes. The membrane was blocked with 5% milk to minimize non-specific antibody binding and then probed with specific primary antibodies. All antibodies were diluted in the blocking buffer and incubated overnight at 4 °C in a wet chamber. The corresponding HRP-conjugated secondary antibodies were incubated with membranes at room temperature for 45 min. Protein bands were visualized immediately after development using Western Lightning Plus-Enhanced Chemiluminescence Substrate (Perkin Elmer Life & Analytical Science). Images were further quantified by ImageJ software.

4.3 Results and Discussion

4.3.1 Isolation of Chromatin Using Bifunctionalized Magnetic Nanoparticles

Functionalized super paramagnetic nanoparticles, where magnetization exists only when an external magnetic field is applied have been extensively used in bio-separation studies (Herr et al., 2006; Kouassi and Irudayaraj, 2006; Lago-Cachón et al., 2014; Ravindranath et al., 2011). For example, in the proposed chromatin immunoprecipitation assay, magnetic nanoparticles was used to capture DNA fragments that wrap histone proteins (associated with specific histone posttranslational modifications) when they are functionalized with the corresponding histone antibodies. These particles can also be used for cell collection and DNA preparation through nonspecific binding (Huang et al., 2010; Zhou et al., 2013b). Here, we first used bi-functional magnetic nanoparticles (MNPs) to simplify the process of chromatin extraction from leucocytes in whole blood to realize the development of lab-on-chip devices where chromatin can be used as substrate.

The carboxyl-functionalized MNPs bind to the leucocytes' cell membrane without specific interaction (shown in Fig.4.1) and the leucocytes were nonspecifically isolated from whole blood by magnetic separation. The MNPs randomly deposit on the cell surfaces rather than targeting specific cell surface markers, indicating the non-specific nature of their interaction (Shan et al., 2012b). Some reports also show that carboxyl-functionalized MNPs can nonspecifically enrich cells from different sources such as blood, saliva, urine and bacterial culture (Shan et al., 2010b; Shan et al., 2012b; Xie et al., 2004a; Xie et al., 2004b). Contaminants such as erythrocytes, carbohydrates, lipids and proteins, were left in the supernatant and removed. Further, washing with PBS 1X was

done to remove contaminants to a large extent. Thus, the MNPs demonstrate their ability to enrich leucocytes from whole blood via an easy, fast and reliable process.

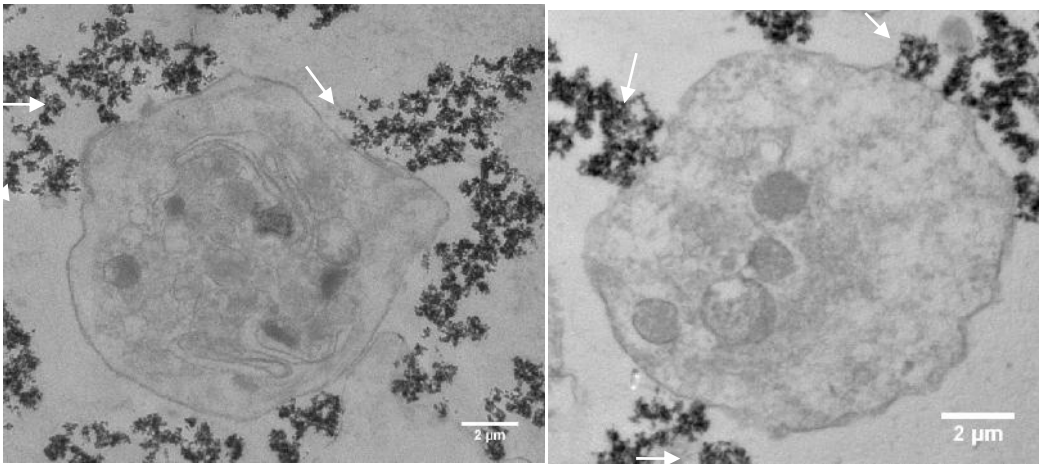

Figure 4.1 Transmission electron microscopy (TEM) images. Leucocytes captured by carboxyl-functionalized magnetic nanoparticles. A few clusters of nanoparticles are visible on the surface of cells (indicated by white arrow).

Besides enrichment of leucocytes, the carboxyl-functionalized MNPs can also be used to isolate the corresponding chromatin released from these cells and hence play a dual role. During chromatin extraction, it is not necessary to remove the nanoparticle-cell complexes since these can be directly lysed in the same tube. After cell lysis, the released chromatin was adsorbed onto the MNP surface with the help of isopropyl alcohol. This step will induce chromatin molecules to transition from an elongated coil conformation to a compacted spherical form. The polycations in solution would mediate the electrostatic interaction between carboxyl coated MNPs and the available phosphate groups on DNA, resulting in chromatin attachment onto the MNP surface (Shan et al.; Zhou and Irudayaraj, 2015a). The attached chromatin could then be eluted from the nanoparticles

with PBS 1X (50 µl). Thus, the enrichment of leucocytes and the adsorption of chromatin can be integrated and the whole extraction can be completed in a single tube.

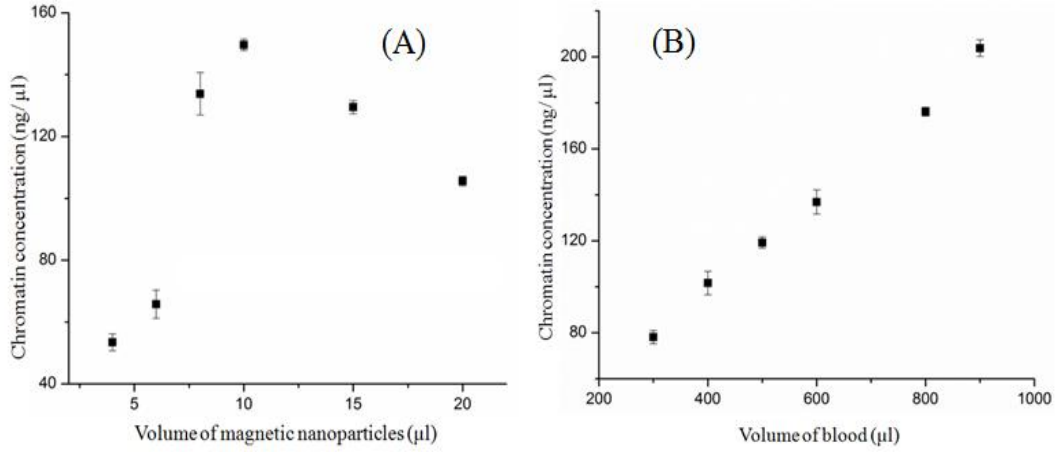

Figure 4.2 Chromatin extraction efficiency. (A) Chromatin extracted from 400 µl of blood with 4-20 µl of MNPs. (B) Chromatin extracted from 300-900 µl of blood with 10 µl of MNPs. All of the chromatin was eluted into 50 µl of PBS 1X.

To determine the chromatin extraction efficiency and to optimize the experimental conditions, different aliquots of MNP suspension were added to a fixed volume (400 µl) of frozen blood. Each extraction was repeated three times. Fig.4.2A shows that chromatin concentration reached a peak when the nanoparticle concentration reached 10 µl of MNPs (100 µg in quantity). This indicates that the enrichment efficiency of leucocytes and elution efficiency of chromatin by MNPs, will determine the chromatin extraction efficiency. Before reaching the peak, the more leucocytes captured the higher is the yield of the chromatin extraction; while after the optimal point, the absorbed chromatin cannot be washed into the elution buffer when excess MNPs are added. By increasing the volume of the blood samples (from 0.3 to 0.9 ml) with the same amount of MNPs (10 µl), increased concentration of chromatin (Fig.4.2B) can be obtained. Though the extraction

of leucocytes in different patient samples varied using our approach, at least 5 μg of chromatin could be extracted from 1 ml of whole blood sample.

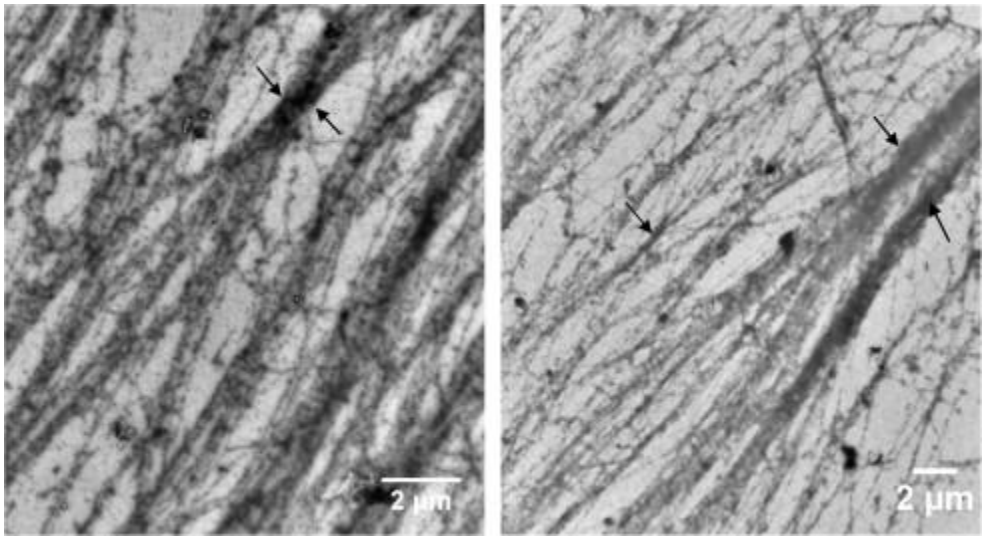

Figure 4.3 TEM images of extracted chromatin in cells from blood - negatively stained with 2% uranyl acetate. Both images show that chromatin is organized into heterochromatin and euchromatin. The heterochromatin is indicated by black arrow. Compared to euchromatin, heterochromatin is much harder to be accessed by transcription factors as well as antibodies.

Fig.4.3 shows the chromatin under TEM via negative staining (2% uranyl acetate, UA). From the image, it can be seen that long and thin chromatin fibers covered the entire carbon coated copper grid. Their length is much longer than the diameter of the nucleus (10~12 μm), indicating that besides nucleosome and higher order chromatin structure, nuclear matrix would also assist in the compaction of the chromatin fibers inside the nucleus. We also noted that some part of the chromatin fibers (indicated with black arrows) are more heavily stained and compacted than other fibers. They might be the heterochromatin, which are hard to be accessed by transcription factors and is highly associated with the down regulation of certain genes residing in these locations. Others

might be euchromatin, which is loosely compacted and can be easily accessed by transcription factors and highly associated with gene expression.

4.3.2 Determination of Epigenetic Modifications by a Two-step EIA

DNA and histone modifications are the two key epigenetic marks that play critical role in gene expression. The stepwise creation of distinct epigenetic patterns throughout the genome drives the formation of different cell lineages during development. These unique patterns dictate gene expression profiles, demarcate individual cell types and are faithfully propagated during replication and cell division to maintain distinct cell lineages (MacAlpine and Almouzni, 2013; Whitehouse and Smith, 2013). Leukemia is a heterogeneous disease with widespread aberration of epigenetic marks (Chen et al., 2010; Conway O' Brien et al., 2014). These epigenetic alterations can be used as biomarkers for cancer detection, diagnosis and prognosis (Herceg and Hainaut, 2007). Most of the efforts have predominantly either studied DNA (Ge et al., 2013; Shahal et al., 2014) or histone modification independently (Fraga et al., 2005; Krivtsov and Armstrong, 2007; Krivtsov et al., 2008; Li et al., 2002) or focused on elucidating the epigenetic patterns of specific genes (Guenther et al., 2008; Okada et al., 2005) because one requires DNA and the other requires histone proteins. For the first time, we attempt to evaluate both DNA and histone modifications globally and simultaneously in a single platform.

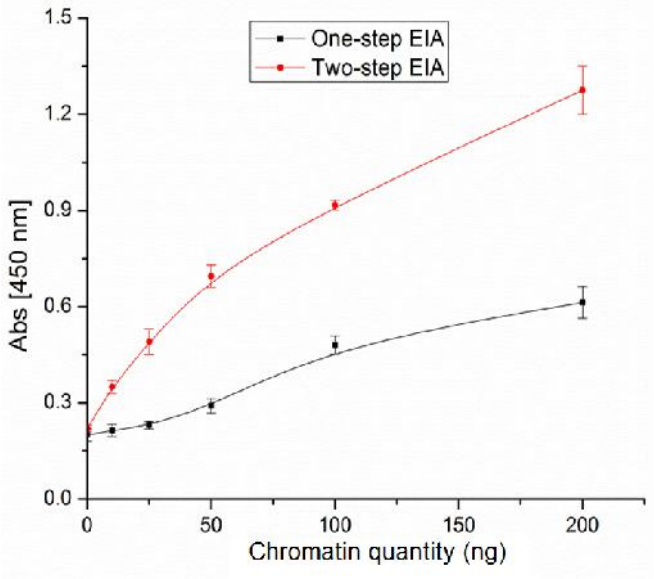

Figure 4.4 Comparison between the two-step EIA and the conventional one-step EIA to detect histone H4 as a test case. The required chromatin for the two-step EIA was 10 ng while the one-step EIA required 100 ng.

To achieve increased signal amplification, we used a two-step (primary antibody, secondary antibody-biotin and streptavidin-HRP) enzyme-linked immunosorbent assay (two-step EIA) to detect epigenetic modifications on DNA and histone proteins using the same sample. We compared our method with the conventional one-step (primary antibody, secondary antibody-HRP) EIA (using histone H4 as a test case), and found that the two-step EIA required 10 ng of chromatin, while the one-step EIA required 100 ng of chromatin (as shown in Fig.4.4). Further, since streptavidin can be labeled with multiple HRP molecules, upon interaction with biotin-labeled antibody an enhanced signal proportional to the number of HRP molecules can be expected from this reaction (Chowdhury et al., 2014).

In order to verify whether the extracted chromatin from blood could be used to determine DNA modifications, we compared our method with the conventional DNA-based EIA.

DNA methylation (5mC) is one of the characteristic hallmarks of mammalian heterochromatin where 5mC marks on DNA are hidden inside the highly compacted chromatin fiber, as shown in Fig.4. 3. DNA hydroxymethylation (5hmC) is mostly associated with euchromatin, which is much more accessible and easier to be detected than 5mC in chromatin. In the extracted DNA by conventional approaches, a compact form does not exist, and 5mC and 5hmC have equal opportunity for assess. Thus, the 5mC/5hmC ratio should be higher in DNA than that in chromatin due to the lack of access by 5mC targeting antibodies in the heterochromatin. Our result shows that the 5mC/5hmC ratio is 1.26 in DNA and 1.21 in chromatin, which is consistent with our hypothesis. The detection of DNA modifications using chromatin as a substrate is similar to using DNA as a substrate. Thus, samples using in our method is suitable for the detection of epigenetic modifications in DNA.

In order to verify whether chromatin could be used to determine histone modifications, we compared the developed two-step EIA with Western Blotting analysis (WB). We used the conjugated linoleic acid (CLA) treated S1 cells as a model to assess its effect on histone H3 lysine 9 di-methylation (H3K9me2). Ethanol (EtOH) was used as a control. Chromatin was extracted by the developed approach from S1 cells and one half of it was used for WB analysis; the other half was used for the two-step EIA analysis. A representative data set was shown in Fig.4.6, the H3K9me2 level drops after treating with CLA: 48.9% in the two-step EIA analysis (Fig.4.6A); 50.85% in WB analysis (Fig.4.6B). There is no significant difference between the two analytical methods. Thus, the chromatin used to detect epigenetic modification in DNA can also be used to detect histone modifications using the proposed method. It should be noted that while Western

Blotting analysis requires loading of separate samples, in our method multiple epigenetic modifications can be detected simultaneously with less sample amount (as much as 200 ng compared to 15 μg) requiring less cells to complete the analysis (Zhou and Irudayaraj, 2015a). Future experiments could extend the limit of multiplexing by other highly sensitive methods such as surface enhanced Raman and plasmon hyperspectral imaging (Lee et al., 2011; Sun et al., 2007).

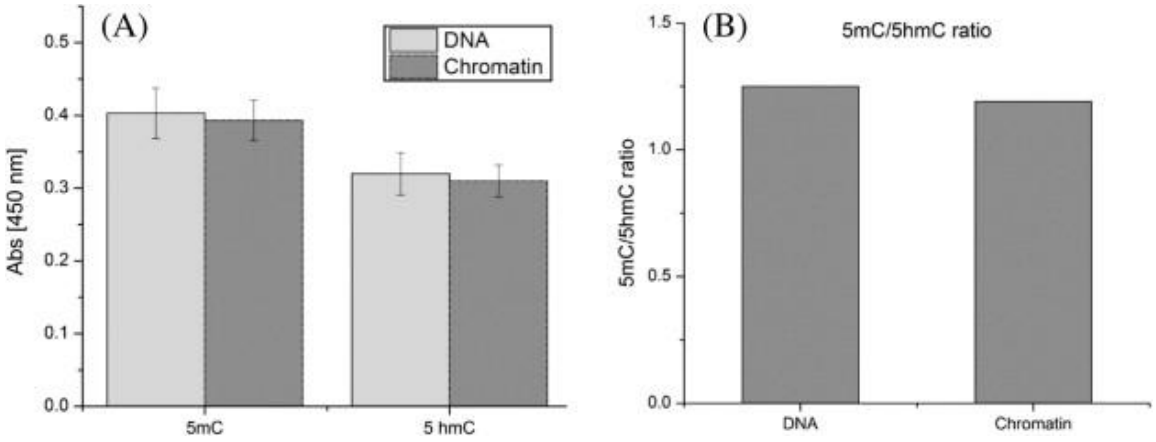

Figure 4.5 Chromatin as substrate for 5mC and 5hmC quantification compared with DNA as substrate. Quantification of 5mC and 5hmC by two-step EIA uses DNA or chromatin as substrate (A), and the corresponding 5mC/5hmC ratio in DNA and chromatin is determined (B). The detection of DNA modifications using chromatin as a substrate is similar to using DNA as a substrate.

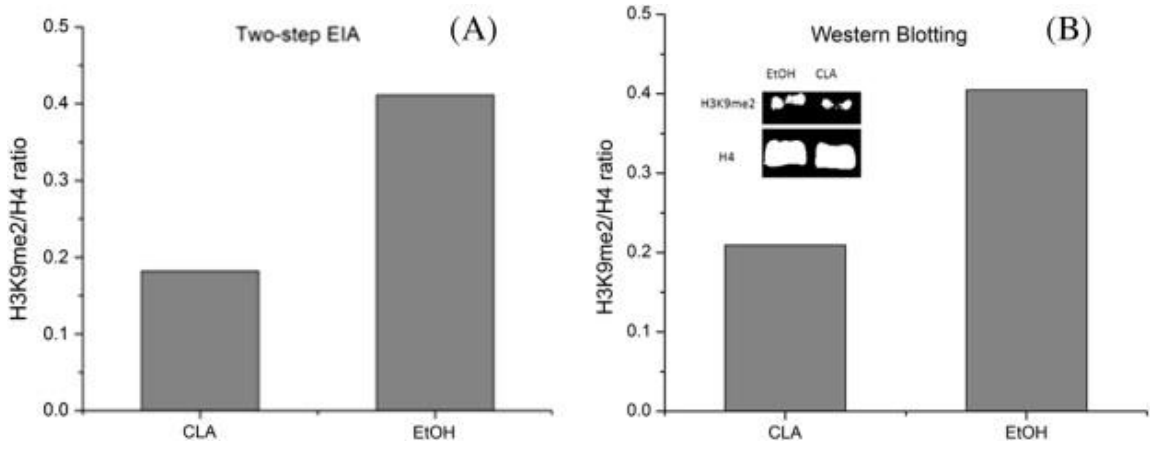

Figure 4.6 Quantification of the H3K9me2/H4 ratio by the two-step EIA (A) compared to Western blotting analysis (B). The two analytical methods give similar result indicating that the global level of H3K9me2 drops after treating the S1 cells with CLA.

4.4 Conclusion

Using the unique surface chemistry of modified magnetic nanoparticles, we report a rapid one-pot chromatin extraction protocol from whole blood and to demonstrate a cross-platform approach for simultaneous detection of epigenetic modifications on DNA and histone proteins. With carboxyl functionalized magnetic nanoparticles, we have demonstrated that leucocytes can be enriched and their chromatin can be adsorbed on to surface modified nanoparticles in a single tube with a few simple steps. Our sample preparation and detection strategy does not require centrifugation, filtration, fragmentation or use of hazardous agents. Using the extracted chromatin as a substrate, we demonstrate that epigenetic modifications on DNA and histone proteins can be simultaneously detected via a biotin-streptavidin mediated enzyme-based immunosorbent assay (two-step EIA), which conventionally is done separately because analyzing DNA

and histone proteins involve separate steps. The developed method was successfully validated with the conventional DNA based EIA and Western Blotting analysis. Our approach is the first demonstration to propose the simultaneous detection of DNA and histone modifications in the extracted chromatin. Future efforts could focus on using the developed approach in a high throughput setting to identify changes in DNA and histone post translational modifications which can be used as biomarkers for health screening, disease prognosis, and for understanding normal blood cell development and leukemogenesis.

CHAPTER 5. CHROMATIN ASSOCIATED RNAS CONTRIBUTE TO HIGHER ORDER CHROMATIN STRUCTURE

5.1 Introduction

Temporal and spatial regulation of higher order chromatin structure is extremely important for epigenetic regulation and control of gene activation and silencing (Fessing, 2014; Lanctot et al., 2007). Many factors such as pH, temperature, ionic-strength, histone variants and chromatin modifiers (DNA methylation tranferases and histone modifiers) have been known to influence both nucleosomal and higher order chromatin structure (Rodríguez-Campos and Azorín, 2007). Nuclear RNAs are an integral component of chromatin and also contribute to local chromatin conformation(Diermeier et al., 2014; Rodríguez-Campos and Azorín, 2007; Schubert and Längst, 2013). It is known that chromatin-induced gene silencing depends on small non-coding RNAs (ncRNAs) which assist in the formation of heterochromatin. Further, dosage compensation and genomic imprinting in animals require the contribution of specific ncRNAs (Cai and Cullen, 2007; Deng and Meller, 2006; Kelley and Kuroda, 2000; Quinodoz and Guttman, 2014). Moreover, some ncRNAs are involved in the recruitment of DNA methyltransferases and histone-modifying complexes to specific loci to modify local chromatin conformation (Peschansky and Wahlestedt, 2013). Altogether, chromatin architecture and epigenetic

memory could be mediated by RNA-directed processes; however, whether RNA itself plays a direct structural role in higher order chromatin structure is unclear.

In this chapter, we show that chromatin associated RNAs play a direct structural role in heterochromatin formation in eukaryotic nucleus. DNA halos were generated from RNase A treated eukaryotic cells using the fluorescent DNA halo assay. RNA is critical for proper condensation and segregation of chromatin in the interphase. These RNAs are not likely to correspond to nascent transcripts since the DNA halos are also found when cells are treated with the RNA synthesis inhibitor α-amanitin. Darkfield microscopy analysis using gold nanoparticles labeled antibody specific for the DNA-RNA hybrid confirmed that the RNA were retained on chromatin through the formation of a DNA-RNA hybrid. When the cells were treated with RNase A, the gold probes were undetectable under darkfield microscopy. We further performed gold nanoparticle labeling of the extracted chromatin and examined by electron microscopy. Surprisingly, most gold probes were enriched in the heterochromatin. RNase A treatment of extracted chromatin would decrease the chromatin fiber thickness. Altogether, these results show that chromatin associated RNAs contribute to heterochromatin formation.

5.2 Material and Methods

5.2.1 Fluorescent DNA Halo Assay

The fluorescent DNA halo assay used in this study was modified from (Guillou et al., 2010). Briefly, MCF7 cells were grown on coverslips overnight to reach 80% confluence. Cells were then permeabilized with 0.5% Trition X-100 for 10 min on ice. After washing

with chilled 1x PBS 3 times, cells were further treated with RNase A (10 µg/ml) at 37 ^{o}C for 30 min, and immersed in a buffer containing 25 mM Tris (pH 8.0), 0.5 M NaCl, 0.2 mM $MgCl_2$, 1 mM PMSF, and protease inhibitors for 1 min, and then in Halo buffer (10 mM Tris at pH 8.0, 2 M NaCl, 10 mM EDTA, protease inhibitors) for 4 min. After washing with 25 mM Tris (pH 8.0), 0.5 M NaCl, 0.2 mM $MgCl_2$, cells were then stained with DAPI (10 µg/ml) for 10 min on ice. The halo radius (R) of each cell was determined by measuring the total area of the nucleus (A_t) and the central area, highly stained with DAPI, of the nuclear scaffold (A_s) using the formula $R= [(A_t-A_s)/\pi]^{1/2}$. In the control experiment, cells were treated with RNase inhibitor instead of RNase A.

5.2.2 Gold Nanoparticles labeled Antibodies Specific for DNA-RNA Hybrids

The gold nanoparticle solution (1 ml, 16 or 40 nm in diameter) was neutralized with 1 µl of Na_2CO_3 (0.5 M) and 100 µl of phosphate buffer (10 mM, pH 7.4) to bring the solution to a physiological pH in a glass tube. 2 µl of monoclonal anti-DNA-RNA hybrid antibody S9.6 solution (5 mg/ml) specific for DNA-RNA hybrid was added to the GNP solution to maintain a final molar concentration of 10 µg/ml of nanoparticle solution. The solution was stirred in a shaker for 2 hours and 5 % (w/v) Casien solution (122 µl) was added following that (Casien is dispersed in 10 mM phosphate buffer). The solution was stirred overnight before centrifugation at a rate of 12,000 RPM for 15 minutes, and redispersed in 100 µl of 0.5% Casien in 10 mM PBS and stored at 4 ^{o}C. In the control experiment, gold nanoparticles were only coated with Casien.

5.2.3 Labeling Chromatin Associated RNAs inside Nucleus

40 nm gold nanoparticles labeled anti-DNA-RNA hybrid antibodies were used to detect chromatin associated RNAs inside the nucleus of MCF7 cells. After cell confluence

reached 80% on glass coverslips, cells were fixed with 4% paraformaldehyde and permeabilized with 0.5% Trition X-100 for 10 min on ice. Cells were then blocked with 0.5% Casien in 0.1x PBS on ice, and then incubated with 200 µl of immunostaining buffer containing 0.5% Casien, gold probes (10 µl) and RNase inhibitors at room temperature for 1h. After washing with 1x PBS, the coverslips were mounted and examined by darkfield microscopy. Two negative control experiments were performed: (1) The cells were immunostained with gold nanoparticles only coated with Casien; (2) Before immunostaining, cells were treated with RNase A.

5.2.4 Native Chromatin Extraction

Native chromatin was extracted from MCF7 cells as previous reported (Zhou et al., 2015; Zhou and Irudayaraj, 2015a). Briefly, fresh MCF7 cells were trypsinized and collected by centrifugation, and then lysed in ice with buffer containing 250 mM SDS, 1 mM EDTA, 0.5 mM EGTA, 1 mM PMSF, protease inhibitors and RNase inhibitors. 8 µl salicylic acid coated magnetic nanoparticles (10 mg/ml) were added to form a chromatin-nanoparticle complex. Ice-cold isopropanol was added and incubated for 10 min on ice. The chromatin-nanoparticle complexes were magnetically separated to the tube wall and washed with ice cold 70% ethanol. Chromatin was further eluted in 1x PBS buffer containing RNase inhibitor. A final magnetic separation step was performed to obtain native chromatin in the supernatant.

5.2.5 Labeling CARs on Extracted Native Chromatin

16 nm gold nanoparticles labeled with the monoclonal anti-DNA-RNA hybrid antibodies S9.6 were used to detect chromatin associated RNA on the extracted native chromatin. Extracted native chromatin (5 µl , OD260 = 1.5) was mounted on the glow discharged

TEM grid, and then the grid was blocked with 0.5% Casien, and further incubated with buffer containing 0.5% Casien, RNase inhibitor and 16 nm gold probes at room temperature for 1h. The grids were washed three times with 10 µl 1x PBS, air dried and then examined by transmission electron microscopy.

5.3 Results and Discussion

Chromatin associated RNAs are an integral component of chromatin that perform critical functions during development and cell differentiation. They have been shown to mediate local chromatin conformation to regulate gene expression by novel mechanisms such as RNA interference, gene co-suppression, gene silencing and imprinting (Amaral et al., 2008). Numerous studies have shown that these RNA-directed processes involve the recruitment of histone-modifiers, DNA methyltransferases and other chromatin associated non-histone proteins, such as HP1 and PRC2, to specific loci in an indirect manner to mediate local chromatin conformation (Caudron-Herger and Rippe, 2012). However, whether the chromatin associated RNA itself plays a direct structural role in chromatin architecture is still unresolved.

Large-scale chromatin loops are important in many aspects of chromatin function. Evidence of chromatin associated RNAs participating in gene activation/silencing during chromatin looping by grouping together neighboring origins is only emerging (Nakama et al., 2012; Wang et al., 2011). RNAs could directly link with chromatin to stabilize long-range interactions between distant chromatin sites. To test this hypothesis, we used the fluorescent DNA halo assay to estimate the average length of DNA loops in interphase

nuclei. Cells were permeabilized with the detergent, and treated with RNase A and further depleted of soluble proteins by extraction with high-salt buffers allowing supercoiled DNA loops to unwind and form a halo around the insoluble proteinaceous nuclear matrix or karyoskeleton (Guillou et al., 2010; Roti and Wright, 1987). If chromatin associated RNAs participate in the formation or stabilization of chromatin loops, their deletion should result in fewer, longer loops, leading in an increase in the average halo radius. Control cells were treated with RNase inhibitors. Deletion of RNA on the chromatin induces a striking increase in the halo radius (Fig.5.1A), indicative of larger DNA loops. By contrast, the RNase inhibitor treatment of cells did not significantly affect the halo size. These RNAs are not likely to correspond to nascent transcripts since the DNA halos are also found when cells are treated with α-amanitin. These experiments are consistent with the hypothesis that chromatin associated RNAs participate in the organization of chromatin inside the nucleus.

As mentioned above, chromatin associated RNAs regulate chromatin loops. However, it is possible that chromatin associated non-histone proteins (e.g. HP1) might mediate chromatin and RNA interaction, and these RNAs would further serve as scaffolds to recruit other chromatin modifiers to adjust chromatin architecture. If RNAs directly interact with chromatin, the mechanism that underlies the association is still unclear. Early studies proposed that the RNAs play an important role in the control of genetic activity by forming hybrids at specific loci on DNA (Bonner et al., 1968; Dahmus and Bonner, 1969). Further, Szeszak and Pihl have indicated that 0.1% of the DNA of rat liver chromatin may be present to form DNA-RNA hybrids (Szeszak and Pihl, 1971). Recently, using an antibody specific for the DNA-RNA hybrid, Nakama et al. found that

some non-coding RNAs were retained on the chromatin and confirmed the formation of DNA-RNA hybrids *in vivo* (Nakama et al., 2012). The detected DNA-RNA hybrids are diminished by the RNase H treatment, which confirmed that the antibody detected the DNA-RNA hybrid. However, due to the low sensitivity of fluorescence microscopy, only a few hybrids were detected.

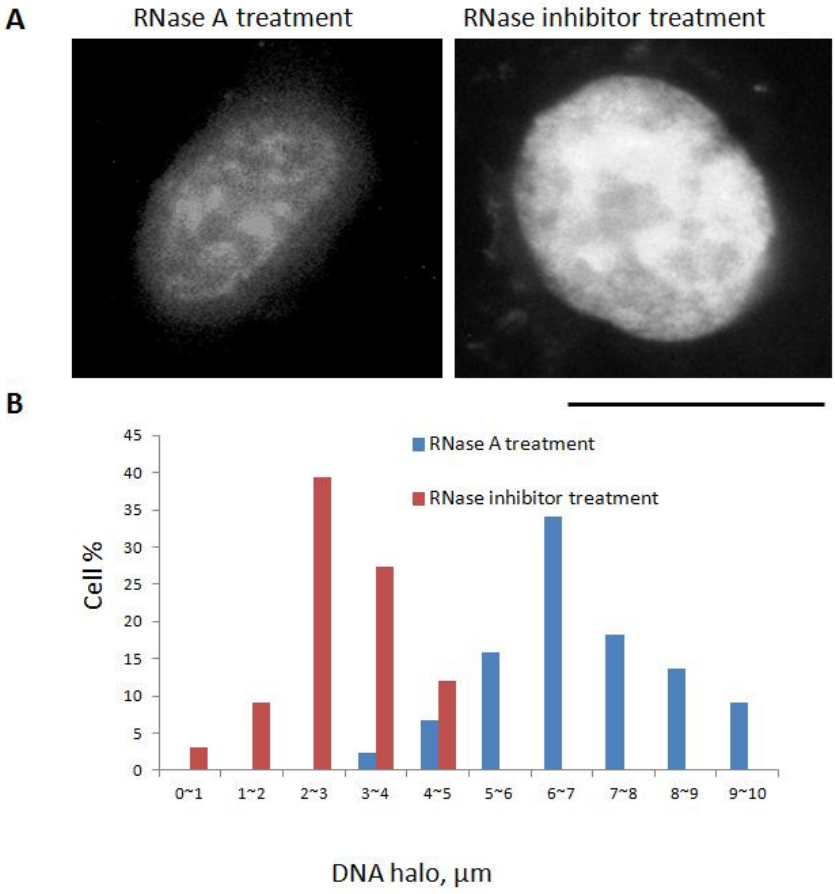

Figure 5.1 Chromatin associated RNAs regulate the length of chromatin loops. (A) MCF7 cells were treated with RNase A (*left*) and RNase inhibitor (*right*), and subjected to treatment to generate DNA halos. Halo radius of each condition was measured (n = 150 for each condition). Bar denotes 10 µm. (B) Histogram showing radius measurements grouped in intervals of 10 (a~b: value ≥a and <b).

In order to increase the sensitivity of immunostaining, gold nanoparticle labeled monoclonal anti-DNA-RNA hybrid antibody S9.6 (Boguslawski et al., 1986) was used to detect DNA-RNA hybrids inside the nucleus and evaluated by darkfield microscopy. Compared to pure gold nanoparticles (GNPs), the antibody/Casien-coated gold nanoparticles show a red shift in the absorption maximum as noted from the UV-vis spectrum (Fig.5.2A), which verifies the successful S9.6/Casien coating on the GNP surface. These 40 nm GNP probes could be detected at the single-molecule level using our home-built Darkfield microscopy platform (Lee et al., 2014).

If there are detectable gold nanoparticles in the cell nucleus immunostained by anti-DNA-RNA hybrid antibody, deletion of RNAs inside the nucleus should result in less or undetectable signals. Negative control cells were treated with gold nanoparticles only coated with Casien. As shown in Fig.5.2B, it was apparent that deletion of RNAs by RNase A digestion caused significantly decreased signals. The negative control cells did not contain detectable signals indicating that there is no non-specific binding of gold nanoprobes inside the nucleus. These experiments indicate that RNAs directly associate with chromatin inside the nucleus by forming DNA-RNA hybrids.

Using the anti-DNA-RNA antibody for immunostaining studies, Nakama et al. found that the hybrids foci co-localized with the heterochromatin associated proteins, and proposed a model for the association of the heterochromatin ncRNA with chromatin. However, due to the low resolution of light microscopy (~200 nm), the co-localization might be due to the association between DNA-RNA hybrids and Chp1 proteins. To determine whether the exact location of chromatin associated RNAs was important; we used transmission

electron microscopy (TEM) at sub-nanometer resolution to detect the foci of the (DNA-RNA) hybrid elements on the extracted native chromatin.

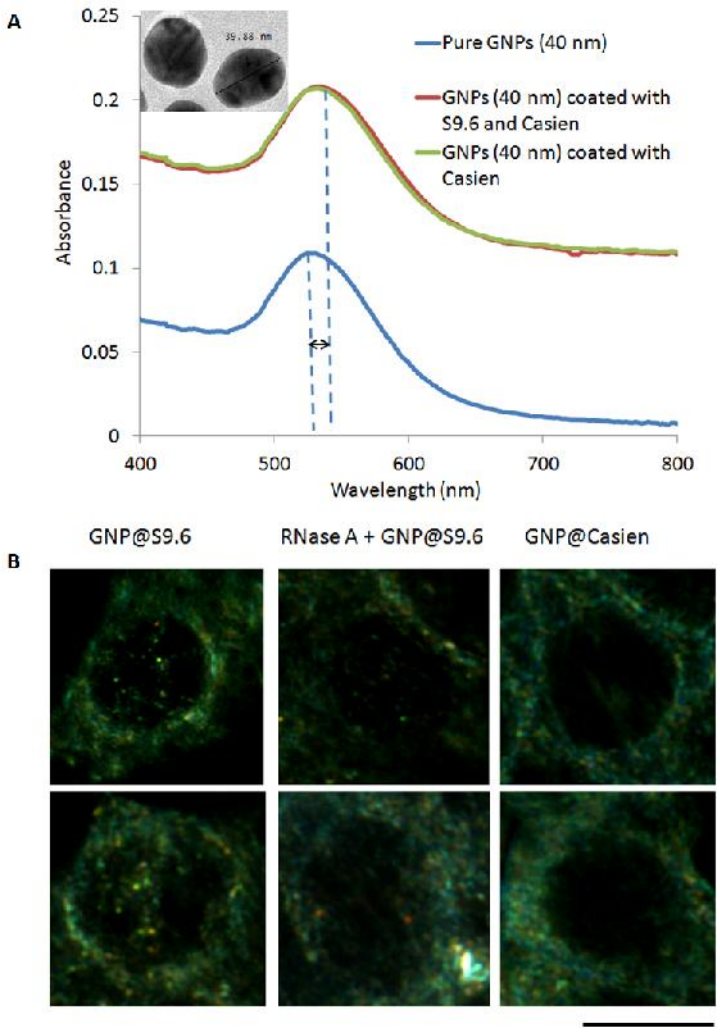

Figure 5.2 Detection of DNA-RNA hybrids *in vivo* using gold nanoparticle labeled anti-DNA-RNA hybrid antibody with darkfield microscopy. (A) Characterization of 40 nm gold nanoparticle probes by TEM and UV-vis spectroscopy. The S9.6/Casien coated gold nanoparticles show a red shift at the absorption maximum. (B) MCF7 cells were immunostained by GNP@S9.6 (*left*), RNase A and GNP@S9.6 (*middle*) and GNP@Casien (*right*). Pretreatment of RNase A diminished signals. Bar, 10 μm.

The anti-DNA-RNA hybrid antibodies were labeled with 16-nm gold nanoparticles, as shown in Fig.5.3A. In TEM the gold nanoparticles used as markers scatter electrons well, making them readily distinguishable from biological samples. The anti-DNA-RNA hybrid antibodies labeled with smaller gold nanoparticles allow easier access to chromatin.

Native chromatin was extracted from MCF7 cells as previously described (Zhou and Irudayaraj, 2015a). The extracted native chromatin was anchored onto the glow discharged carbon surfaces of TEM grids providing affinity towards biological samples. Depending upon the sample preparation procedure, the chromatin can generally take two different forms on the TEM grids. When chromatin is directly deposited on the grids and allowed to air dry, chromatin was stacked on the grids and formed an artificial fractal structure containing several DNA loops, as shown in Fig .3B (I). The stacked chromatin made it difficult to distinguish heterochromatin and euchromatin. Alternatively, applying a piece of filter paper on the edge of TEM grids after depositing the chromatin solution chromatin structures that are well aligned was noted, as shown in Fig.5.3B (II and III). On the aligned chromatin, the euchromatin is distinguishable from the heterochromatin. Most of the gold nanoparticle marked DNA-RNA hybrid foci were located on the heterochromatin (Fig.5.3B (II)). These RNAs are not likely to correspond to nascent transcripts as they are also found to bind to the heterochromatin when cells are treated with RNA synthesis inhibitor, α-amanitin. Interestingly, we further observed that the chromatin formed a “branching structure” between the heterochromatin and euchromatin. Several DNA-RNA hybrids were located on the branch structure, as shown in Fig.5.3B (III). To further determine whether the RNAs contribute to chromatin conformation, we

treated the extracted chromatin with RNase A and examined under TEM, and found that the heterochromatin was seldom visible and the fiber thickness decreased, as shown in Fig.5.3C. These experiments indicated that most chromatin associated RNAs directly contribute to heterochromatin formation, which is consistent with the results obtained by Nakama et al (Nakama et al., 2012).

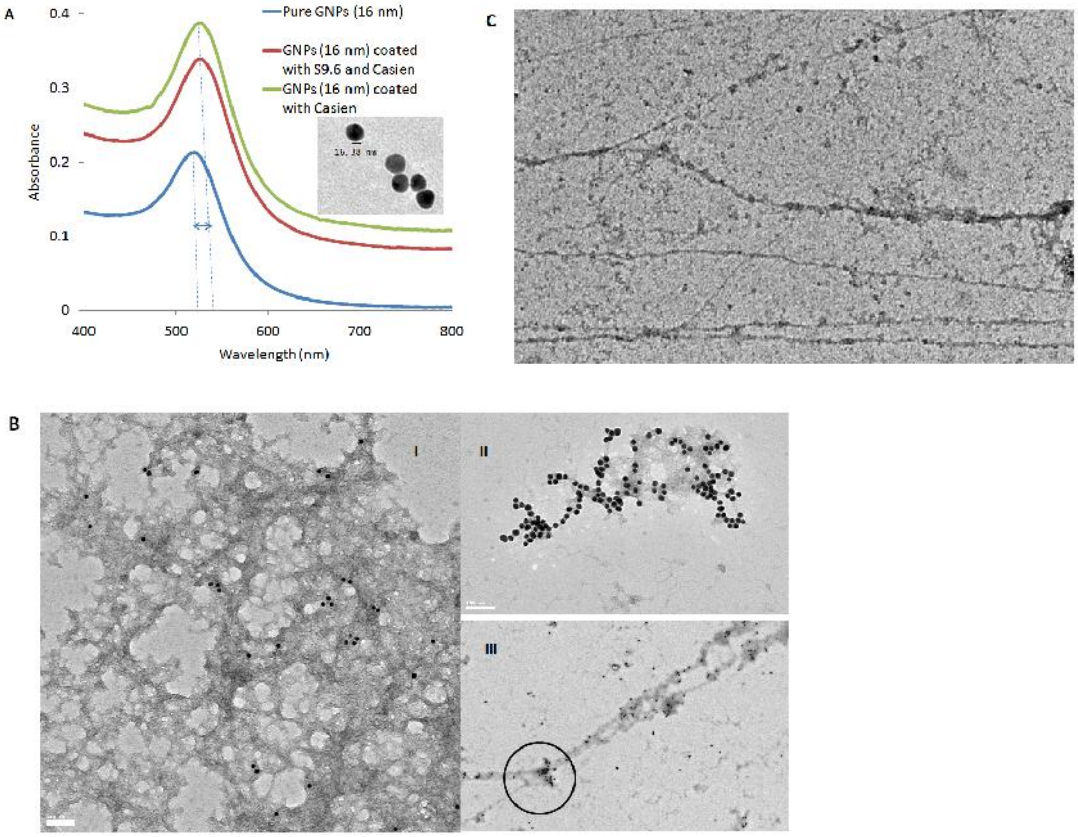

Figure 5.3 Detection of DNA-RNA hybrids on extracted chromatin using gold nanoparticle labeled anti-DNA-RNA hybrid antibodies under TEM. (A) Characterization of 16 nm gold nanoparticle probes by both transmission electron microscopy and UV-vis spectroscopy. The S9.6/Casien coated gold nanoparticles show a red shift at absorption maximum. (B) Native chromatin extracted from MCF7 cells was immunostained with 16-nm gold nanoprobes. (I) DNA-RNA hybrid foci on fractal DNA loops. (II) Hybrid foci on the heterochromatin were heavily marked by gold nanoprobes. (III) Hybrid foci on the branching structure indicated by a black circle. (C) RNAase A treatment caused disruption of heterochromatin and decreasing chromatin fiber thickness.

5.4 Conclusion

In conclusion, we found that chromatin associated RNAs directly associated with heterochromatin through DNA-RNA hybridization contributes to higher order chromatin structure. Results from fluorescence DNA halo assay suggest that deletion of nuclear RNAs significantly altered chromatin organization *in vivo*. Similar effects have been reported as follows: a mild acid treatment that release histones causes the formation of a DNA halo around isolated nuclei (Cook and Brazell, 1975). RNAi silencing of cohesin, which plays a critical role in architectural organization of chromatin, would induce larger DNA halo radii (Guillou et al., 2010). Using the monoclonal anti-DNA-RNA hybrid antibody S9.6 we confirmed that the nuclear RNAs were associated with DNA by forming DNA-RNA hybrids. We used the same antibody to detect the foci of chromatin associated RNA at subnanometer resolution by TEM and found that most of these colocalize on the heterochromatin. Deletion of these RNAs causes disruption of heterochromatin and decreases chromatin fiber thickness. We also found that the chromatin associated RNAs located at the chromatin branching structure is a transitional structure between heterochromatin and euchromatin. These RNAs may have a function to prevent heterochromatin spreading to euchromatin, as proposed (Cohen and Jia, 2014). Further studies will involve the development of an unbiased chromatin associated RNAs extraction platform backed by transcriptomic analyses.

CHAPTER 6. RAPID AND UNBIASED EXTRACTION OF CHROMATIN ASSOCIATED RNAS FROM PURIFIED NATIVE CHROMATIN

6.1 Introduction

Chromatin associated RNAs (CARs) are an integral component of chromatin that has diverse architectural functions inside the nucleus where they are found associated with heterochromatin (Nakama et al., 2012), euchromatin (Hall et al., 2014), and the nuclear matrix (Nickerson et al., 1989). Purification of CARs is extremely important for down-stream applications such as transcriptomic analyses. Conventionally, CARs are typically isolated from soluble chromatin, which is collected from different fractions in a sucrose gradient for overnight centrifugation after soluble chromatin has been released from the isolated nuclei by MNase digestion. The total assay time, including nuclei preparation, chromatin purification and RNA isolation, is about 16 h. Unfortunately, the RNAs isolated from soluble chromatin-containing fractions often do not fully represent the true CARs population, since RNAs also associate with insoluble heterochromatin fragments. For example, repetitive RNAs can form more complex and less soluble structures with heterochromatin (Hall et al., 2014). Moreover, when compared to mRNA, the half life of CARs vary over a wide range with some less than 2 h (Clark et al., 2012). Although the sequences of CARs extracted by conventional methods can be systematically identified

the global level using high-throughput genomic platforms (Mondal et al., 2010), these approached often exhibit some bias due to the fact that some RNAs resistant to extraction and some RNAs are degraded during the long handling process. Thus, developing an ultrafast and unbiased method for the extraction of CARs is essential to ensure the accuracy of transcriptomic analyses.

One of the most important and time-consuming steps during CARs extraction is the isolation of native chromatin. In contrast to the conventional method that requires high speed centrifugation for a prolonged period of time to purify soluble chromatin, we recently developed methods using magnetic nanoparticles (SAMNPs) that allow for a rapid, unbiased and cost-effective method for purifying chromatin (Zhou et al., 2015; Zhou and Irudayaraj, 2015a). When free RNA (most of these are rRNAs and mRNAs) and chromatin were released from lysed mammalian cells, nucleic acids were non-specifically bound to SAMNPs forming free RNA-SAMNPs while chromatin formed chromatin-SAMNPs complexes. The complexes and free magnetic nanoparticles were magnetically separated from the sample solution. If extraction of CARs is desired, both the free RNA-SAMNPs and the free SAMNPs must first be removed before chromatin-SAMNPs complexes can be submitted for CARs extraction.

This problem can be addressed by adapting magnetophoretic chromatography using a liquid-type filter (Kwon et al., 2013; Kwon et al., 2015). A solution containing the free SAMNPs, free RNA-SAMNPs and chromatin-SAMNPs are placed onto a viscous PEG solution in a 200-µl pipette tip to form two separated liquid layers due to differences in viscosities. When an external magnetic field is placed below the tip, only the chromatin-SAMNPs complexes pass through the interface and reach the bottom of the tip. Both the

free RNA-SAMNPs complexes and the free SAMNPs remain trapped at the interface between the solutions. The magnetophoretic chromatography can be achieved in 10 min and the collected chromatin-SAMNPs complexes can then be directly used for CARs extraction.

In this chapter, we present a rapid and unbiased method to extract chromatin associated RNAs by introducing magnetophoretic chromatography to purify chromatin using salicylic acid coated magnetic nanoparticles. SAMNPs have dual functions. They can be used for enriching mammalian cells from the culture media and further used for capturing chromatin from the lysed cells. In this study, magnetophoretic chromatography was applied to isolate the chromatin-SAMNPs complexes from both free SAMNPs and from the free RNA-SAMNPs complexes. The collected chromatin-SAMNPs complexes were then used for CAR extraction. The total assay time, including cell and chromatin purification and CARs extraction, can be completed within 2h.

6.2 Experiment

6.2.1 Chromatin Isolation and Magnetophoretic Chromatography

Hydrophilic SAMNPs were prepared according to the previous reported method (Zhou et al., 2013a). The concentration was adjusted to 10 mg/ml. The SAMNPs were added into the cell culture media containing trypsinized MCF7 cells and incubated for 5 min at room temperature. The cell-SAMNPs complexes were magnetically separated and lysed in buffer containing 250 mM SDS, 1 mM EDTA, 1 mM PMST, 0.5 mM EGTA and 2% protease inhibitor Cocktail. The complexes were pipetted up and down slowly 20 times

with a 200-ul pipette tip and further incubated for 10 min. Isopropanol was added to the suspension to form nucleic acids-SAMNPs complexes and incubated for another 10 min on ice. The mixture containing chromatin-SAMNPs, mRNA-SAMNPs complexes and free SAMNPs was separated from the solution by an external magnetic field (SuperMag Multitube Separator), and then re-dispersed in 50-µl 1x PBS. The PBS buffer containing the chromatin-SAMNPs was transferred onto the 200-ul pipette tip containing 80 µl of a 25 wt% PEG solution. The chromatin-SAMNPs complexes were separated from the free SAMNPs and free RNA-SAMNPs complexes by magnetophoretic chromatography for about 10 min.

6.2.2 CARs extraction

The collected chromatin-SAMNPs complexes were directly submitted for CARs extraction using E.Z.N.A. Total RNA Kit I (OMEGA bio-tek). In a parallel study, CARs were extracted from isolated nuclei (Nuclei Isolation Kit, Sigma-Aldrich). The concentration and purity of CARs was determined using a Nanodrop spectrophotometer. The CARs were aliquoted into two parts; one was directly used for agarose gel electrophoresis and the other was used for preparing cDNA using the iScript cDNA synthesis kit (Bio-Rad).

6.2.3 Quantitative (real-time) PCR (qPCR)

The qPCR reactions were performed to validate the enrichment of a subset of frequently reported CARs, and beta-actin mRNA was used as a negative control. The qPCR quantification was performed using the standard curve method with FastStart Universal SYBR Green (Roche) using the LightCycler 96 system (Roche). The primer sequences used in various qPCR reactions are provided in Table 6.1 (Tang et al., 2013). The relative

level of each CAR was calculated compared to the beta-actin mRNA both in the magnetophoretic chromatography purified CARs and in isolated nuclei.

6.3 Results and Discussion

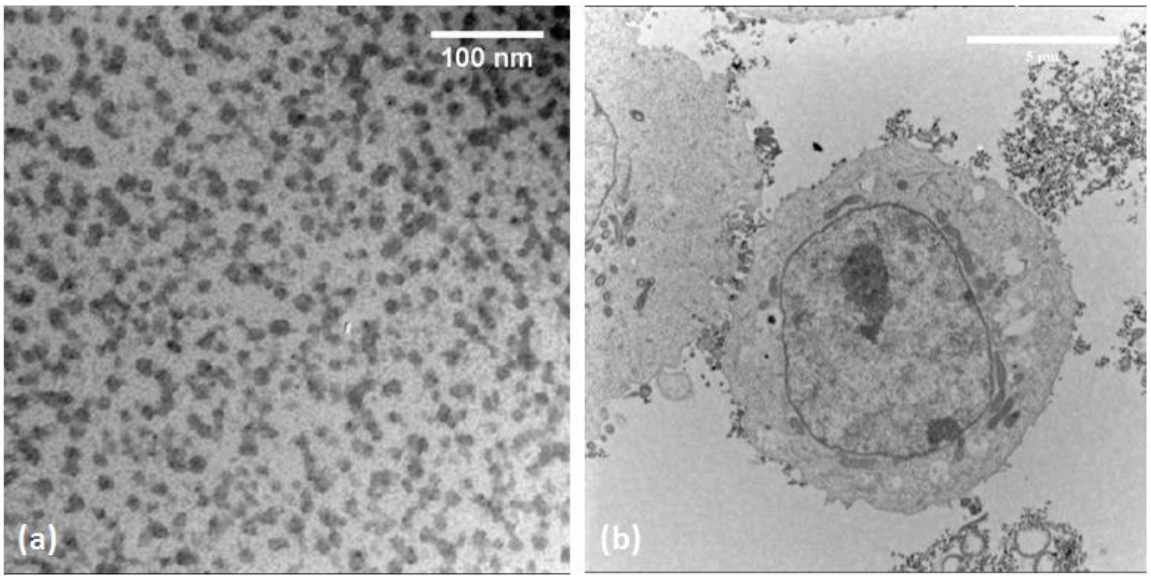

Figure.6.1 TEM images of (a) SAMNPs and (b) MCF7 cells with SAMNPs. SAMNPs were monodispersed in water and formed clusters when interacting with MCF7 cells in cell culture media.

Fig.6.1a shows transmission electron microscopy (TEM) images of SAMNPs. The average size of SAMNPs was measured as 10 nm with narrow size distributions. The SAMNPs are monodispersed in water with a hydrodynamic diameter of approximately 122.7 nm and a zeta potential of 38.1 mV (Zhou et al., 2013a). When added into buffers such as cell culture media containing amounts of salts (6.4 g/l NaCl, 3.7 g/l $NaHCO_3$, 0.4 g/l KCl, 0.2 g/l $CaCl_2$ etc), the ions perturb the surface charge of SAMNPs. The

SAMNPs would form clusters and non-specifically attach to the cell membrane of MCF7 cells, as shown in Fig.6.1b.

The formed cell-SAMNPs complexes and free SAMNPs are separated under an external magnetic field. Compared to the free SAMNPs, the cell-SAMNPs are separated more efficiently than free SAMNPs since the magnetic force exerted on the magnetic particles is proportional to their apparent volume (Kwon et al., 2015). The small size of SAMNPs helps to retain the superparamagnetic properties (Sun and Zeng, 2002). Thus, each SAMNPs cluster consists of a few hundred 10-nm iron oxide nanoparticles, which still possess paramagnetic properties with even higher separation efficiency.

The mixture of cell-SAMNPs complexes and free SAMNPs was magnetically separated from the cell culture media using a permanent magnet (SuperMag Multitube Separator), and then re-suspended in lysis buffer. Nucleic acids, including free RNA and chromatin, were released when the cell membrane and nuclear membrane were dissolved in the lysis buffer. The SAMNPs clusters released from the cell membrane and free SAMNPs were re-dispersed in the lysis buffer and further interacted with the released nucleic acids. Adding chaotropic agents, such as isopropanol, assists nucleic acids to wrap around SAMNPs and cause co-aggregation. Thus, a mixture of free RNA-SAMNPs, chromatin-SAMNPs complexes as well as free SAMNPs was formed and magnetically separated from the lysis buffer with an external magnetic field, and then re-dispersed in 50 µl of 1x PBS for subsequent magnetophoretic chromatography, Fig.6.2a.

Conventionally, extraction of chromatin associated RNAs utilizes three experimental steps: i) nuclei isolation; ii) soluble chromatin purification; iii) RNA extraction from the collected soluble chromatin. However, both nuclei isolation and the soluble chromatin

purification processes are tedious, time consuming and result in significant sample loss. Moreover, the CARs are extracted only from soluble chromatin and RNAs associated heterochromatin is lost during conventional CARs preparation. And due to short half lives of RNA, CARs degrade during the prolonged extraction process causing a bias for the full sequence analysis of CARs. In contrast, chromatin isolation by the established magnetic isolation process is fast and convenient (Zhou and Irudayaraj, 2015b), although there is still the issue of free RNA adsorbing to the magnetic nanoparticle surface, which could introduce artifacts for down-stream sequence analysis of CARs. Thus, it is essential to remove free RNA before transcriptomic analysis of CARs. Most of the free RNAs are mRNA and rRNA in the cytoplasm. Though high temperature could degrade the free RNAs without sacrificing DNA quality and quantity (Shan et al., 2011), the CARs degrade as well. Thus, it is necessary to develop a fast, simple and cost-effective method to remove free RNA without causing degradation of CARs.

This issue is addressed by adapting magnetophoretic chromatography using a liquid-type filter (Kwon et al., 2013; Kwon et al., 2015). Before magnetophoretic separation, all of the magnetic objects were dispersed uniformly in the upper layer of liquid in the pipette tip. When a permanent magnet was placed under the pipette tip, the chromatin-SAMNPs complexes, the free RNA-SAMNPs complexes and free SAMNPs were attracted toward the magnetic pole. Multiple forces affect these complexes through the PEG solution, such as the magnetic force (F_m), gravitational force (F_g), buoyant force (F_b) and drag force (F_d). F_m exerted on an object is proportional to its apparent volume; F_b is proportional to the surface area of the object; F_d is proportional to the solution viscosity, which is directly associated with the concentration of PEG solution (Kwon et al., 2015). Compared to the

free RNA-SAMNPs complexes and the free SAMNPs, the chromatin-SAMNPs complexes are much greater in size due to the large size of chromatin. Thus, the chromatin-SAMNPs complexes have a higher probability of passing through the PEG solution than the free RNA-SAMNPs and the free SAMNPs. To let the chromatin-SAMNPs complexes pass through and keep both the free RNA-SAMNPs complexes and the free SAMNPs within the interface between the PBS solution and PEG solution, the concentration of PEG solution was optimized and determined at 25% (m/v). As shown in Fig.6.2a, the chromatin-SAMNPs complexes were well separated from the free RNA-SAMNPs complexes and the free SAMNPs in the experimental time scale (10 min). Only the chromatin-SAMNPs complexes can reach the bottom of the pipette tip after the magnetophoretic chromatography process; and the free RNAs-SAMNPs complexes are trapped at the interface between the solutions.

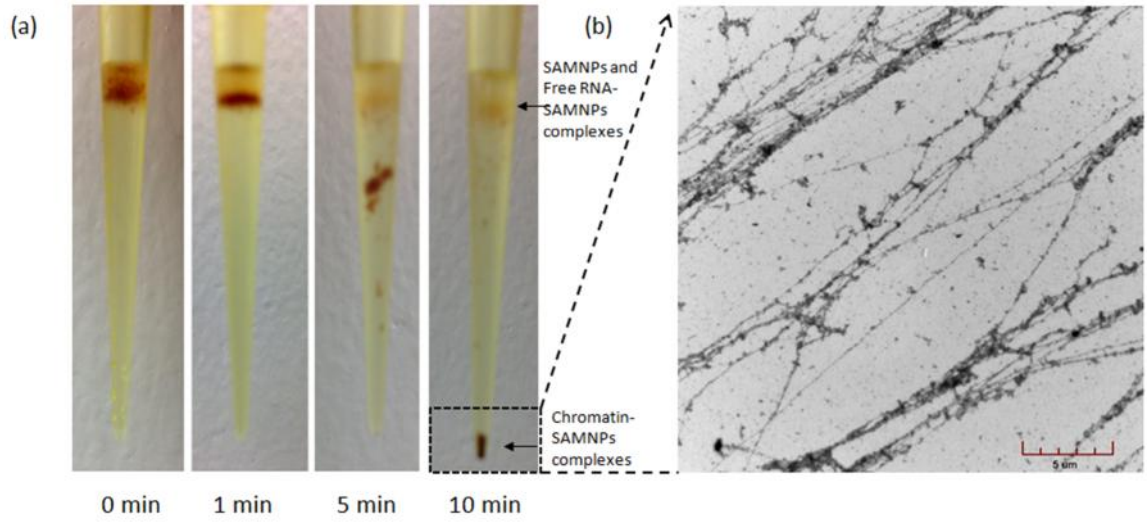

Figure.6.2 Optical images of the pipette tip during magnetophoretic chromatography of chromatin-SAMNPs in 25% (m/v) PEG solution (a). In the experiment time scale, the chromatin-SAMNPs complexes were formed at the bottom of the tip; while the free RNA-SAMNPs and free SAMNPs were kept between the interphase of the two solutions. TEM images of chromatin released from the chromatin-SAMNPs complexes in PBS solution (b).

Due to the reversible process of chromatin and SAMNPs interaction, removing the free SAMNPs from the collected chromatin-SAMNPs complexes would increase the released chromatin in solution. In a compared study, 10 µg of chromatin was extracted from 1 million MCF7 cells using our previously reported method (Zhou and Irudayaraj, 2015a); while 14 µg of chromatin was extracted from the same amount of MCF7 cells using the magnetophoretic chromatography method. The extracted chromatin was visualized by TEM, as shown in Fig.6.2b.

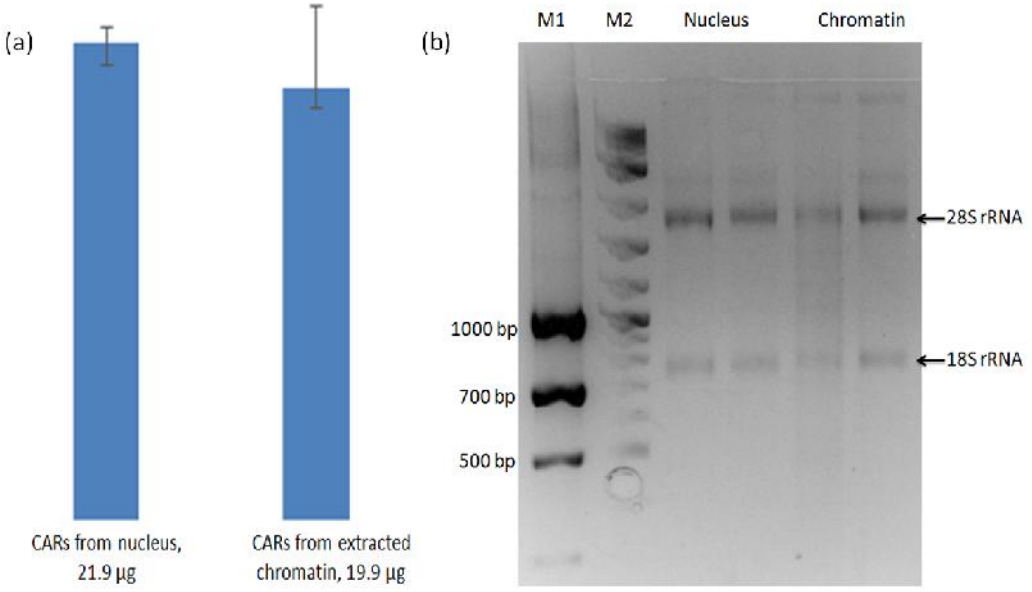

Figure.6.3 (a) Quantity of CARs extracted from isolated nuclei and magnetophoretic chromatography collected chromatin from 4 million cells. (b) Agarose gel electrophoresis analysis of CARs on a 2% RNase denatured gel.

After magnetophoretic chromatography, the chromatin-SAMNPs complexes were collected and submitted for chromatin associated RNAs extraction using a commercial kit, which was completed within 45 min. In a parallel study, CARs were extracted from the isolated nuclei using the same kit. The purity of CARs was determined by

OD_{260}/OD_{280} with a value of 2.05, which indicated there was negligible genomic DNA contamination. The quantity of extracted CARs was also determined, as shown in Fig.6.3a. Agarose gel electrophoresis analysis of the isolated CARs indicated that the major RNAs were rRNA due to rRNA-tree formed at the nucleoli (Hontz et al., 2008). Interestingly, we found a CAR band with size about 15 kb in the CARs extracted from magnetophoretic chromatography collected chromatin. These could possibly imply the chromatin associated long non-coding RNAs.

The quality of CARs was evaluated by real-time PCR (qPCR). The fold change of each CAR was calculated according to the CARs extracted from nuclei, as shown in Fig.6.4. The level of β-actin in the extracted CARs, as an internal control, was 5 times lower in the magnetophoretic chromatography collected chromatin compared to CARs extracted from nuclei. As expected, the CARs (MEG3, Neat1, HULC and MALAT1) were 3-8 times higher in the magnetophoretic chromatography collected chromatin than in the nuclear fraction. This is due to the removal of free RNAs unbound to chromatin during the magnetophoretic chromatography process. Interesting HOTAIR was decreased in the collected chromatin, possibly because HOTAIR is primarily located in the cytoplasm of carcinoma cells (Lv et al., 2013).

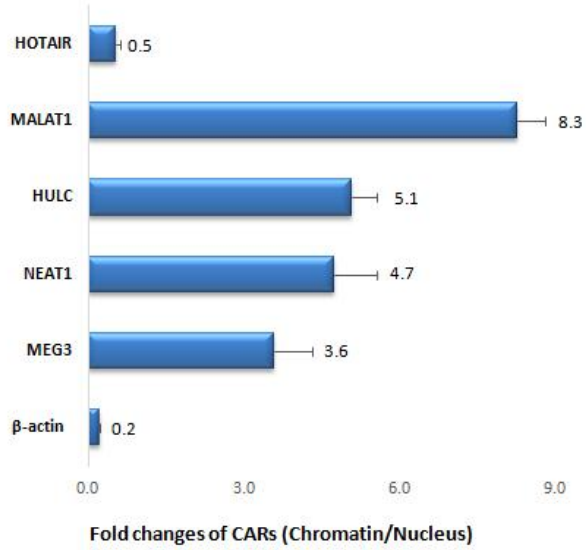

Figure.6.4 The fold change of CARs extracted from magnetophoretic chromatography collected chromatin compared to that from isolated nuclei. The CARs (MEG3, Neat1, HULC and MALAT1) were 3-8 times higher in the magnetophoretic chromatography collected chromatin than in the nuclear fraction, while β-actin and HOTAIR was lower.

In conclusion, we have developed a novel assay to extract chromatin associated RNAs using magnetophoretic chromatography. The total assay time including cell separation, chromatin collection and chromatin associated RNA extraction can be completed within 2h. The SAMNPs could non-specifically adsorb on to the chromatin with the help of isopropanol, to realize the subsequent unbiased extraction of CARs. Magnetophoretic chromatography was used to separate chromatin-SAMNPs complexes from free RNA-SAMNPs complexes and the free SAMNPs. This novel strategy not only improves the chromatin extraction efficiency, but also assists in the extraction of CARs by removing free RNAs. The mild and ultrafast magnetic separation process keeps CARs from degrading. Thus, we have developed an ultrafast, unbiased and cost-effective method for

the extraction of CARs, which is essential to ensure the accuracy of transcriptomic analyses.

Table 6.1: Nucleotide sequence of primers for qPCR.

Name	Primer sequence
HOTAIR-F	5’-CAGTGGGGAACTCTGACTCG-3’
HOTAIR-R	5’-GTGCCTGGTGCTCTCTTACC-3’
NEAT1-F	5’-TGGCTAGCTCAGGGCTTCAG-3’
NEAT1-R	5’-TCTCCTTGCCAAGCTTCCTTC-3’
HULC-F	5'-TCATGATGGAATTGGAGCCTT-3'
HULC-R	5'-CTCTTCCTGGCTTGCAGATTG-3'
MALAT1-F	5'-TAGGAAGACAGCAGCAGACAGG-3'
MALAT1-R	5'-TTGCTCGCTTGCTCCTCAGT-3'
MEG3-F	5'-GCCAAGCTTCTTGAAAGGCC-3'
MEG3-R	5'-TTCCACGGAGTAGAGCGAGTC-3'
β-actin-F	5′-AGCGAGCATCCCCCAAAGTT-3’
β-actin-R	5′-GGGCACGAAGGCTCATCATT-3’

CHAPTER 7. CHROMATIN FIBERS HAVE A RBANCHING STRUCTURE

7.1 Introduction

According to textbooks, the approximately 2 meters of genomic DNA progressively folds and packs itself into compact chromatin forming 10 nm “beads-on-a-string” fiber, 30 nm chromatin fiber and thicker fibers with diameter beyond 30 nm. The detailed structure of *in vitro* reconstituted 30-nm chromatin fiber, double helix twisted by tetranucleosomal units, has been resolved using single particle cryogenic electron microscopy (cryo-EM) (Song et al., 2014). However, other studies using cryogenic electron tomography (cryo-ET) (Eltsov et al., 2008), small-angle X-ray scattering (SAXS) (Maeshima et al., 2014), and electron spectroscopic imaging experiments do not support the exist of 30-nm chromatin fiber *in vivo*. Recently stochastic optical reconstruction microscopy (STORM) with ~20 nm resolution was applied to visualize and quantify chromatin fiber width by imaging fluorescence tagged core histone proteins (Ricci et al., 2015), and it observed that heterogeneous “nucleosome clutches” occupy discrete domains along the chromatin fiber, and chromatin structure is heterogeneous containing both the 10 nm and the 30 nm fiber. A recent advancement in cryo-ET, using cryogenic focused ion beam (cryo-FIB) to study sectioned Hela nuclei, found that the 30-nm chromatin fiber had a speckled

appearance inside the nuclear sections (Li et al., 2015), which is consistent with the finding of nucleosomal clutches.

The heterogeneous *in vivo* chromatin fiber undergoes regulated condensation-decondensation reactions. This explains the existence of heterochromatin and euchromatin, as well as the regulation of gene expression depending on if the chromatin is “closed” or “opened”. However, how does the 30-nm fiber interact with the 10-nm fiber? What is the higher order chromatin structure beyond 30-nm fiber? Cryo-ET provides a powerful tool to bridge the resolution gap between molecular structures of individual proteins as revealed by cryo-EM single particle method and larger cellular architectures as observed by the optical microscopy. However, due to the condensed nature of the nucleus and chromatin as well as the similar contrast between chromatin and its surrounding proteins and ions, little information could be obtained from the 3D reconstructed images. We have partially addressed the problem by extracting native chromatin from mammalian cells, and further preserving its native structure in vitreous ice. We observed that the native chromatin holds a branching structure. Moreover, the chromatin organizes into branching structure at different levels, and the structure commonly exists in different types of mammalian cells such as human MCF7 cells, Hela cells, S1 cells and healthy blood cells as well as mouse neural stem cells.

7.2 Experiment

Human MCF7 cells, Hela cells and mouse neural stem cells were cultured using standard protocols. Healthy human blood samples were gained from Basudev Chowdhury as part of the study entitled, “Quantification of 5-methylcytosine, 5-hydroxymethylcytosine and 5-carboxylcytosine from the blood of cancer patients by an enzyme-based immunoassay”.

Native chromatin was extracted using solid phase reversible immobilization (SPRI) method by salicylic acid coated magnetic nanoparticles (SAMNPs). Briefly, the cells were either enriched by centrifugation or by magnetic separation. The collected cells were lysed in buffer containing 250 mM SDS, 1 mM EDTA, 1 mM PMSF, 0.5 mM EGTA and 2% protease inhibitor Cocktail, following by adding SAMNPs. The complexes were pipetted up and down slowly 20 times with a 200-uL pipette tip and further incubated for 10 min. Isopropanol was added to the suspension to form nucleic acids-SAMNPs complexes and incubated for another 10 min on ice. The chromatin-SAMNPs complexes were further isolated by an external magnetic field, and washed once with 70% (v/v) ethanol. The chromatin was eluted by adding 50 µl 1x PBS solution. The concentration of chromatin was determined by a Nanodrop spectroscopy.

Cryo ET sample preparation and data collection. The extracted native chromatin samples with a concentration of 220 ng/µl were used. 10 µl of chromatin sample was mixed with 12 µl of 10 nm gold nanoparticle solution. An aliquot of 3 µl of the mixture was absorbed onto the glow-discharged 400 mesh Lacey carbon holey grids (Ted Pella, INC, CA, USA) for 1 min, manually blotted by putting a piece of #1 filter paper on the edge of the grid

using 1 min blotting time at 50% humidity, and then plunged into liquid ethane cooling by liquid nitrogen inside an FEI Vitrobot Mark III (FEI, Eindhoven). The grids were transferred into an FEI Titan Krios electron microscope (FEI, Eindhoven) equipped with a field emission gun and operated at 300 kV. Cryo-EM micrographs of chromatin samples were obtained using a K2 direct electron director and at 11,000 x nominal magnification corresponding to a pixel size of 1.3 Å/pixel on the specimen level. The images of the chromatin branching structure were automatically recorded using the software package Leginon. The nominal defocus was set to -4 µm for all sessions. An angular range was set to -56 to +56 degree with increments of 2 degrees. Before image acquisition, the microscope was carefully aligned at a reference position by using parallel illumination and by minimizing the beam tile with a coma-free alignment procedure. The total dosage for each tomography series was set to ~ 80 e-/Å2, and the dose for each frame was approximately 0.98 e-/Å2.

Before image processing, the sub-frames at each tilt angle were motion corrected and then averaged. The averaged tilted images were stacked into a series by newstack and addtostack functions. All togographic reconstructions were obtained with the program Imod (http://bio3d.colorado.edu/).

Negative stained electron tomography sample preparation and data collection. The extracted native chromatin samples with a concentration of 50 ng/µl were used. 10 µl of chromatin sample was mixed with 10 µl of 16 nm gold nanoparticle solution. An aliquot of 4µl of the mixture was absorbed onto the glow-discharged 200 mesh carbon continuous grids (Ted Pella, INC, CA, USA) for 1 min, manually blotted by putting a piece of #1 filter paper on the edge of the grid, and stained with 4 µl of uranyl acetate

(UA, 2%) for 10s. After removing the UA, the grids were briefly washed with 4 µl water and further air dried. The grids were transferred into an FEI T20 electron microscope (FEI, Eindhoven) equipped with a LaB6 filament and operated at 200 kV. Negative stained micrographs of chromatin samples were obtained using a Gatan camera and at different magnifications. The images of the chromatin branching structure were automatically recorded using the software package SerialEM. The nominal defocus was set to -4 µm for all sessions. An angular range was set to -70 to +70 degree with increments of 2 degrees. Before image acquisition, the microscope was carefully aligned. The produced tomography stacks were reconstructed by IMOD (http://bio3d.colorado.edu/).

7.3 Results and Discussion

We have determined a three-dimensional (3D) cryogenic electron microscopy (cryo-EM) structure of chromatin fibers extracted from MCF7 eukaryotic cells, as shown in Fig.7.1. The native chromatin fibers were extracted by solid phase reversible immobilization (SPRI) using salicylic acid coated magnetic nanoparticles (SAMNPs) as a carrier, and stored in the physiological conditions in1x PBS (containing 137 mM NaCl, 2.7 mM KCl, 10 mM Na_2HPO_4 and 1.8 mM KH_2PO_4). To preserve the native chromatin structure, neither pre-fixation by paraformaldehyde or glutaraldehyde nor fragmentation by MNase digestion or solication was introduced during the extraction process. Slow pipetting was performed to minimize the mechanical shearing force on the native chromatin. The concentration of extracted native chromatin fibers was determined using a Nanodrop

spectrophotometer with a concentration of 220 ng/µl (Fig. 7.2). The length of extracted native chromatin could reach 100 µm on a 200 mesh continuous carbon coated grid. However, due to high viscosity of concentrated chromatin and its large size, mounting chromatin on holey grids such as c-flat and Quotainfoil in cryogenic conditions is challenging. Either no chromatin was observed or chromatin fibers stored in thick vitreous ice which impeded tomography data collection. Moreover, the chromatin was easy to tangle together forming amorphous structure as shown in Fig. 7.3.

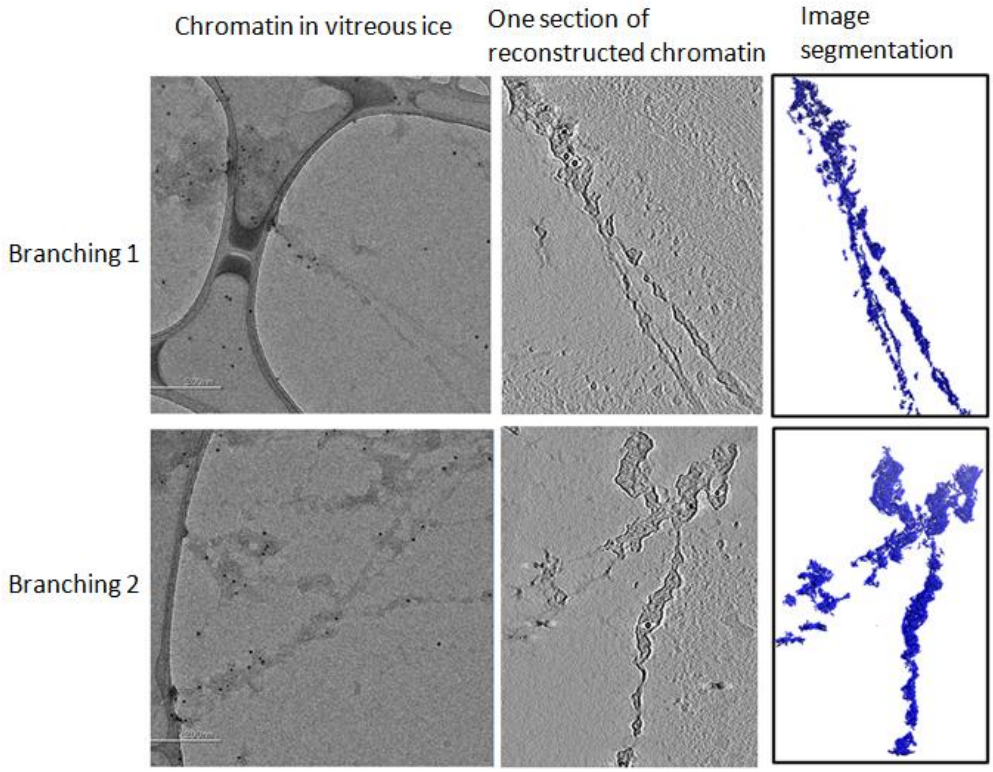

Figure 7.1 Chromatin branching structure. Extracted native chromatin in vitreous ice (left), one section of reconstructed chromatin using IMOD (middle) and Image segmentation of chromatin using Chimera (right).

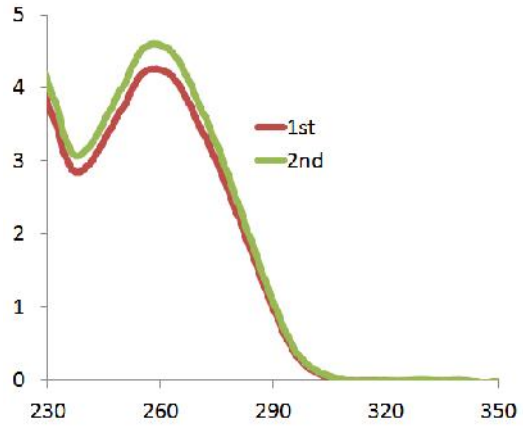

Figure 7.2 The absorption spectra of extracted chromatin.

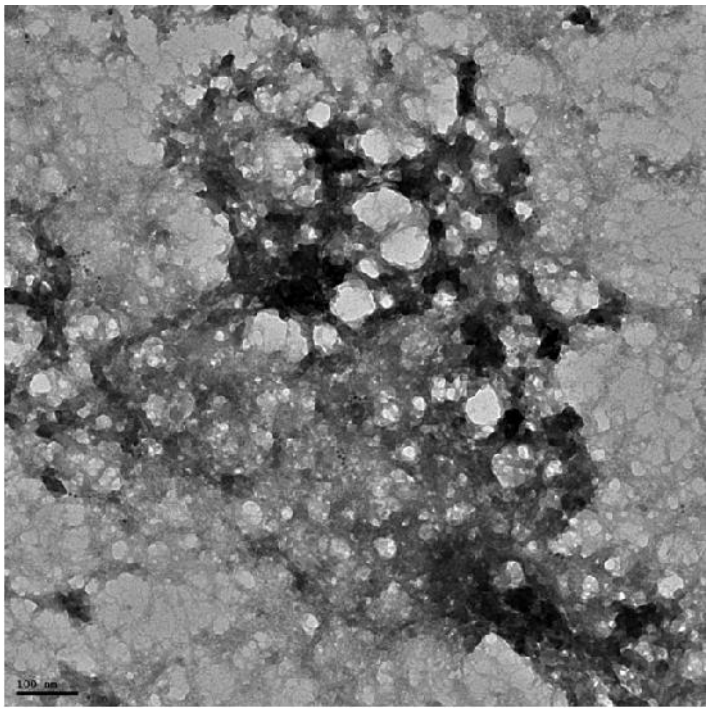

Figure 7.3 Unligned chromatin fibers forming an amorphous structure.

These challenges were resolved by manual blotting by putting filter paper on the edge of lacey carbon holey grids. The viscous concentrated chromatin fibers remain on the glow discharged grids after manual blotting; whereas after automatically blotting the chromatin

fibers disappeared due to sticking to the filter paper. The manual filtering process introduces a mild force within the liquid to align the chromatin fibers in one specific direction allowing their fibers not tangled and allowing fine structure observed more easily. Moreover, the holes of Lacey carbon holey girds are thick enough to keep a single layer of chromatin fibers in a thin layer of vitreous ice with optimized blotting time. Appling the native chromatin extraction technique and the optimized conditions for preparing chromatin sample in vitreous ice, we observed that the native chromatin fibers hold a branching structure (Fig. 7.1). The long chromatin fibers in vitreous ice could be directly visualized because of the high contrast of DNA molecules. Compared to reports from other group showing chromatin arranged in parallel array, we observed that chromatin had a branching structure. After 3D reconstruction of the tomography images using IMOD, we found that the branching structure was not formed by randomly twisted chromatin fibers as cryogenic electron tomography has the powder to determine the small distance between twisted but not well attached chromatin fibers. Here, we termed the thick regions on the branching structure as “roots”, and the thin region as “branches”. Chromatin insides the nucleus requires multiple levels of condensation and folding to fit its huge size into the relative small nucleus. At the same time, some ordered structure is necessary to allow it to open and unwind to meet demands such as replication and translation. The branching structure at the 30 nm chromatin fiber level would be a good example of a structure designed to meet these demands. Genes located in the root in the form of 30 nm fibers are silenced, while genes located in the branches in the form of 10 nm fibers have higher chance of being expressed. Moreover, the 30-nm fibers might have

various conformational states that are involved in the transition from inactive heterochromatin to euchromatin that is active in transcription or replication. However, the 30 nm chromatin fibers still need to be condensed further, higher levels of chromatin condensation and thicker chromatin fibers are necessary. Whether the 30 nm chromatin fibers form other thicker fibers is currently unknown. Due to the discontinuities of Lacey carbon holey grids and dose sensitivity of vitreous ice, we observed the MCF7 chromatin fibers at room temperature on continuous carbon grids and stained with UA (2%) to increase the contrast. Surprisingly, we found that higher order structure of chromatin fibers beyond 30 nm also possess a branching structure. Moreover, different types of branching structure were observed, as shown in Fig.7.4. We performed statistical analysis on the different branching structures. Based on the diameter of the root, the branch structure can be classified into at least 4 categories (Fig. 5): L1 (fibers > 241 nm), L2 (181~240 nm), L3 (31~180 nm) and L4 (11~30 nm). We measured tens of branching structure and found out the distribution of branching structure at different levels according to the diameter of root, as shown in Fig. 5. The chromatin fiber diameter distribution of all the observed branching structures was also given in Fig. 5. It also indicated that the portion of chromatin fibers with a diameter 30 ± 10 nm is 27% among the observed branching structures. Given that the major chromatin fibers were the basic 10 nm bead-on-a-string structure; the portion of 30 nm chromatin fibers was relatively low inside the nucleus. This is in consistent with the cryogenic section data observed by Li. et al where the 30 nm chromatin fibers inside the nucleus had a speckled pattern. The branching structure was also observed in other eukaryotic cells, such as cultured human Hela cells, mouse neural stem cells and human white blood cells, as shown in Fig.

6~8, respectively. Thus, the branching structure of chromatin fibers is a general structure inside eukaryotic cells.

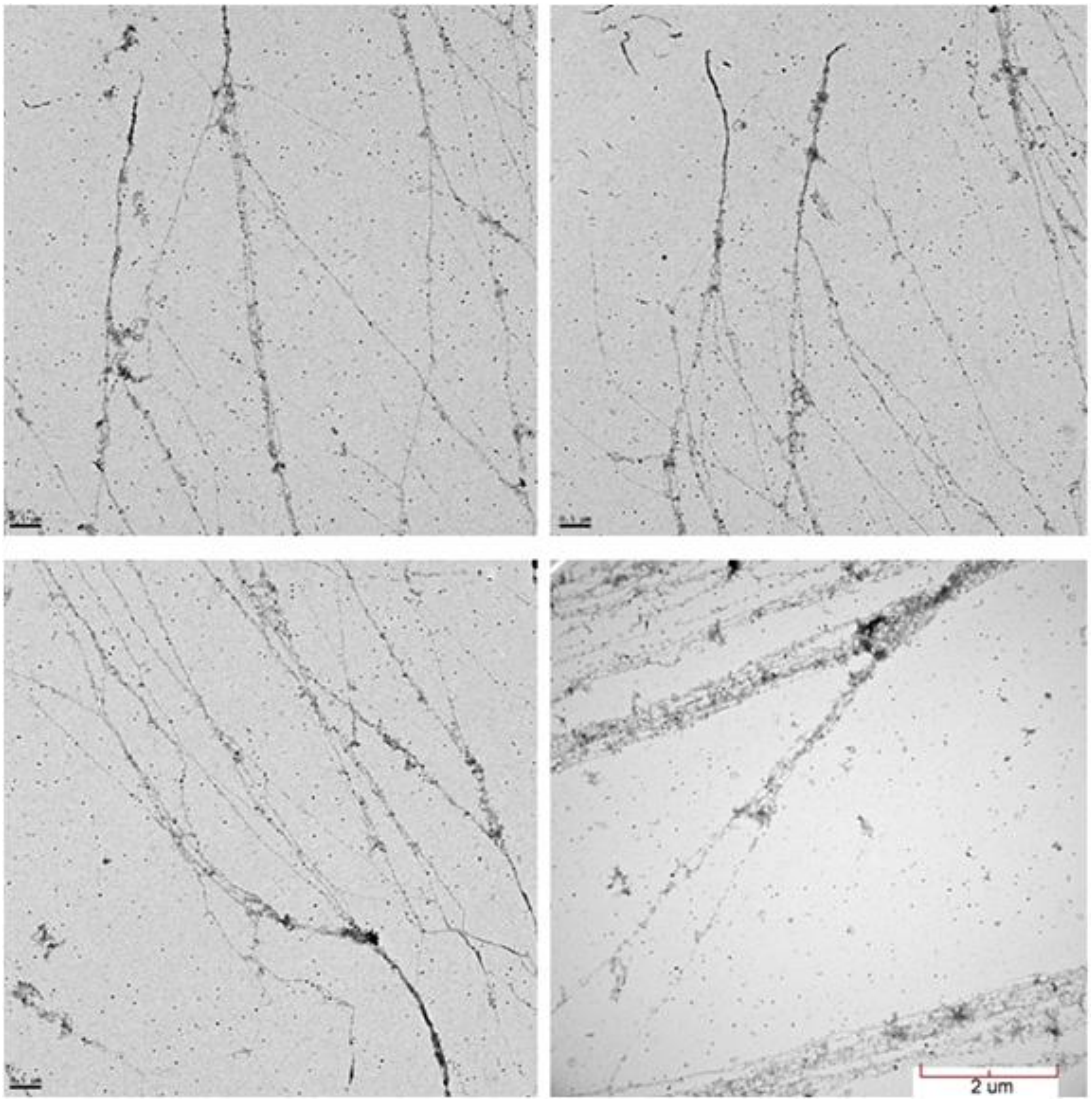

Figure 7.4 The chromatin branching structure of MCF7 cells. The branching structure is formed at different levels.

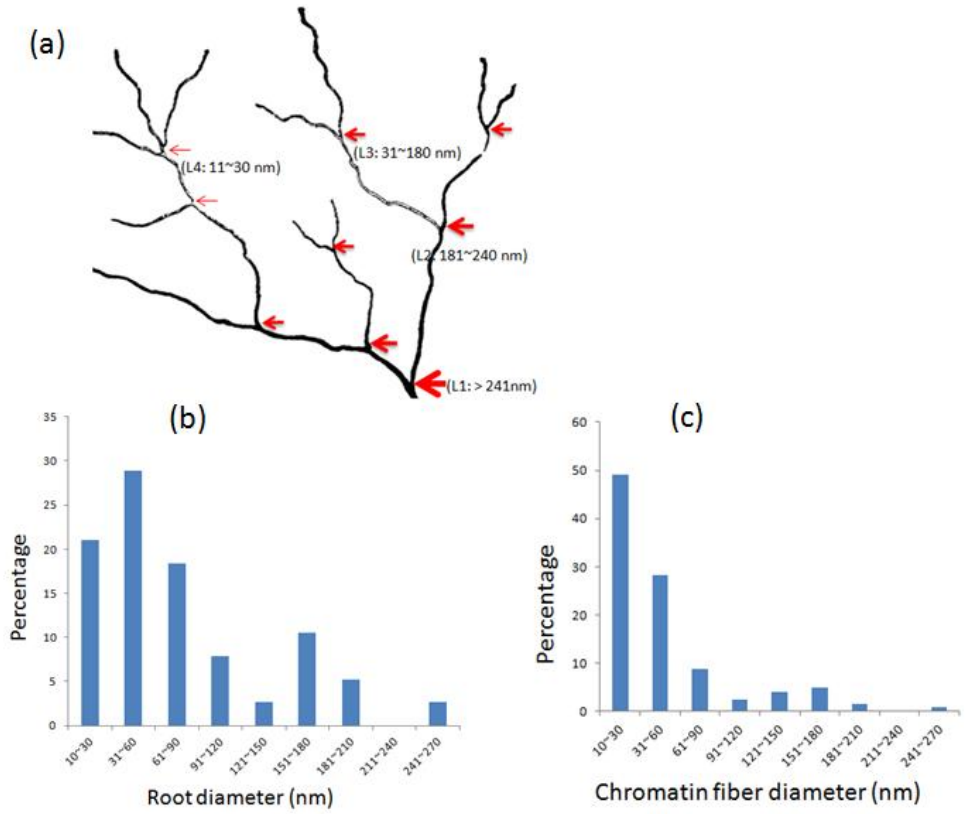

Figure 7.5 (a) Schematic diagram of chromatin branching structure at four levels. The roots (red arrow) have diameter at levels of 11~30 nm, 31~180 nm, 181~240 nm, > 241 nm. (b) statistical analysis of root diameter. (c) statistical analysis of chromatin fiber diameter.

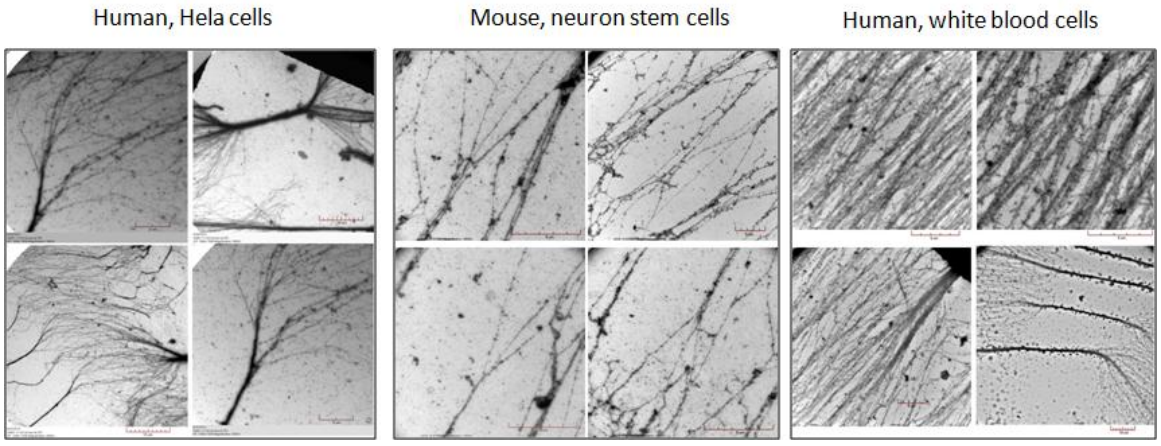

Figure 7.6 Chromatin branching structure exists in eukaryotic cells: human Hela cells (left), mouse neural stem cells (middle) and human white blood cells.

LIST OF REFERENCES

LIST OF REFERENCES

Abad, P.C., Lewis, J., Mian, I.S., Knowles, D.W., Sturgis, J., Badve, S., Xie, J., and Lelièvre, S.A. (2007). NuMA influences higher order chromatin organization in human mammary epithelium. Molecular biology of the cell *18*, 348-361.

Adomas, A., and Wade, P. (2013). Chromatin Structure and Gene Expression: Function Follows Form. In Environmental Epigenomics in Health and Disease, R.L. Jirtle, and F.L. Tyson, eds. (Springer Berlin Heidelberg), pp. 189-205.

Akbarzadeh, A., Samiei, M., and Davaran, S. (2012). Magnetic nanoparticles: preparation, physical properties, and applications in biomedicine. Nanoscale Research Letters *7*, 144-144.

Amaral, P.P., Dinger, M.E., Mercer, T.R., and Mattick, J.S. (2008). The Eukaryotic Genome as an RNA Machine. Science *319*, 1787-1789.

Bartke, T., Vermeulen, M., Xhemalce, B., Robson, S.C., Mann, M., and Kouzarides, T. (2010). Nucleosome-Interacting Proteins Regulated by DNA and Histone Methylation. Cell *143*, 470-484.

Basu, S., Chatterjee, S., Bandyopadhyay, A., and Sarkar, K. (2013). Potential application of superparamagnetic nanoparticles for extraction of bacterial genomic DNA from contaminated food and environmental samples. Journal of the Science of Food and Agriculture *93*, 788-793.

Bednar, J., Horowitz, R.A., Dubochet, J., and Woodcock, C.L. (1995). Chromatin conformation and salt-induced compaction: three-dimensional structural information from cryoelectron microscopy. J Cell Biol *131*, 1365-1376.

Bednar, J., Horowitz, R.A., Grigoryev, S.A., Carruthers, L.M., Hansen, J.C., Koster, A.J., and Woodcock, C.L. (1998). Nucleosomes, linker DNA, and linker histone form a unique structural motif that directs the higher-order folding and compaction of chromatin. Proc Natl Acad Sci U S A *95*, 14173-14178.

Beveridge, J.S., Stephens, J.R., and Williams, M.E. (2011). The use of magnetic nanoparticles in analytical chemistry. Annual Review of Analytical Chemistry *4*, 251-273.

Bhorjee, J.S., and Pederson, T. (1973). Chromatin. Its isolation from cultured mammalian cells with particular reference to contamination by nuclear ribonucleoprotein particles. Biochemistry *12*, 2766-2773.

Bhorjee, J.S., and Pederson, T. (1976). Rapid, preparative-scale purification of chromatin proteins. Biochimica et Biophysica Acta (BBA) - Nucleic Acids and Protein Synthesis *418*, 154-159.

Boguslawski, S.J., Smith, D.E., Michalak, M.A., Mickelson, K.E., Yehle, C.O., Patterson, W.L., and Carrico, R.J. (1986). Characterization of monoclonal antibody to DNA · RNA and its application to immunodetection of hybrids. Journal of Immunological Methods *89*, 123-130.
Bonner, J., Dahmus, M.E., Fambrough, D., Huang, R.-c.C., Marushige, K., and Tuan, D.Y.H. (1968). The Biology of Isolated Chromatin: Chromosomes, biologically active in the test tube, provide a powerful tool for the study of gene action. Science *159*, 47-56.
Cai, X., and Cullen, B.R. (2007). The imprinted H19 noncoding RNA is a primary microRNA precursor. RNA *13*, 313-316.
Cardoso, M.C., Schneider, K., Martin, R.M., and Leonhardt, H. (2012). Structure, function and dynamics of nuclear subcompartments. Current Opinion in Cell Biology *24*, 79-85.
Carruthers, L.M., Bednar, J., Woodcock, C.L., and Hansen, J.C. (1998). Linker histones stabilize the intrinsic salt-dependent folding of nucleosomal arrays: mechanistic ramifications for higher-order chromatin folding. Biochemistry *37*, 14776-14787.
Caudron-Herger, M., and Rippe, K. (2012). Nuclear architecture by RNA. Current Opinion in Genetics & Development *22*, 179-187.
Cedar, H., and Bergman, Y. (2009). Linking DNA methylation and histone modification: patterns and paradigms. Nat Rev Genet *10*, 295-304.
Chambers, W.H., Taylor, J.R., and Klesius, P.H. (1983). Isolation of bovine polymorphonuclear leukocytes by density gradient centrifugation. Veterinary Immunology and Immunopathology *5*, 197-202.
Chen, J., Odenike, O., and Rowley, J.D. (2010). Leukaemogenesis: more than mutant genes. Nat Rev Cancer *10*, 23-36.
Chowdhury, B., Cho, I.-H., Hahn, N., and Irudayaraj, J. (2014). Quantification of 5-methylcytosine, 5-hydroxymethylcytosine and 5-carboxylcytosine from the blood of cancer patients by an enzyme-based immunoassay. Analytica chimica acta *852*, 212-217.
Ciccia, A., and Elledge, S.J. (2010). The DNA Damage Response: Making It Safe to Play with Knives. Molecular Cell *40*, 179-204.
Clark, M.B., Johnston, R.L., Inostroza-Ponta, M., Fox, A.H., Fortini, E., Moscato, P., Dinger, M.E., and Mattick, J.S. (2012). Genome-wide analysis of long noncoding RNA stability. Genome research *22*, 885-898.
Cohen, A.L., and Jia, S. (2014). Noncoding RNAs and the borders of heterochromatin. Wiley Interdisciplinary Reviews: RNA *5*, 835-847.
Conway O' Brien, E., Prideaux, S., and Chevassut, T. (2014). The Epigenetic Landscape of Acute Myeloid Leukemia. Advances in Hematology *2014*, 15.
Cook, P.R., and Brazell, I.A. (1975). Supercoils in human DNA. Journal of Cell Science *19*, 261-279.
Cremer, T., and Cremer, C. (2001). Chromosome territories, nuclear architecture and gene regulation in mammalian cells. Nature reviews genetics *2*, 292-301.
Cremer, T., and Cremer, M. (2010). Chromosome Territories. Cold Spring Harbor perspectives in biology *2*.
Cuddapah, S., Barski, A., Cui, K., Schones, D.E., Wang, Z., Wei, G., and Zhao, K. (2009). Native Chromatin Preparation and Illumina/Solexa Library Construction. Cold Spring Harbor Protocols *2009*, pdb.prot5237.

Dahmus, M.E., and Bonner, J. (1969). Nucleoproteins in regulation of gene function. Paper presented at: Fed Proc.
DeAngelis, M.M., Wang, D.G., and Hawkins, T.L. (1995). Solid-phase reversible immobilization for the isolation of PCR products. Nucleic Acids Research *23*, 4742-4743.
Deng, X., and Meller, V.H. (2006). Non-coding RNA in fly dosage compensation. Trends in Biochemical Sciences *31*, 526-532.
Diermeier, S.D., Schubert, T., and Längst, G. (2014). Deep Sequencing of Small Chromatin-Associated RNA: Isolation and Library Preparation. In Functional Analysis of DNA and Chromatin (Springer), pp. 343-353.
Eltsov, M., MacLellan, K.M., Maeshima, K., Frangakis, A.S., and Dubochet, J. (2008). Analysis of cryo-electron microscopy images does not support the existence of 30-nm chromatin fibers in mitotic chromosomes in situ. Proceedings of the National Academy of Sciences *105*, 19732-19737.
Fessing, M.Y. (2014). Gene Regulation at a Distance: Higher-Order Chromatin Folding and the Coordinated Control of Gene Transcription at the Epidermal Differentiation Complex Locus. Journal of Investigative Dermatology *134*, 2307-2310.
Fraga, M.F., Ballestar, E., Villar-Garea, A., Boix-Chornet, M., Espada, J., Schotta, G., Bonaldi, T., Haydon, C., Ropero, S., Petrie, K., *et al.* (2005). Loss of acetylation at Lys16 and trimethylation at Lys20 of histone H4 is a common hallmark of human cancer. Nat Genet *37*, 391-400.
Fussner, E., Ching, R.W., and Bazett-Jones, D.P. (2011a). Living without 30 nm chromatin fibers. Trends in Biochemical Sciences *36*, 1-6.
Fussner, E., Ching, R.W., and Bazett-Jones, D.P. (2011b). Living without 30nm chromatin fibers. Trends in Biochemical Sciences *36*, 1-6.
Gardner, K.E., Allis, C.D., and Strahl, B.D. (2011). Operating on chromatin, a colorful language where context matters. Journal of Molecular Biology *409*, 36-46.
Ge, C., Yu, L., Fang, Z., and Zeng, L. (2013). An Enhanced Strip Biosensor for Rapid and Sensitive Detection of Histone Methylation. Analytical Chemistry *85*, 9343-9349.
Glozak, M.A., Sengupta, N., Zhang, X., and Seto, E. (2005). Acetylation and deacetylation of non-histone proteins. Gene *363*, 15-23.
Greenblatt, S.M., and Nimer, S.D. (2014). Chromatin modifiers and the promise of epigenetic therapy in acute leukemia. Leukemia *28*, 1396-1406.
Groth, A., Rocha, W., Verreault, A., and Almouzni, G. (2007). Chromatin Challenges during DNA Replication and Repair. Cell *128*, 721-733.
Guenther, M.G., Lawton, L.N., Rozovskaia, T., Frampton, G.M., Levine, S.S., Volkert, T.L., Croce, C.M., Nakamura, T., Canaani, E., and Young, R.A. (2008). Aberrant chromatin at genes encoding stem cell regulators in human mixed-lineage leukemia. Genes & development *22*, 3403-3408.
Guillou, E., Ibarra, A., Coulon, V., Casado-Vela, J., Rico, D., Casal, I., Schwob, E., Losada, A., and Méndez, J. (2010). Cohesin organizes chromatin loops at DNA replication factories. Genes & development *24*, 2812-2822.
Gutierrez, S., and Romero-Oliva, F. (2013). Epigenetic changes: a common theme in acute myelogenous leukemogenesis. Journal of Hematology & Oncology *6*, 57.

Hall, L.L., Carone, D.M., Gomez, A.V., Kolpa, H.J., Byron, M., Mehta, N., Fackelmayer, F.O., and Lawrence, J.B. (2014). Stable C 0 T-1 Repeat RNA is abundant and is associated with euchromatic interphase chromosomes. Cell *156*, 907-919.
Hansen, J.C. (2002). Conformational dynamics of the chromatin fiber in solution: determinants, mechanisms, and functions. Annu Rev Bioph Biom *31*, 361-392.
Harlow, R., and Wells, J. (1975). Preparation of membrane-free chromatin bodies from avian erythroid cells and analysis of chromatin acidic proteins. Biochemistry *14*, 2665-2674.
Hawkins, T.L., O'Connor-Morin, T., Roy, A., and Santillan, C. (1994). DNA purification and isolation using a solid-phase. Nucleic Acids Research *22*, 4543.
Heard, E., and Bickmore, W. (2007). The ins and outs of gene regulation and chromosome territory organisation. Current Opinion in Cell Biology *19*, 311-316.
Herceg, Z., and Hainaut, P. (2007). Genetic and epigenetic alterations as biomarkers for cancer detection, diagnosis and prognosis. Molecular Oncology *1*, 26-41.
Herr, J.K., Smith, J.E., Medley, C.D., Shangguan, D., and Tan, W. (2006). Aptamer-Conjugated Nanoparticles for Selective Collection and Detection of Cancer Cells. Analytical Chemistry *78*, 2918-2924.
Hontz, R.D., French, S.L., Oakes, M.L., Tongaonkar, P., Nomura, M., Beyer, A.L., and Smith, J.S. (2008). Transcription of multiple yeast ribosomal DNA genes requires targeting of UAF to the promoter by Uaf30. Molecular and Cellular Biology *28*, 6709-6719.
Horowitz-Scherer, R.A., and Woodcock, C.L. (2006). Organization of interphase chromatin. Chromosoma *115*, 1-14.
Huang, Y.-F., Wang, Y.-F., and Yan, X.-P. (2010). Amine-Functionalized Magnetic Nanoparticles for Rapid Capture and Removal of Bacterial Pathogens. Environmental science & technology *44*, 7908-7913.
Jiang, X., Jiang, X., Feng, S., Tian, R., Ye, M., and Zou, H. (2007). Development of Efficient Protein Extraction Methods for Shotgun Proteome Analysis of Formalin-Fixed Tissues. Journal of Proteome Research *6*, 1038-1047.
Kelley, R.L., and Kuroda, M.I. (2000). Noncoding RNA Genes in Dosage Compensation and Imprinting. Cell *103*, 9-12.
Kornberg, R.D., Lapointe, J.W., and Lorch, Y. (1989). [1] Preparation of nucleosomes and chromatin. In Methods in Enzymology, M.W. Paul, and D.K. Roger, eds. (Academic Press), pp. 3-14.
Kouassi, G.K., and Irudayaraj, J. (2006). Magnetic and Gold-Coated Magnetic Nanoparticles as a DNA Sensor. Analytical Chemistry *78*, 3234-3241.
Krivtsov, A.V., and Armstrong, S.A. (2007). MLL translocations, histone modifications and leukaemia stem-cell development. Nat Rev Cancer *7*, 823-833.
Krivtsov, A.V., Feng, Z., Lemieux, M.E., Faber, J., Vempati, S., Sinha, A.U., Xia, X., Jesneck, J., Bracken, A.P., Silverman, L.B., *et al.* (2008). H3K79 Methylation Profiles Define Murine and Human MLL-AF4 Leukemias. Cancer Cell *14*, 355-368.
Křížová, J., Španová, A., Rittich, B., and Horák, D. (2005). Magnetic hydrophilic methacrylate-based polymer microspheres for genomic DNA isolation. Journal of Chromatography A *1064*, 247-253.

Kulić, I., and Schiessel, H. (2003). Chromatin dynamics: nucleosomes go mobile through twist defects. Physical Review Letters *91*, 148103.
Kwon, D., Joo, J., Lee, J., Park, K.-H., and Jeon, S. (2013). Magnetophoretic Chromatography for the Detection of Pathogenic Bacteria with the Naked Eye. Analytical Chemistry *85*, 7594-7598.
Kwon, D., Lee, S., Ahn, M.M., Kang, I.S., Park, K.-H., and Jeon, S. (2015). Colorimetric detection of pathogenic bacteria using platinum-coated magnetic nanoparticle clusters and magnetophoretic chromatography. Analytica chimica acta *883*, 61-66.
Lago-Cachón, D., Rivas, M., López-Larrea, C., López-Vázquez, A., Martínez-Paredes, G., and García, J.A. (2014). HeLa cells separation using MICA antibody conjugated to magnetite nanoparticles. physica status solidi (c) *11*, 1043-1047.
Lanctot, C., Cheutin, T., Cremer, M., Cavalli, G., and Cremer, T. (2007). Dynamic genome architecture in the nuclear space: regulation of gene expression in three dimensions. Nat Rev Genet *8*, 104-115.
Lee, K., Cui, Y., Lee, L.P., and Irudayaraj, J. (2014). Quantitative imaging of single mRNA splice variants in living cells. Nat Nano *9*, 474-480.
Lee, K., Drachev, V.P., and Irudayaraj, J. (2011). DNA−Gold Nanoparticle Reversible Networks Grown on Cell Surface Marker Sites: Application in Diagnostics. ACS Nano *5*, 2109-2117.
Li, J., Chen, P., Sinogeeva, N., Gorospe, M., Wersto, R.P., Chrest, F.J., Barnes, J., and Liu, Y. (2002). Arsenic Trioxide Promotes Histone H3 Phosphoacetylation at the Chromatin of CASPASE-10 in Acute Promyelocytic Leukemia Cells. Journal of Biological Chemistry *277*, 49504-49510.
Li, X., Feng, H., Zhang, J., Sun, L., and Zhu, P. (2015). Analysis of chromatin fibers in Hela cells with electron tomography. Biophys Rep *1*, 51-60.
Liu, G., and Liu, P. (2010). Synthesis of monodispersed crosslinked nanoparticles decorated with surface carboxyl groups via soapless emulsion polymerization. Colloids and Surfaces A: Physicochemical and Engineering Aspects *354*, 377-381.
Liu, X., and Harada, S. (2001). DNA Isolation from Mammalian Samples. In Current Protocols in Molecular Biology (John Wiley & Sons, Inc.).
Lucchini, R., Wellinger, R.E., and Sogo, J.M. (2001). Nucleosome positioning at the replication fork. EMBO J *20*, 7294-7302.
Luger, K., Dechassa, M.L., and Tremethick, D.J. (2012). New insights into nucleosome and chromatin structure: an ordered state or a disordered affair? Nat Rev Mol Cell Biol *13*, 436-447.
Lv, X.-B., Lian, G.-Y., Wang, H.-R., Song, E., Yao, H., and Wang, M.-H. (2013). Long Noncoding RNA HOTAIR Is a Prognostic Marker for Esophageal Squamous Cell Carcinoma Progression and Survival. PLoS One *8*, e63516.
MacAlpine, D.M., and Almouzni, G. (2013). Chromatin and DNA Replication. Cold Spring Harbor perspectives in biology *5*.
Maeshima, K., Imai, R., Hikima, T., and Joti, Y. (2014). Chromatin structure revealed by X-ray scattering analysis and computational modeling. Methods *70*, 154-161.
McKnight, S.L., and Miller Jr, O.L. (1977). Electron microscopic analysis of chromatin replication in the cellular blastoderm drosophila melanogaster embryo. Cell *12*, 795-804.

Monahan, J.J., and Hall, R.H. (1975). Preparation of chromatin from tissue culture cells—A convenient method. Analytical Biochemistry *65*, 187-203.
Mondal, T., Rasmussen, M., Pandey, G.K., Isaksson, A., and Kanduri, C. (2010). Characterization of the RNA content of chromatin. Genome research *20*, 899-907.
Murphy, J.C., Wibbenmeyer, J.A., Fox, G.E., and Willson, R.C. (1999). Purification of plasmid DNA using selective precipitation by compaction agents. Nat Biotech *17*, 822-823.
Nakama, M., Kawakami, K., Kajitani, T., Urano, T., and Murakami, Y. (2012). DNA–RNA hybrid formation mediates RNAi-directed heterochromatin formation. Genes to Cells *17*, 218-233.
Nickerson, J.A., Krochmalnic, G., Wan, K.M., and Penman, S. (1989). Chromatin architecture and nuclear RNA. Proceedings of the National Academy of Sciences *86*, 177-181.
Okada, Y., Feng, Q., Lin, Y., Jiang, Q., Li, Y., Coffield, V.M., Su, L., Xu, G., and Zhang, Y. (2005). hDOT1L Links Histone Methylation to Leukemogenesis. Cell *121*, 167-178.
Pederson, T. (1977). Isolation and characterization of chromatin from the cellular slime mold, Dictyostelium discoideum. Biochemistry *16*, 2771-2777.
Peschansky, V.J., and Wahlestedt, C. (2013). Non-coding RNAs as direct and indirect modulators of epigenetic regulation. Epigenetics *9*, 3-12.
Prodělalová, J., Rittich, B., Španová, A., Petrová, K., and Beneš, M.J. (2004). Isolation of genomic DNA using magnetic cobalt ferrite and silica particles. Journal of Chromatography A *1056*, 43-48.
Quinodoz, S., and Guttman, M. (2014). Long noncoding RNAs: an emerging link between gene regulation and nuclear organization. Trends in cell biology *24*, 651-663.
Ragoczy, T., Bender, M.A., Telling, A., Byron, R., and Groudine, M. (2006). The locus control region is required for association of the murine β-globin locus with engaged transcription factories during erythroid maturation. Genes & development *20*, 1447-1457.
Ravindranath, S.P., Wang, Y., and Irudayaraj, J. (2011). SERS driven cross-platform based multiplex pathogen detection. Sensors and Actuators B: Chemical *152*, 183-190.
Rego, A., Sinclair, P.B., Tao, W., Kireev, I., and Belmont, A.S. (2008). The facultative heterochromatin of the inactive X chromosome has a distinctive condensed ultrastructure. Journal of Cell Science *121*, 1119-1127.
Ricci, Maria A., Manzo, C., García-Parajo, M.F., Lakadamyali, M., and Cosma, Maria P. (2015). Chromatin Fibers Are Formed by Heterogeneous Groups of Nucleosomes In Vivo. Cell *160*, 1145-1158.
Rodríguez-Campos, A., and Azorín, F. (2007). RNA Is an Integral Component of Chromatin that Contributes to Its Structural Organization. PLoS One *2*, e1182.
Roti, J., and Wright, W. (1987). Visualization of DNA loops in nucleoids from HeLa cells: assays for DNA damage and repair. Cytometry *8*, 461-467.
Šafařík, I., and Šafaříková, M. (1999). Use of magnetic techniques for the isolation of cells. Journal of Chromatography B: Biomedical Sciences and Applications *722*, 33-53.
Saha, A., Wittmeyer, J., and Cairns, B.R. (2006). Chromatin remodelling: the industrial revolution of DNA around histones. Nat Rev Mol Cell Biol *7*, 437-447.

Saiyed, Z.M., Parasramka, M., Telang, S.D., and Ramchand, C.N. (2007). Extraction of DNA from agarose gel using magnetic nanoparticles (magnetite or Fe3O4). Analytical Biochemistry *363*, 288-290.
Sarkar, T.R., and Irudayaraj, J. (2008). Carboxyl-coated magnetic nanoparticles for mRNA isolation and extraction of supercoiled plasmid DNA. Analytical Biochemistry *379*, 130-132.
Schubert, T., and Längst, G. (2013). Changes in higher order structures of chromatin by RNP complexes. RNA biology *10*, 175-179.
Shahal, T., Gilat, N., Michaeli, Y., Redy-Keisar, O., Shabat, D., and Ebenstein, Y. (2014). Spectroscopic Quantification of 5-Hydroxymethylcytosine in Genomic DNA. Analytical Chemistry *86*, 8231-8237.
Shan, Z., Jiang, Y., Guo, M., Bennett, J.C., Li, X., Tian, H., Oakes, K., Zhang, X., Zhou, Y., Huang, Q., *et al.* Promoting DNA loading on magnetic nanoparticles using a DNA condensation strategy. Colloids and Surfaces B: Biointerfaces, 247-254.
Shan, Z., Li, C., Zhang, X., Oakes, K.D., Servos, M.R., Wu, Q., Chen, H., Wang, X., Huang, Q., Zhou, Y., *et al.* (2011). Temperature-dependent selective purification of plasmid DNA using magnetic nanoparticles in an RNase-free process. Analytical Biochemistry *412*, 117-119.
Shan, Z., Wu, Q., Wang, X., Zhou, Z., Oakes, K.D., Zhang, X., Huang, Q., and Yang, W. (2010a). Bacteria capture, lysate clearance, and plasmid DNA extraction using pH-sensitive multifunctional magnetic nanoparticles. Analytical Biochemistry *398*, 120-122.
Shan, Z., Wu, Q., Wang, X., Zhou, Z., Oakes, K.D., Zhang, X., Huang, Q., and Yang, W. (2010b). Bacteria capture, lysate clearance, and plasmid DNA extraction using pH-sensitive multifunctional magnetic nanoparticles. Analytical Biochemistry *398*, 120-122.
Shan, Z., Zhou, Z., Chen, H., Zhang, Z., Zhou, Y., Wen, A., Oakes, K.D., and Servos, M.R. (2012a). PCR-ready human DNA extraction from urine samples using magnetic nanoparticles. J Chromatogr B Analyt Technol Biomed Life Sci *881-882*, 63-68.
Shan, Z., Zhou, Z., Chen, H., Zhang, Z., Zhou, Y., Wen, A., Oakes, K.D., and Servos, M.R. (2012b). PCR-ready human DNA extraction from urine samples using magnetic nanoparticles. Journal of Chromatography B *881–882*, 63-68.
Sharma, S., Kelly, T.K., and Jones, P.A. (2010). Epigenetics in cancer. Carcinogenesis *31*, 27-36.
Shishehbore, M., Afkhami, A., and Bagheri, H. (2011). Salicylic acid functionalized silica-coated magnetite nanoparticles for solid phase extraction and preconcentration of some heavy metal ions from various real samples. Chemistry Central Journal *5*, 1-10.
Song, F., Chen, P., Sun, D., Wang, M., Dong, L., Liang, D., Xu, R.-M., Zhu, P., and Li, G. (2014). Cryo-EM Study of the Chromatin Fiber Reveals a Double Helix Twisted by Tetranucleosomal Units. Science *344*, 376-380.
Sun, L., Yu, C., and Irudayaraj, J. (2007). Surface-Enhanced Raman Scattering Based Nonfluorescent Probe for Multiplex DNA Detection. Analytical Chemistry *79*, 3981-3988.
Sun, S., and Zeng, H. (2002). Size-Controlled Synthesis of Magnetite Nanoparticles. Journal of the American Chemical Society *124*, 8204-8205.

Szeszak, F., and Pihl, A. (1971). Content of DNA · RNA hybrids in rat liver chromatin. Biochimica et Biophysica Acta (BBA) - Nucleic Acids and Protein Synthesis *247*, 363-367.
Takizawa, T., Meaburn, K.J., and Misteli, T. (2008). The Meaning of Gene Positioning. Cell *135*, 9-13.
Tang, L., Zhang, W., Su, B., and Yu, B. (2013). Long noncoding RNA HOTAIR is associated with motility, invasion, and metastatic potential of metastatic melanoma. BioMed Research International *2013*.
Tremethick, D.J. (2007). Higher-order structures of chromatin: the elusive 30 nm fiber. Cell *128*, 651-654.
Unal, B., Durmus, Z., Kavas, H., Baykal, A., and Toprak, M.S. (2010). Synthesis, conductivity and dielectric characterization of salicylic acid–Fe3O4 nanocomposite. Materials Chemistry and Physics *123*, 184-190.
van Steensel, B. (2011). Chromatin: constructing the big picture. EMBO J *30*, 1885-1895.
Voso, M.T., D'Alò, F., Greco, M., Fabiani, E., Criscuolo, M., Migliara, G., Pagano, L., Fianchi, L., Guidi, F., Hohaus, S., *et al.* (2010). Epigenetic changes in therapy-related MDS/AML. Chemico-Biological Interactions *184*, 46-49.
Wan, J., Cai, W., Meng, X., and Liu, E. (2007). Monodisperse water-soluble magnetite nanoparticles prepared by polyol process for high-performance magnetic resonance imaging. Chemical Communications *0*, 5004-5006.
Wang, K.C., Yang, Y.W., Liu, B., Sanyal, A., Corces-Zimmerman, R., Chen, Y., Lajoie, B.R., Protacio, A., Flynn, R.A., Gupta, R.A., *et al.* (2011). A long noncoding RNA maintains active chromatin to coordinate homeotic gene expression. Nature *472*, 120-124.
Whitehouse, I., and Smith, D.J. (2013). Chromatin dynamics at the replication fork: there's more to life than histones. Current Opinion in Genetics & Development *23*, 140-146.
Woodcock, C.L., and Dimitrov, S. (2001). Higher-order structure of chromatin and chromosomes. Curr Opin Genet Dev *11*, 130-135.
Woodcock, C.L., and Ghosh, R.P. (2010). Chromatin higher-order structure and dynamics. Cold Spring Harb Perspect Biol *2*, a000596.
Woodcock, C.L., Safer, J.P., and Stanchfield, J.E. (1976a). Structural repeating units in chromatin. I. Evidence for their general occurrence. Exp Cell Res *97*, 101-110.
Woodcock, C.L., Sweetman, H.E., and Frado, L.L. (1976b). Structural repeating units in chromatin. II. Their isolation and partial characterization. Exp Cell Res *97*, 111-119.
Xie, X., Nie, X., Yu, B., and Zhang, X. (2007). Rapid enrichment of leucocytes and genomic DNA from blood based on bifunctional core–shell magnetic nanoparticles. Journal of Magnetism and Magnetic Materials *311*, 416-420.
Xie, X., Zhang, X., Yu, B., Gao, H., Zhang, H., and Fei, W. (2004a). Rapid extraction of genomic DNA from saliva for HLA typing on microarray based on magnetic nanobeads. Journal of Magnetism and Magnetic Materials *280*, 164-168.
Xie, X., Zhang, X., Zhang, H., Chen, D., and Fei, W. (2004b). Preparation and application of surface-coated superparamagnetic nanobeads in the isolation of genomic DNA. Journal of Magnetism and Magnetic Materials *277*, 16-23.

Zhang, Y., Hu, Z., Qin, H., Liu, F., Cheng, K., Wu, R.a., and Zou, H. (2013). Cell Nucleus Targeting for Living Cell Extraction of Nucleic Acid Associated Proteins with Intracellular Nanoprobes of Magnetic Carbon Nanotubes. Analytical Chemistry.
Zhang, Y., Hu, Z., Qin, H., Wei, X., Cheng, K., Liu, F., Wu, R.a., and Zou, H. (2012). Highly Efficient Extraction of Cellular Nucleic Acid Associated Proteins in Vitro with Magnetic Oxidized Carbon Nanotubes. Analytical Chemistry *84*, 10454-10462.
Zhou, Z., Cho, I.I.H., Shan, Z., and Irudayaraj, J. (2015). Cross-platform detection of epigenetic modifications from extracted chromatin in leucocytes from blood. Analytical Chemistry Research *4*, 39-44.
Zhou, Z., and Irudayaraj, J. A native chromatin extraction method based on salicylic acid coated magnetic nanoparticles and characterization of chromatin. Analyst *140*, 938-944.
Zhou, Z., Kadam, U.S., and Irudayaraj, J. One-stop genomic DNA extraction by salicylic acid-coated magnetic nanoparticles. Anal Biochem *442*, 249-252.

VITA

VITA

Zhongwu Zhou received a Bachelor of Agronomy degree in 2009 and a Master of Biochemistry and Molecular Biology degree in 2011 at Sichuan Agricultural University. He joined the PhD program in the Department of Agricultural and Biological Engineering at Purdue University (West Lafayette) in the spring of 2012. With his colleagues, he developed several techniques, such as genomic DNA extraction, native chromatin extraction, chromatin associated RNAs extraction and epigenetic marks detection, to study chromatin. One of his most important discoveries is that chromatin has a branching structure, like a tree.